

Alma Mater Studiorum – Università di Bologna

DOTTORATO DI RICERCA IN
ONCOLOGIA E PATOLOGIA SPERIMENTALE

XXVII Ciclo

Settore Concorsuale di afferenza: 06/A2
Settore Scientifico disciplinare: MED/04

**PRECLINICAL DEVELOPMENT OF
ANTI-CANCER STRATEGIES AGAINST
HUMAN HER-2**

Presentata da Dott. Massimiliano Dall’Ora

Coordinatore Dottorato

Chiar.mo Prof.
Pier-Luigi Lollini

Relatore

Chiar.mo Prof.
Pier-Luigi Lollini

Esame finale anno 2015

CONTENTS

INTRODUCTION	5
1. HER-2	7
1.1 Role and function	7
1.2 HER-2-driven transformation	10
1.3 HER-2 isoforms	11
2. HER-2-positive breast cancer and approved therapies	14
2.1 Clinically approved anti-HER-2 agents	14
2.2 Resistance to current anti-HER-2 therapies	16
3. Preclinical models and experimental approaches targeting HER-2	18
3.1 Preclinical mouse models	18
3.1.1 HER-2 and $\Delta 16$ transgenic models	19
3.1.2 Transplantation models	20
3.2 Experimental approaches targeting HER-2	24
3.2.1 Drugs	24
3.2.2 Virotherapy	26
3.2.3 Vaccines	28
MATERIALS AND METHODS	31
1. Cells	33
2. Mice	34
3. HER-2 and $\Delta 16$ expression	35
3.1 Indirect immunofluorescence and cytofluorimetric analysis	35
3.2 Real-time PCR	36
4. Sensitivity to drugs in 3-D culture	37
5. MEK inhibition and signaling	38
6. Viability tests	39
7. Preclinical models	39
7.1 Spontaneous carcinogenesis in transgenic models	39
7.2 Syngeneic transplantation models and therapy	40

7.3 Xenogeneic transplantation models and therapy	41
7.3.1 NVP-BKM120 therapy and metastasis quantification	41
7.3.2 R-LM249 therapy and metastasis quantification	42
7.4 Immunoprevention	43
7.4.1 Vaccine schedules	43
7.4.2 ELISA (Enzyme-Linked ImmunoSorbent Assay)	44
7.4.3 MLTC (Mixed Lymphocyte Tumor Cell Culture)	45
7.4.4 Indirect immunofluorescence and cytofluorimetric analysis	45
7.4.5 HER-2 inhibition and signaling	45
7.4.6 Xenogeneic transplantation model and passive immunization	46
8. Statistical analysis	47
RESULTS	49
1. F1 Model	51
1.1 Carcinogenesis	51
1.2 Metastasis	52
1.3 HER-2 and $\Delta 16$ expression	53
2. Anti-cancer strategies against HER-2	54
2.1 Drugs	54
2.1.1 Trastuzumab	54
2.1.2 Lapatinib	55
2.1.3 Dasatinib	55
2.1.4 NVP-BKM120	56
2.1.5 MEK inhibition	58
2.2 Oncolytic virus R-LM249	59
2.2.1 <i>In vitro</i> sensitivity	59
2.2.2 Therapy of localized HER-2-positive breast cancer	60
2.2.3 Therapy of disseminated HER-2-positive breast cancer	61
2.2.4 Therapy of disseminated HER-2-positive ovarian cancer	62
2.3 Anti-HER-2 vaccines	63

2.3.1 Immunoprevention of HER-2-positive breast cancer	63
2.3.2 Immune responses to anti-HER-2 vaccines	64
2.3.3 Anti-HER-2 antibodies	65
FIGURES AND TABLES	67
DISCUSSION	101
CONCLUSIONS	117
SCIENTIFIC PUBLICATIONS DURING PHD PERIOD	121
REFERENCES	125

INTRODUCTION

1. HER-2

The Human Epidermal Growth Factor Receptor-2 (HER-2) is a 185 kDa transmembrane receptor tyrosine kinase. It belongs to the Epidermal Growth Factor Receptor family (EGFR family), also known as ErbB family because of the homology with the oncogene of the avian erythroblastosis virus (v-erbB). Besides HER-2, this family is composed of three more members: EGFR (HER-1), HER-3 and HER-4 (Yarden and Sliwkowski, 2001). Dysregulation (mutations or overexpression) of ErbB members has been strongly related to the initiation and maintenance of several solid tumors (Yarden and Pines, 2012; Arteaga and Engelman, 2014).

1.1 Role and function

ErbB proteins are widely expressed in cells of mesodermal and ectodermal origins and they are functionally important for the development of many organs, including skin, brain, lungs and gastrointestinal system. Furthermore, the employment of knockout models for EGFR or HER-2 showed the relevance of these proteins for mammary morphogenesis (Yarden and Sliwkowski, 2001; Moasser, 2007).

EGFR family receptors consist of an extracellular domain with two cysteine-rich regions, a transmembrane domain and an intracellular tyrosine kinase domain (Figure I). After the binding to the extracellular domain of a ligand, i.e. the Epidermal Growth Factor (EGF) family, an activating conformational change occurs in the receptor, promoting the interaction with a monomer of the same kind (homodimerization) or with another member of the ErbB family (heterodimerization). Coupling two monomers (heterodimers are preferred to homodimers) causes transphosphorylation of tyrosines in the intracellular domain and the engagement of specific effectors that activate signal transduction (Yarden and Sliwkowski, 2001; Moasser, 2007). The most activated cascades downstream to ErbB dimers are Ras- and Shc-activated mitogen-activated protein kinase (MAPK), PI3K-AKT, JAK-STAT and PLC γ pathways (Yarden and Sliwkowski, 2001).

Introduction

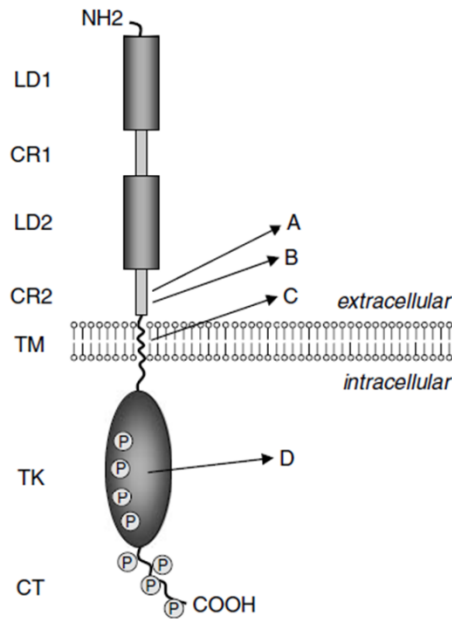


Figure I. HER-2 structure and mutations. LD1 and LD2, ligand-binding regions; CR1 and CR2, cysteine-rich regions; TM, transmembrane domain; TK, tyrosine kinase domain; CT, carboxy-terminal tail. **(A)** Site of somatic mutations found in tumors arisen in mice transgenic for Neu. **(B)** Site of $\Delta 16$ deletion. **(C)** Site of NeuT mutation. **(D)** Site of mutations found in rare cases of human lung cancers (Moasser, 2007).

The activation of HER receptors triggers a multi-layered signaling network (Figure II), whose specificity and potency depend on the composition of ligands (at least 12) and monomers (input layer), along with the variety of intracellular effectors and regulators (signal-processing layers). The physiological outputs consist of cell division, migration, adhesion, differentiation and apoptosis. Ligand-mediated receptor endocytosis allows the turning off of the signaling network (Yarden and Sliwkowski, 2001).

HER-2 is the only member of the EGFR family with unknown ligands. It constitutively exists in the activated conformation and, among ErbB members, it has the strongest catalytic activity. Furthermore, it is considered as preferred partner of ligand-induced heterodimers and the complex between HER-2 and the catalytically inactive HER-3 is the most active signaling heterodimer of the family (Yarden and Pines, 2012).

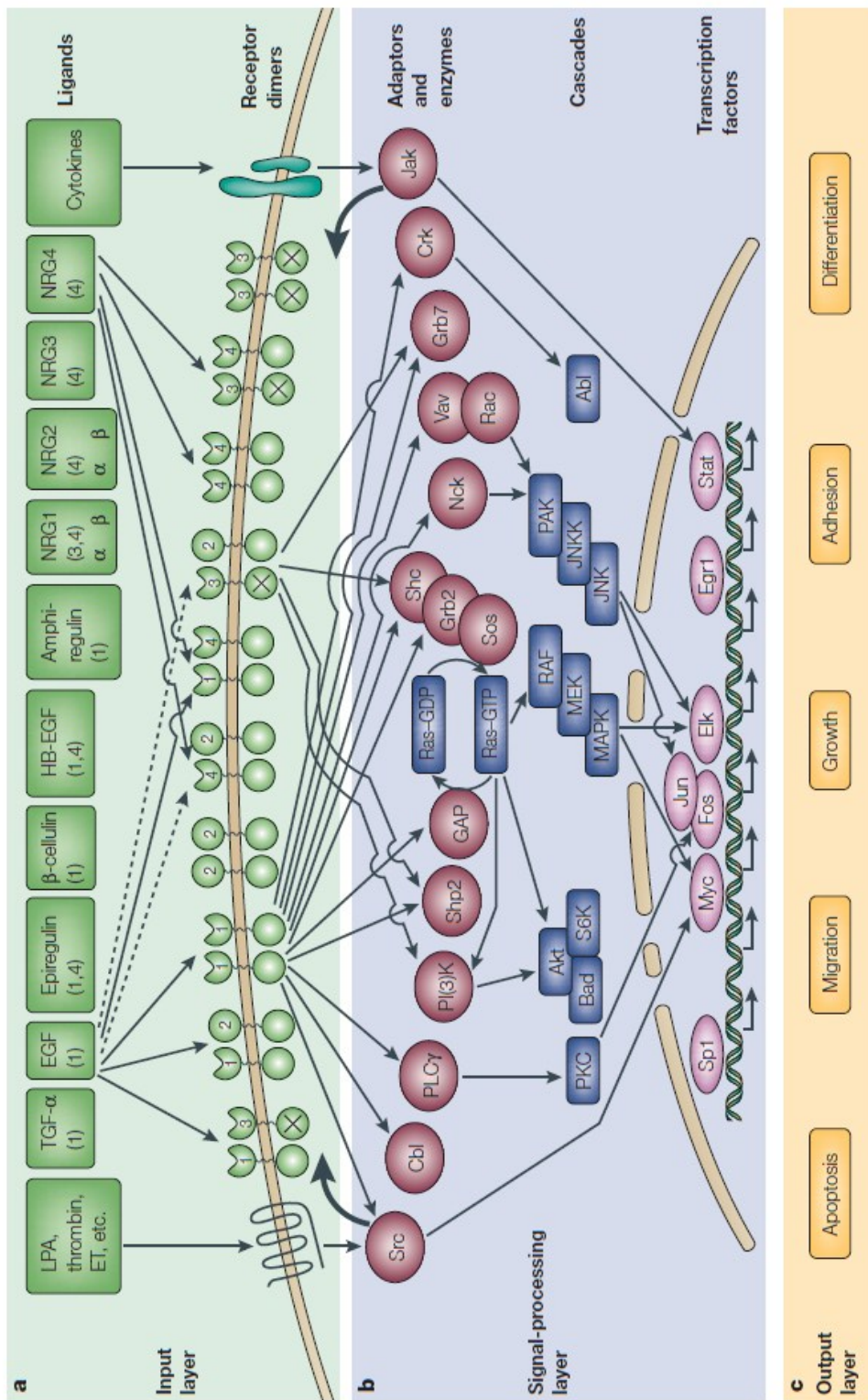


Figure II. The ERbB signaling network.

(A) The input layer is composed of ligands and combinations of HER monomers. (B) Intracellular effectors of many signaling pathways represent the signal-processing layer. (C) Cellular processes (output layer) triggered by the signaling network (Yarden and Sliwkowski, 2001).

1.2 HER-2-driven transformation

In 1984, HER-2 was first connected to cancer when Schechter and colleagues isolated from carcinogen-induced rat neuroblastomas its mutated ortholog, called NeuT (Schechter *et al.*, 1984). Since then, numerous studies have been conducted to shed light into HER-2/Neu-driven transformation.

NeuT transforming ability was attributed to a point mutation in the transmembrane domain. Other mutations (including a deletion), found in the juxtamembrane region of the extracellular domain, were associated to HER-2/Neu-driven mammary tumorigenesis in *in vitro* and *in vivo* models (Figure I).

HER-2 tumorigenic ability in humans was mainly related to the overexpression of the wild-type form of the receptor (Moasser, 2007). Hence, HER-2 overexpression alone seems oncogenic in humans without the need of activating mutations as in Neu/HER-2 transgenic mice. However, in more recent studies somatic mutations of HER-2 were detected in human cancers with no HER-2 gene amplification by next-generation sequencing. In particular, missense mutations in the catalytic and extracellular domains or duplications/insertions in exon 20 were found in lung adenocarcinoma and lobular breast, bladder, gastric and endometrial cancers (Bose *et al.*, 2013; Arteaga and Engelman, 2014).

HER-2 overexpression, caused by gene amplification or transcriptional deregulation, was reported in human breast, gastric, esophageal, ovarian, endometrial and lung cancers (Arteaga and Engelman, 2014). It determines a high availability of catalytically activated HER-2 on cell surface, that can homo- or heterodimerize with other monomers and trigger a high-potent intracellular signaling. As already described, HER-2/HER-3 is the most active heterodimer among EGFR family. HER-3, that strongly activates the PI3K-AKT pathway, is always phosphorylated in human HER-2-positive breast cancer, that has been found highly dependent on this survival and anti-apoptotic cascade (Lee-Hoeflich *et al.*, 2008; Chakrabarty *et al.*, 2013). On the contrary, HER-2 directly activates MAPK proliferative cascade but not PI3K-AKT pathway. Hence, HER-3 is an important partner for HER-2 and the combination between these two monomers enhances cell survival and proliferation and avoids apoptosis in HER-2-driven cancers (Yarden and Pines, 2012; Arteaga and Engelman, 2014).

In addition, when coupled with other ErbB monomers, HER-2 increases ligand-binding affinity and delays the ligand-induced receptor endocytosis, prolonging signal transduction. Transforming ability of HER-2 can also be enhanced by its interaction with other cell surface receptors apart from ErbB members, e.g. the insulin-like growth factor 1 (IGF-1) and the hepatocyte growth factor, further extending the concept of multi-layered network previously described (Emde *et al.*, 2012).

Apart from full-length HER-2 overexpression, the investigation of HER-2-driven transformation and the search for activating mutations in human HER-2-positive breast cancers led to the identification of truncated forms and a splice variant of HER-2, described in next section.

1.3 HER-2 isoforms

Carboxy-terminal fragments of HER-2 (CTFs, also called p95HER-2) were identified in about 30% of human HER-2-positive breast cancers. They originate by proteolytic shedding of the extracellular domain of full-length HER-2 or by traduction of HER-2 mRNA from internal initiation codons. p95HER-2 fragments are able to homodimerize on cell membrane, leading to a much more rapid and acute signal transduction than that driven by HER-2-containing dimers. The presence of CTFs in human HER-2-positive breast tumors has been associated to a worse prognosis and to a higher risk of metastatic progression; furthermore, they showed Trastuzumab-resistance (Arribas *et al.*, 2011). However, two recent studies connected CTF expression in human samples of HER-2-positive breast cancer to a good Trastuzumab response (Scaltriti *et al.*, 2014; Parra-Palau *et al.*, 2014).

Besides CTFs, Morancho and colleagues observed the existence of N-terminal fragments (H2NTF) in 60% of human HER-2-positive breast cancers. The intracellular catalytic domain is absent in H2NTF, but it can interact with HER-2 and the other ErbB members, inhibiting their functions. Acting as dominant negative molecule, the presence of H2NTF has been related to a better prognosis (Morancho *et al.*, 2013).

In addition to the truncated isoforms of HER-2, a splice variant lacking

Introduction

exon 16 (initially called Δ HER2, here referred to as Δ 16) was identified in 1998 by Kwong and Hung in human cancer cell lines. The in-frame deletion is localized in the same region of the extracellular domain that is mutated in Neu/HER-2 transgenic models (Figure I) (Kwong and Hung, 1998). Due to the loss of two cysteine residues in the juxtamembrane region, a conformational change in the extracellular domain of HER-2 occurs, promoting intermolecular disulfide bonds with other Δ 16 monomers (Castiglioni *et al.*, 2006).

The formation of stable and constitutively active homodimers results in a stronger activation of the signal transduction. In particular, an increased activation of PI3K-AKT and MAPK pathways was observed in MCF-7 and MCF-10A transfected with Δ 16 and compared with cells transfected with full-length HER-2 (Mitra *et al.*, 2009; Alajati *et al.*, 2013).

Furthermore, three different studies correlated the oncogenic properties of Δ 16 isoform to Src kinase activation. Mitra and colleagues identified Src kinase as a critical upstream effector of both PI3K-AKT and MAPK cascades in MCF-7 transfected with Δ 16, and they showed a physical interaction between Δ 16 and Src on the cell membrane, assuming a Δ 16-mediated Src activation. Phospho-Src was also detected in 44% of human Δ 16-expressing breast tumors (Mitra *et al.*, 2009). Confirming these findings, molecular studies on tumors arisen in a Δ 16 transgenic model (see section 3.1.1) showed that Δ 16 constitutively-activated homodimers were able to trigger a Src-mediated signal transduction (Marchini *et al.*, 2011). The strong correlation between activated Δ 16 dimers/monomers and phospho-Src was highlighted also by Castagnoli and colleagues both on a cell line derived from a tumor of a Δ 16 transgenic mouse (Milan 6, also described in the Results of this thesis) and on human HER-2-positive breast tumors. However, they did not observe Src-dependent activation of PI3K-AKT and MAPK pathways (Castagnoli *et al.*, 2014).

Phenotypically, the high potency of signal transduction led by Δ 16 determined an increased proliferation and a decrease in the death of cells transfected with the splice variant of HER-2 (Castiglioni *et al.*, 2006; Mitra *et al.*, 2009; Alajati *et al.*, 2013). In migration and invasion assays, a higher ability of

Introduction

Δ 16-expressing cells (MCF-7 or MCF-10A) in respect to HER-2-transfected cell lines was observed by Alajati and colleagues and by Mitra and co-workers. In particular, the latter group associated this metastatic potential to Src activation (Mitra *et al.*, 2009; Alajati *et al.*, 2013).

In *in vivo* experiments, the subcutaneous or intramammary injection of Δ 16-transfected cells in immunodeficient mice revealed the tumorigenic ability of this HER-2 variant (Castiglioni *et al.*, 2006; Alajati *et al.*, 2013). In addition, Alajati and colleagues showed that the intramammary or intravenous administration of cells was able to induce metastasis formation in 66% and 71% of immunodeficient mice respectively (Alajati *et al.*, 2013).

Δ 16 isoform has been found as 8-10% of HER-2 transcript amount in half HER-2-positive breast cancer patients and in 90% of women with locally disseminated disease (Castiglioni *et al.*, 2006; Mitra *et al.*, 2009).

In vitro resistance to Trastuzumab was observed in Δ 16-expressing cells in the studies conducted by Castiglioni and Mitra (Castiglioni *et al.*, 2006; Mitra *et al.*, 2009). On the contrary, other authors, focusing on *in vivo* experiments, demonstrated Trastuzumab susceptibility of Δ 16-expressing tumors. Alajati and colleagues injected Δ 16-transfected human cell line MCF-10A in immunodeficient mice, while in the study conducted by Castagnoli and colleagues Trastuzumab was administered to mice carrying the splice variant of HER-2 and to mice that had previously received the intramammary injection of MILAN 6 (Alajati *et al.*, 2013; Castagnoli *et al.*, 2014). In the latter study, a retrospective analysis showed that patients with primary human HER-2-positive breast cancer had a lower relapse rate, after treatment with Trastuzumab, if tumors coexpressed at high levels both Δ 16 and phospho-Src (Castagnoli *et al.*, 2014).

2. HER-2-positive breast cancer and approved therapies

HER-2-positive breast cancer is characterized by overexpression of HER-2, either through gene amplification (20% of breast cancers) or through transcriptional deregulation (5%) (Moasser, 2007; Arteaga and Engelman, 2014). HER-2 amplification is an early event in breast tumorigenesis and is maintained during progression to advanced disease (Moasser, 2007). In these patients, metastases are primarily detected in visceral organs, i.e. lungs and liver (Cadoo *et al.*, 2013). Overall, women with this subtype of breast cancer have a worse prognosis (Moasser, 2007).

2.1 Clinically approved anti-HER-2 agents

Besides conventional therapies (surgery, radiotherapy and cytotoxic chemotherapy), the development of HER-2-targeted therapies improved overall response rates, time to progression and overall survival in HER-2-positive breast cancer patients (Singh *et al.*, 2014).

Trastuzumab is a humanized immunoglobulin G₁ antibody that binds to an epitope in juxtamembrane region IV of HER-2 (Table I). It is able to inhibit cleavage of HER-2 ectodomain (preventing the formation of CTF), uncouple ligand-independent HER-2 homodimers (partially inhibiting downstream signaling) and trigger antibody-dependent cell-mediated cytotoxicity (ADCC) and adaptive immunity to HER-2 (Arteaga and Engelman, 2014). It is approved by FDA (Food and Drug Administration) and EMA (European Medicine Agency) and represents the standard of care for patients with early or advanced HER-2-positive breast cancer (Emde *et al.*, 2012).

However, after Trastuzumab approval an increase in the incidence of brain metastases was observed in patients. The progressive high number of HER-2-positive breast cancer patients with metastatic spread in the brain (up to half of women) has been attributed to the reduction in mortality, the effectiveness of Trastuzumab in killing metastatic cells in other organs and to its incapability to cross the blood-brain barrier (Palmieri *et al.*, 2007; Giordano *et al.*, 2014; Singh *et*

Introduction

al., 2014).

Three more anti-HER-2 drugs have been developed and approved for clinical treatment of patients that fail first-line therapy with Trastuzumab: Lapatinib, Pertuzumab and T-DM1 (Table I).

Lapatinib is a HER-2/EGFR dual inhibitor. Thanks to its small size, it is able to reversibly compete with ATP for the ATP-binding site in the kinase domain of HER-2 and EGFR. As a result, it inhibits signal transduction downstream to HER-2, including PI3K-AKT and MAPK pathways (Arteaga and Engelman, 2014). To enhance clinical benefit, typical regimens for Trastuzumab resistant patients with advanced disease consist of Lapatinib administration in combination with capecitabine or Trastuzumab (Yan *et al.*, 2014).

Pertuzumab is a humanized monoclonal antibody that binds to subdomain II of the extracellular portion of HER-2. It is able to prevent ligand-dependent heterodimerization of HER-2 with other HER members, including the high potent HER-2/HER-3 dimer. As a result, inhibition of signaling pathways is observed (Arteaga and Engelman, 2014; Yan *et al.*, 2014). Due to their different targeted epitopes on HER-2 extracellular domain, Trastuzumab and Pertuzumab combination has been approved for the treatment of HER-2-positive breast cancer (Arteaga and Engelman, 2014).

Trastuzumab-derivative of maytansyne 1 (T-DM1) is an antibody-drug conjugate, approved in 2013 for the treatment of metastatic HER-2-positive breast cancer. A molecule of Trastuzumab and 3.5 molecules of the compound are linked together by a covalent non-reducible thioether bond. T-DM1 combines Trastuzumab mechanism of action to the cytotoxic microtubule-depolymerizing ability of DM1. Hence, after Trastuzumab-mediated HER-2 binding, the conjugate is internalized and degraded by lysosomes. Then, DM-1 is released in the cytoplasm, causing lysis of HER-2-positive cancer cells (Arteaga and Engelman, 2014; Yan *et al.*, 2014).

Table I. Clinically approved anti-HER-2 agents (modified from Arteaga and Engelman, 2014)

Drug	Type of molecule	Mechanism of action	FDA approval
Trastuzumab	humanized IgG ₁ , binds juxtamembrane domain IV	inhibits ectodomain cleavage and ligand-independent HER-2-containing dimers; ADCC and adaptive immunity to HER-2	1998 (metastatic breast) 2006 (adjuvant early breast) 2010 (advanced gastric)
Lapatinib	small molecule	reversible, ATP-competitive TKI	2006 (advanced breast)
Pertuzumab	humanized IgG ₁ , binds heterodimerization domain II	inhibits ligand-induced HER-2-containing dimers	2012 (metastatic breast) 2013 (neoadjuvant breast)
T-DM1	antibody-drug conjugate	same as Trastuzumab plus inhibition of microtubules and cell lysis (DM-1)	2013 (advanced breast)

2.2 Resistance to current anti-HER-2 therapies

Despite undeniable improvements in the treatment of patients, metastatic HER-2-positive breast cancer is still an incurable disease. Many patients display intrinsic (without initial response to treatment) or acquired (after an initial clinical response to the drug) resistance (Arteaga and Engelman, 2014).

Among HER-2 isoforms, as described in section 1.3, CTF and $\Delta 16$ expression in HER-2-positive breast cancer was connected to Trastuzumab intrinsic resistance, while H2NTF was related to a better prognosis in patients treated with the monoclonal antibody. However, further studies on $\Delta 16$ and p95HER-2 proposed a beneficial role of these isoforms in patients treated with Trastuzumab (Alajati *et al.*, 2013; Castagnoli *et al.*, 2014; Scaltriti *et al.*, 2014; Parra-Palau *et al.*, 2014).

Resistance to anti-HER-2 single-agent treatment was defined as “bypass track resistance” by Arteaga and Engelman (Arteaga and Engelman, 2014). In fact, the administration of a single drug is not sufficient to block the wide signaling network driven by ErbB receptors and the inhibition of a single receptor

Introduction

or pathway determine the activation of the others and the generation of feedback loops (Yarden and Pines, 2012; Arteaga and Engelman, 2014). Focusing on the input layer of ErbB network, Trastuzumab resistance was associated to increased levels of ErbB ligands, and activation of TGF β receptors was involved in this mechanism (Ritter *et al.*, 2007; Wang *et al.*, 2008). Furthermore, IGF-1 overexpression and dimerization with HER-2 cause resistance to Trastuzumab (Huang *et al.*, 2010). In addition, incapability of anti HER-2 agents to inhibit HER-2 could be attributed to the downregulation of the receptor (detected in patients treated with Trastuzumab) or/and to the not uncommon clinical observation of heterogeneous tumors containing HER-2-positive and negative cells (Mittendorf *et al.*, 2009; Arteaga and Engelman, 2014).

Many mechanisms promoting anti-HER-2 resistance were detected in the signal-processing layer. Somatic mutations or amplifications in the PI3K-AKT pathway (PI3K, mTOR, PTEN) have been found in 30% of HER-2-positive breast tumors, conferring resistance to current treatments (Arteaga and Engelman, 2014). Activity of Src kinase family members was also involved in HER-2 inhibitors resistance, partially by phosphorylation and inhibition of the tumor suppressor PTEN and consequent constitutive activation of PI3K-AKT pathway (Zhang *et al.*, 2011; Rexer *et al.*, 2011). Furthermore, as described above, opposite results were obtained in the studies conducted by Mitra and Castagnoli regarding the role of $\Delta 16$ /Src coexpression in HER-2-positive tumors and Trastuzumab resistance.

Defects in apoptosis and cell-cycle control were also found in resistant cancers. High levels of Survivin, a caspases inhibitor, were detected in HER-2-positive breast tumors resistant to Trastuzumab or Lapatinib. In addition, amplification of cyclin E and downregulation of the Cdk inhibitor p27^{KIP1} has been associated to Trastuzumab resistance (Arteaga and Engelman, 2014).

3. Preclinical models and experimental approaches targeting HER-2

The study of breast cancer in humans is highly problematic for different reasons. First, early genetic events that lead to tumor formation are difficult to detect as they usually occur before the clinical presentation of the disease. In addition, comparisons among patients are hampered by the high heterogeneity of human breast tumors. Furthermore, early stages of the metastatic cascade are difficult to detect in patients for the low number of invasive cells involved in the process.

Hence, the need to shed light on all cancer stages and to test new therapeutic strategies to overcome resistance to clinically approved therapies drove the development of preclinical models (Ottewell *et al.*, 2006; Saxena and Christofori, 2013).

3.1 Preclinical mouse models

The use of mice as preclinical models relies on anatomical, physiological and genetic similarities. Besides, mice have a small size, are easy to breed and they have a short gestation time, as well as a relatively short life (Jonkers and Derksen, 2007).

The ideal preclinical model of breast cancer should mimic the genetic and phenotypic changes that occur in patients. During the years, several mouse models have been developed, each of which is able only to partially reproduce the human situation. The most used preclinical models for the study of breast cancer are the genetically engineered mice (GEM) and transplantation models (Ottewell *et al.*, 2006).

GEM are developed to express (transgenic mice) or to lack (knockout mice) a gene of interest. They have been widely employed to study the early stages (initiation and progression) of many cancers but, due to the low incidence of metastases, they seem inappropriate for advanced disease studies (Ottewell *et al.*, 2006; Saxena and Christofori, 2013).

Introduction

Transplantation models consist of the injection of murine (syngeneic model) or human (xenogeneic model) cancer cells in mice. They are useful for studies on the various cancer stages as well as for the evaluation of new therapeutic approaches (Saxena and Christofori, 2013).

3.1.1 HER-2 and $\Delta 16$ transgenic models

The first genetically modified models developed for the study of HER-2-positive breast cancer were transgenic for the rat homologue Neu, either the normal or the mutated form (NeuT) (Muller *et al.*, 1988; Guy *et al.*, 1992). Despite their usefulness in shedding light on HER-2/Neu driven transformation in breast cancer, they could not be used for the investigation of human HER-2-targeted therapies.

To overcome this issue, transgenic models for wild-type HER-2 were generated. The first model that successfully reproduced HER-2-positive mammary carcinogenesis in mice was developed by Finkle and colleagues in 2004. In this model, also employed in the study described in this thesis and referred to as HER-2 model, overexpression of HER-2 in the mammary gland (but also in many other tissues) was achieved by the integration of 30-50 copies of the transgene on murine chromosome 6 under the promotion of the Murine Mammary Tumor Virus (MMTV). A tumor-free survival study was conducted on female transgenic mice with an endpoint of 52 weeks. 73% of mice developed asynchronous mammary tumors, with a mean latency of 36 weeks of age. Furthermore, lung metastases were detected in 40% of mice with tumors. As briefly described in section 1.2, the search for a transforming “second hit” on HER-2 proto-oncogene led to the identification of in-frame deletions, point mutations and insertions in more than 80% mammary tumors of mice overexpressing HER-2. These somatic mutations, as Neu mutations and splice deletion of exon 16, were localized in the cysteine-rich juxtamembrane region of HER-2. In a much lower extent, mutations were also found in the transmembrane domain of HER-2 (Finkle *et al.*, 2004).

The identification of $\Delta 16$ in human HER-2-positive breast tumors drove Marchini and colleagues in the generation of a preclinical model carrying this

HER-2 isoform under the promotion of MMTV ($\Delta 16$ HER2-LUC model, here referred to as $\Delta 16$ model and also described in the Results of this thesis) (Marchini *et al.*, 2011). Firefly luciferase was included as reporter transgene to allow the bioluminescent visualization of $\Delta 16$ expression in murine tissues. The integration of only 5 copies of the transgene in murine chromosome 5 was sufficient to determine the exclusive mammary overexpression of $\Delta 16$. After just a mean latency of 15 weeks of age, a multiple asynchronous tumors spread in all virgin $\Delta 16$ females was observed (4-5 tumors/mouse were detected in animals between 12 and 19 weeks of age). Furthermore, at 25 weeks of age lung metastases were already present. All these findings, in addition to the absence of further transforming mutations on $\Delta 16$ gene, highlighted the high transforming and invasive ability of $\Delta 16$ (Marchini *et al.*, 2011).

3.1.2 Transplantation models

The injection of murine cancer cells in an immunocompetent syngeneic mouse allows the study of the interactions among tumor, surrounding microenvironment and host immune responses. Cell lines can derive from spontaneous murine tumors or from carcinogen-, transgene- or gene knockout-induced tumors (Saxena and Christofori, 2013). According to the injection route (see below), the tumorigenic and/or the metastatic ability of different cell lines can be evaluated. Furthermore, susceptibility to new therapies (e.g. active or passive immunological strategies) in an immunocompetent host can be properly studied (Ottewell *et al.*, 2006).

Xenotransplantation refers to the delivery/implantation of human cells or tissues into immunodeficient mice, in order to prevent an immune rejection by the host (Jonkers and Derksen, 2007; Saxena and Christofori, 2013). Xenograft models are relatively easy and cheap to generate, and allow the study of human tumor growth and metastasis development, as well as the effectiveness of therapeutic agents on human tumor cells or tissues (Ottewell *et al.*, 2006). Many mouse strains carrying different gene mutations and therefore exhibiting various levels of immunodeficiency have been developed over the years, including *nude* and $\text{Rag}^{-/-}; \text{Il2rg}^{-/-}$ mice (Table II) (Thomsen *et al.*, 2008).

Introduction

In *nude* mice a single homozygous base deletion on Foxn1^{nu} gene in chromosome 11 determines a phenotype of hairlessness, athymia and T-cell deficiency (Hirasawa *et al.*, 1998). Their partially compromised immune system allows the local growth of injected human cells, but it is not sufficient to promote the spread of metastases. Indeed, NK cells are able to kill circulating human tumor cells, complicating the study of tumor progression and invasion of distant organs (Naito *et al.*, 1987).

The search for new useful models led to the development of Rag2^{-/-};Il2rg^{-/-} mice. This immunodeficient strain is double knockout for the Recombination Activating gene 2 (Rag2) and for the Interleukin 2 Receptor Gamma chain gene (Il2rg) (Goldman *et al.*, 1998). The homozygous mutation of Rag2, that usually participates in V(D)J recombination reaction for the formation of T cells receptors and B cells immunoglobulins, determines the absence of mature T and B cells in mice (Oettinger *et al.*, 1990; Shinkai *et al.*, 1992). Mice knockout for Il2rg gene, that encodes for the common gamma chain of IL-2, IL-4, IL-7, IL-9, IL-15 and IL-21 receptors, are defective in mature T and B cells and totally deficient in NK cells (Cao *et al.*, 1995; Kovanen and Leonard, 2004). As a result, knockout mice for both genes are severely immunocompromised and prone to the growth of human cancer cells (Goldman *et al.*, 1998). Furthermore, Nanni and colleagues showed the ability of this model in mimicking human metastatic spread (Nanni *et al.*, 2010).

Besides mice, the selection of the most appropriate cell line to be injected is an important issue in order to obtain a highly efficient preclinical model. To amplify the growing and invasive intrinsic ability of tumor cells, selection of increasingly aggressive variants is performed. For example, to select human breast cancer metastatic variants, Francia and colleagues injected MDA-MB-231 triple negative cells subcutaneously or intramammary in immunodeficient mice; then, metastatic colonies were isolated and cultured *in vitro*. Many consecutive *in vivo-in vitro* stages were performed to obtain a highly metastatic cell line. The same group of scientists first developed a HER-2-positive breast cancer metastatic model, transducing MDA-MB-231 with HER-2 gene and selecting metastatic variants as described above (Francia *et al.*, 2011).

Introduction

The selection of tumor sublines can be usefully employed to obtain metastatic variants with a specific targeted organ. The use of these cell lines allows investigational studies on metastatic organ-tropism as well as on therapeutic strategies for the treatment of specific colonized organs (Saxena and Christofori, 2013). Focusing on breast cancer-induced brain metastases, in the studies conducted by Bos and Francia MDA-MB-231 sublines highly metastatic to the brain were selected (Bos *et al.*, 2009; Francia *et al.*, 2011). After transducing MDA-MB-231 and MCF-7 with HER-2 and selecting variants, Palmieri and colleagues developed a HER-2-positive metastatic model for brain metastases (Palmieri *et al.*, 2007; Gril *et al.*, 2011).

Depending on the route of cancer cells delivery in syngeneic or xenogeneic mice, different aspects of tumor and metastatic processes of breast cancer can be evaluated. The subcutaneous (s.c.) injection of cells is a quick and easy tool to produce and monitor tumor growth, due to the high vascularization and convenient anatomical location of skin. On this model susceptibility to new localized strategies can be successfully evaluated (Ottewell *et al.*, 2006). Unfortunately, this ectopic transplantation model fails to mimic advanced breast cancer, i.e. the development of metastases (Saxena and Christofori, 2013).

Orthotopic injection of a breast cancer cell line into the organ from which cells were isolated (intramammary, i.ma.), allows to better mimic all aspects of breast cancer disease, including tumor histology, vascularity, tumor-stroma interaction, gene expression profiles and spontaneous metastases development. However, the metastatic spread has a relative high latency, and primary tumor resection could be required to observe advanced disease in mice (Ottewell *et al.*, 2006; Saxena and Christofori, 2013).

For studies focused on late phases of the metastatic process, as well as for the development of anti-metastatic strategies, tumor cells are injected directly into the systemic circulation, allowing a rapid development of induced metastases. According to the injection site, metastases in different organs can be observed. The administration of cells in the lateral tail vein (intravenous injection) is the most common way to obtain induced metastases. The first colonized organ are the lungs, with further metastases to other organs, including the brain. Intracarotid

Introduction

and intracardiac injections allow the development of metastases in the brain bypassing the pulmonary circulation. The latter route is also able to cause the growth of metastatic colonies in liver, ovaries, adrenal glands and bones. Finally, after intraportal and intrasplenic injection liver metastases are observed. A particular systemic delivery consists of the intraperitoneal injection of tumor cells, that causes local invasion (Khanna and Hunter, 2005; Ottewell *et al.*, 2006; Saxena and Christofori, 2013; Daphu *et al.*, 2013).

Table II. Immunodeficient mouse strains developed for xenotransplantation (modified from Thomsen *et al.*, 2008).

Mouse strain	Characteristics
<i>Nude</i>	Thymic agenesis
XID	Defect B cells signaling
<i>Beige</i>	Defect in lysosomal trafficking regulator gene
NOD	Interaction between several genes important for antigen presentation and T cells function
SCID	DNA repair defect, V(D)J recombination defect
γc^{null}	Lack of receptors for IL-2, IL-4, IL-7, IL-9 and IL-15
$\beta 2M^{null}$	No expression of MHC class I due to lack of β -2-microglobulin
Pfp^{null}	No production of perforin in lytic granules
$Rag1^{null}$	Inability to form V(D)J recombination, lack of B and T cell receptor
<i>Beige/Nude/XID</i>	Combined effect of <i>bg</i> , <i>nude</i> and <i>xid</i> mutations
SCID/ <i>Beige</i>	Combined effect of <i>scid</i> and <i>bg</i> mutations
NOD/SCID	V(D)J recombination defect added to NOD anomalies
NOD/SCID/ $\beta 2M^{null}$	V(D)J recombination defect, no MHC class I. Various NOD anomalies
NOD/ $Rag1^{null}$	No V(D)J recombination and NOD defects
NOD/SCID/ γc^{null}	Combined effect of SCID and γc^{null} on NOD background
NOD/ $Rag1^{null}$ / Pfp^{null}	No V(D)J recombination or perforin production and NOD defects
$Rag2^{-/-}; Il2rg^{-/-}$	Lack of B, T and NK cells

3.2 Experimental approaches targeting HER-2

Due to the complexity of ErbB network and the high incidence of resistance to current anti-HER-2 agents, new therapeutic strategies targeting HER-2 are required.

In addition to the formulation of new anti HER-2 biological agents and chemical compounds, relatively recent approaches targeting HER-2 include cancer virotherapy (HER-2 retargeted viruses) and cancer immunoprevention and immunotherapy (anti-HER-2 vaccines) (Campadelli-Fiume *et al.*, 2011; Lollini *et al.*, 2011).

3.2.1 Drugs

Treatment of HER-2-positive breast cancer with a single anti-HER-2 agent does not potently suppress HER-2 signaling. A strategy to overcome “bypass track resistance” consists of combining multiple anti-HER-2 drugs at the same time. As described in section 2.1, dual HER-2 inhibition has been already approved for Trastuzumab in combination with Lapatinib or Pertuzumab, but other combinatorial regimens are under study in on-going clinical trials. In these studies HER-2 targeted agents are also combined with other biological therapies or with chemotherapy. Furthermore, besides dual inhibition of HER-2, some trials include a third drug (Table III) (Yan *et al.*, 2014; Arteaga and Engelman, 2014).

Besides combinatorial regimens, the efficacy of several new drugs targeting HER-2 is currently investigated in clinical trials, including that of Neratinib (a dual irreversible inhibitor of HER-2/EGFR), Margetuximab (a chimeric anti-HER-2 monoclonal antibody with a Fc domain optimized for ADCC), LJM716 (a neutralizing antibody against HER-3 in order to block HER-2/HER-3 dimer) and ²¹²Pb-TCMC-Trastuzumab (an alpha particle releasing radioactive lead conjugated to Trastuzumab) (Table III) (Yan *et al.* 2014).

Instead of targeting HER-2 receptor, new experimental molecules focus on the inhibition of its signaling network. Due to its hyper-activation in HER-2-positive breast cancers, PI3K-AKT cascade is one of the main targets of this strategy. Many PI3K-AKT inhibitors are being developed and investigated, including NVP-BKM120 (Novartis), which has a demonstrated ability to cross the

Introduction

blood-brain barrier. This small molecule compound, that competes for ATP binding, inhibits all four class I PI3K isoforms and is also active against the most common somatic PI3K α mutations (Maira *et al.*, 2012; Saini *et al.*, 2013).

Similarly, MEK inhibitors, including UO126 (DuPont), are being studied in clinical trials. These kinase inhibitors specifically bind to a hydrophobic pocket adjacent to, but not overlapping with, the ATP-binding site (non-ATP competitive inhibitors) of MEK1, MEK2 or both isoforms. MEK inhibition allows the blocking of many upstream signaling pathways that converge to MAPK cascade, although many HER-2-positive breast cancers showed resistance to the treatment with only a MEK inhibitor because of PI3K cascade hyper-activation (Chappell *et al.*, 2011). In addition, PI3K inhibition alone has been associated to enhanced HER signaling and acquired dependency on ERK (downstream to MEK) in HER-2-positive breast tumors (Serra *et al.*, 2011). Therefore, combined anti-MEK/anti-PI3K regimens are under evaluation, as well as combinations that include intracellular signaling inhibitors and anti-HER-2 agents (Table III) (Saini *et al.*, 2013, Arteaga and Engelman, 2014).

Focusing on Src suppression, Mitra and co-workers showed that Dasatinib, a small molecule that inhibits Src kinase family but also receptor tyrosine kinases, was able to suppress the growth, proliferation and invasion ability of HER-2 and $\Delta 16$ -expressing cell lines (Mitra *et al.*, 2009). Zhang and colleagues detected a higher Src activation in a brain-seeking selected variant of BT-474 (BT-474.Br) if compared with the parental cell line and showed its important role in disrupting the blood-brain barrier and promoting brain metastases formation. In accordance with this findings, they demonstrated that the combinatorial regimen of small molecule Src inhibitor Saracatinib and HER-2-targeted Lapatinib was able to reduce HER-2-positive brain metastasis incidence and to increase overall survival of *nude* mice that had previously received the injection of BT-474.Br (Zhang *et al.*, 2013).

Among other experimental drugs targeting HER-2, agents inhibiting VEGF, Hsp90 and matrix metalloproteinases are currently investigated (Table III) (Emde *et al.*, 2012; Hurvitz *et al.*, 2013).

Table III. Experimental drugs targeting HER-2 in HER-2-positive breast cancer (modified from Yan *et al.*, 2014; Arteaga and Engelman, 2014).

Therapy	Regimen
anti-HER-2	Neratinib Margetuximab LJM716 212Pb-TCMC-Trastuzumab T-DM1+Pertuzumab Trastuzumab+Neratinib Trastuzumab+LJM716
anti-signaling effectors	MEK inhibitors (UO126) PI3K inhibitors (BKM120) Src inhibitors (Dasatinib)
other targets	Hsp90, VEGF, matrix metalloproteinases inhibitors
anti-HER-2 + other biological therapies	Trastuzumab+erlotinib (EGFR tyrosine kinase inhibitor) Trastuzumab+everolimus (mTOR inhibitor) Lapatinib+bevacizumab (anti-VEGF-A monoclonal antibody) T-DM1+PI3K inhibitor Trastuzumab+ Pertuzumab+PI3K inhibitor Trastuzumab+LJM716+PI3K inhibitor
anti-HER-2 + chemotherapy	anti-HER-2 agents + capecitabine/ docetaxel/ gemcitabine/paclitaxel

3.2.2 Virotherapy

Cancer virotherapy exploits virus ability to infect, replicate into and kill tumor cells (Lollini *et al.*, 2009). Indeed, the observation that natural viral infections caused cancer regression led to the entry of viruses in cancer therapy.

First pioneering studies were based on the notion that virus families have evolved specificities for different cell types, and this tissue-tropism can be exploited for therapeutic development (Miest and Cattaneo, 2014). However, the use of wild-type viruses was frequently associated to high toxicity (Campadelli-Fiume *et al.*, 2011). The advent of genetic engineering allowed to obtain less aggressive viruses, but the attenuation interfered with the viral therapeutic efficacy. Nowadays, viruses are engineered to have greater tumour specificity and/or efficacy than their parental strains. Viruses from nine different families are currently under evaluation in clinical trials: Adenoviridae, Picornaviridae, Herpesviridae, Paramyxoviridae, Parvoviridae, Reoviridae, Poxviridae, Retroviridae and Rhabdoviridae (Miest and Cattaneo, 2014).

Introduction

The first study on genetically modified Herpesviridae, conducted by Martuza and colleagues in 1991, demonstrated the therapeutic ability of an attenuated Herpes Simplex Virus type 1 (HSV-1) in human gliomas (Martuza *et al.*, 1991).

HSV, that is a DNA virus, is particularly appropriate as oncolytic virus for many reasons. First, it is a common pathogen in humans, causing a self-limiting disease. In worst cases, specific therapies are available (e.g. acyclovir). In addition, its large genome makes the virus suitable for genetic engineering and allows the insertion of heterologous genes. Finally, HSV envelope glycoproteins well tolerate modifications (Campadelli-Fiume *et al.*, 2011).

Three main strategies have been employed to generate oncolytic HSV: the conditional replication of the virus in tumor cells, the potentiation of anti-tumor activity by the insertion of cytokines genes in virus DNA, and the retargeting of HSV to tumor cells (Campadelli-Fiume *et al.*, 2011).

Focusing on the last strategy, retargeted oncolytic viruses were developed combining the notions that viruses use cell surface molecules to enter into cells and that there are tumors that express/overexpress specific receptors on cancer cell membrane (e.g. HER-2 overexpression in HER-2-positive breast cancer) (Lollini *et al.*, 2009). In detail, the entry-fusion apparatus of HSV consists of four glycoproteins: gB and gC mediate virus attachment to glycosaminoglycans, while gD binds cell receptor nectin1 or HVEM (herpesvirus entry mediator), triggering the gH/gL- and gB-mediated virion-cell fusion (Campadelli-Fiume *et al.*, 2011).

In 2009 Menotti and colleagues were able to fully detarget a HSV-1 from nectin1 and HVEM and to retarget it to HER-2. The HER-2 retargeted virus (called R-LM249) was obtained by replacing the gD Ig-folded core (half of gD ectodomain) with another Ig-folded molecule, a single-chain antibody (scFv) against HER-2 (Figure III). The engineered gene also contained the Enhanced Green Fluorescent Protein (EGFP) sequence for an easy fluorescent imaging detection of the virus. R-LM249 entered into and lysed only HER-2-overexpressing tumor cells (SK-OV-3, ovarian cancer cell line resistant to Trastuzumab), barely infecting MCF-7 (intermediate-low HER-2 expression, breast cancer). SJ-Rh4 (HER-2-negative rhabdomyosarcoma) was not infected by

the virus. In *in vivo* experiments, R-LM249 intratumor treatment succeeded in slowing down tumor growth in *nude* mice bearing SK-OV-3 subcutaneous tumors (Menotti *et al.*, 2009).

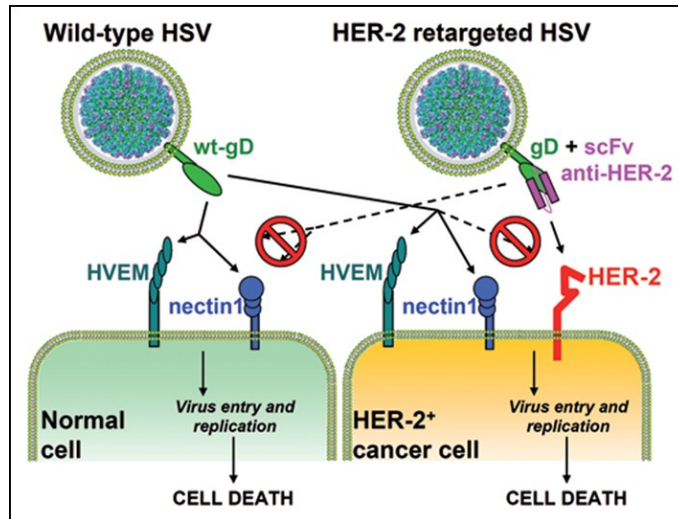


Figure III. Tropism of Wild-type and HER-2 retargeted HSVs (Lollini *et al.*, 2009)

3.2.3 Vaccines

Starting from the observation that immunodeficient mice are more susceptible to spontaneous or chemical carcinogenesis than wild-type mice, immunoprevention of non-infectious tumors has been widely studied. Antigen-specific (i.e. vaccines or monoclonal antibodies) and non-antigen specific approaches (cytokines and immunostimulants) are investigated in preclinical and clinical studies to delay or prevent tumor onset and progression (Lollini *et al.*, 2011).

Active immunization with vaccines exploits the expression in tumors of specific antigens, called oncoantigens, that drive carcinogenesis (Lollini *et al.*, 2006). According to their localization, three classes of oncoantigens have been identified: class I includes cell surface molecules, while extracellular or intracellular oncoantigens belong to class II and III respectively (Lollini *et al.*, 2011). Thus, overexpressed HER-2 on breast cancer cells (class I oncoantigen) is the perfect target for vaccines construction (Lollini *et al.*, 2013).

Introduction

The ideal vaccine should activate humoral and cellular response against tumor and induce immunological memory. Furthermore, it should be safe, easy to develop and administer. Several formulations of vaccines targeting HER-2-positive breast cancer have been tested in preclinical and clinical trials, including peptide-, protein- or DNA-based vaccines, as well as whole-tumor cell and dendritic cell vaccines (Milani *et al.*, 2013).

In the Laboratory of Immunology and Biology of Metastasis a cellular vaccine composed of three immunogenic stimuli was developed to prevent mammary carcinoma in mice transgenic for the mutated rat isoform of HER-2 (BalbNeuT mice). The vaccine was composed of cells with a high expression of Neu (specific stimulus) and of two potent adjuvants: the allogeneic class I major histocompatibility complex molecules (MHC) of the cells and murine IL-12 (non-antigen specific stimuli). The latter adjuvant was delivered i.p. (systemic administration) or vaccine cells were transfected with IL-12 genes to obtain a local release. IL-12 was chosen because of its potent activity as stimulant of T helper 1 anti-tumor response and because of its anti-angiogenic properties (Boggio *et al.*, 1998). Vaccination was able to break tolerance towards Neu: at one year of age, all vaccinated mice were still tumor-free, while control mice had already developed mammary tumors (Nanni *et al.*, 2001; De Giovanni *et al.*, 2004). HER-2-Cell vaccine, described in the Results of this thesis (De Giovanni *et al.*, 2014), was developed according to the notions acquired in these previous studies.

Exploiting the same principle that drove them to the development of the cell vaccine, De Giovanni and co-workers showed the efficacy of a DNA vaccine in preventing carcinogenesis of BALBNeuT with a p53 knockout allele. The vaccine was composed of three plasmids encoding the extracellular/transmembrane domain of Neu, IL-12 and allogeneic MHC respectively. Electroporation of animals was used as adjuvant stimulus, to promote the opening of cell membrane pores and the entry of plasmids in cells (De Giovanni *et al.*, 2009).

In 2010 Quaglino and colleagues compared the immunopreventive efficacy of four DNA vaccines against HER-2/Neu. Two plasmids encoded for the

Introduction

fully rat or human extracellular and transmembrane domains, while HuRT (also described in the Results of this thesis as HURT-DNA vaccine) and RhuT were engineered as chimeric plasmids of HER-2 and Neu extracellular and transmembrane domains. HuRT encoded a protein with 390 NH₂-terminal residues from extracellular HER-2 domain, while 299-COOH aminoacids derived from Neu. Almost symmetrically, Rhut plasmid encoded a protein with 410 NH₂-terminal aa from extracellular Neu and the remainder from HER-2. The intramuscular injection of both chimeric plasmids and the adjuvant electroporation were able to elicit a stronger immunopreventive response in wild-type and HER-2/Neu transgenic mice if compared to non-chimeric vaccines (Quaglino *et al.*, 2010).

MATERIALS AND METHODS

1. Cells

Five human cell lines were used in this thesis: BT-474, MDA-MB-453 (HER-2-positive breast cancer), MDA-MB-231 (HER-2-negative breast cancer), SK-OV-3 (HER-2-positive ovarian cancer) and MCF-10A (epithelial breast tissue of a woman with fibrocystic disease). HER-2-positive cell lines were kindly given by Dr. Serenella Pupa (Istituto Nazionale dei Tumori, Milan, Italy). MDA-MB-231 cell line was purchased from American Type Culture Collection (ATCC). For the experiments on MEK inhibition, MCF-10A and BT-474 were kindly provided by Prof. Yosef Yarden (Weizmann Institute of Science, Rehovot, Israel). Human tumor cells were routinely cultured in Roswell Park Memorial Institute 1640 (RPMI 1640) medium supplemented with 10% heat-inactivated foetal bovine serum (FBS) (Life Technologies, Milan, Italy). MCF-10A were cultured in DMEM:F12 medium (Gibco BRL, Grand Island, NY, USA) supplemented with 10 µg/ml insulin, 0.1 µg/ml cholera toxin, 0.5 µg/ml hydrocortisone, 5% heat-inactivated horse serum (Gibco BRL) and 10 ng/ml Epidermal Growth Factor (EGF).

To better visualize metastases in the multiorgan metastasis model, MDA-MB-453 were transfected with a plasmid expressing Enhanced Green Fluorescent Protein (pEGFP-N1, Clontech, Mountain View, CA) using Lipofectamine 2000 (Life Technologies). Stable transfectant were selected adding the G418 (Life Technologies) at a final concentration of 1000 µg/ml to the medium.

Six mouse mammary tumor cell lines were employed in this project: MAMBO 89, MILAN 6, 143-VS, 302-IVD, 156-VS and 156-IS. They were established from spontaneous primary mammary carcinomas arisen in HER-2 model (MAMBO 89), Δ16 model (MILAN 6) and F1 model (143-VS, 302-IVD, 156-VS and 156-IS). MILAN 6 was obtained and stabilized by Dr. Serenella Pupa, the other cell lines were obtained in the Laboratory of Immunology and Biology of Metastasis. Murine cell lines were stabilized (excluded MAMBO 89) and cultured in MammoCult (StemCell Technologies, Canada) supplemented with 1% FBS. MAMBO 89 cell line was stabilized in Dulbecco's Modified Eagle Medium (DMEM; Life Technologies) +10% FBS, supplemented with Bovine

Materials and methods

Pituitary Extract 30 µg/ml (BPE; BD Biosciences, USA) and MITO Serum Extender 1:200 (BD Biosciences).

All mediums were supplemented with penicillin 100 U/ml and streptomycin 100 µg/ml (Sigma-Aldrich, Milan, Italy). All cell lines were maintained at 37°C in a humidified 5% CO₂ atmosphere.

For the maintenance culture, cells were washed with Phosphate Buffer Saline (PBS; Life Technologies) and harvested by trypsin (0.05%)-EDTA (0.002%) treatment (Life Technologies). Cell number and viability was determined through erythrosine dye exclusion (Sigma-Aldrich) and hemocytometer count.

2. Mice

FVB-huHER-2 mice (Finkle *et al.*, 2004), here referred to as HER-2 model, were obtained from Genentech Inc. (South San Francisco, CA, USA). This line carries in heterozygosis the human full-length normal HER-2 gene under the control of the Murine Mammary Tumor Virus (MMTV) promoter on a FVB background. HER-2 gene heterozygosis was maintained by crossing HER-2^{+/-} male mice with non-transgenic FVB female mice (purchased from Charles River, Calco, Italy).

Δ16-HER2-LUC (Marchini *et al.*, 2011), here referred to as Δ16 model, were kindly given by Prof. Augusto Amici (University of Camerino, Italy). This line carries in heterozygosis the human splice variant Δ16 gene under the control of MMTV promoter on a FVB background. Δ16 gene heterozygosis was maintained as described above for HER-2 model.

F1 mice, transgenic for both genes, were obtained in the Laboratory of Immunology and Biology of Metastasis by crossing Δ16 male mice with HER-2 female mice.

Transgenic mice were screened by routine genotyping with PCR analysis (Finkle *et al.*, 2004; Marchini *et al.*, 2011).

Balb/c Rag2^{-/-};Il2rg^{-/-} breeders were kindly given by Drs. T. Nomura and M. Ito of the Central Institute for Experimental Animals (Kawasaki, Japan). Mice

were bred under sterile conditions and used for the experiments described here at 10-20 weeks of age. This line is double knockout for the Recombination Activating gene 2 (Rag2) and for the Interleukin 2 Receptor Gamma chain gene (Il2rg) (Goldman *et al.*, 1998).

Athymic Crl:CD-1-Foxn1^{nu/nu} mice (referred to as *nude* mice) were purchased from Charles River and kept under sterile conditions.

All animals were bred in the animal facility of the Laboratory of Immunology and Biology of Metastasis (Department of Specialistic, Diagnostic and Experimental Medicine, University of Bologna, Italy). Virgin female mice were used in the experiments. Experiments were authorized by the institutional review board of the University of Bologna and done according to Italian and European guidelines.

3. HER-2 and Δ 16 expression

The expression of total HER-2 on cell surface was evaluated in tumors and cell lines from HER-2, Δ 16 and F1 models and in BT-474 by indirect immunofluorescence and cytofluorimetric analysis. The expression of HER-2 and Δ 16 transcripts was investigated in the same tumors and cell lines by Real-time PCR.

3.1 Indirect immunofluorescence and cytofluorimetric analysis

After necropsy, tumor masses were minced with scissors, incubated for 5 minutes with trypsin and passed through a 70 μ m cell strainer (Becton Dickinson, Bedford, MA, USA) to obtain a homogeneous cell suspension. Before the incubation with the primary antibody, tumor suspensions were incubated with anti-mouse CD16/CD32 clone 2.4G2 (1:100 dilution; PharMingen, San Diego, CA). Next, tumor and cell suspensions were incubated with anti-human HER-2 clone MGR-2 primary antibody (1:100 dilution; Alexis Biochemical, Enzo Life Science, Lansen, Switzerland). Then, samples were incubated with the secondary

fluorescein-conjugated mouse monoclonal antibody (IgG AlexaFluor 488, 1:100 dilution; Life Technologies). Fluorescence intensity was determined through flow cytometry (FACScan, Becton Dickinson).

3.2 Real-time PCR

RNA was extracted using TRIzol protocol (“Total RNA Isolation Reagent”; Life Technologies). Tissue samples were first disrupted using a mortar and pestle and grinded to a fine powder in liquid nitrogen. The suspension was then transferred in appropriate tubes allowing liquid nitrogen to evaporate and then TRIzol was added to extract total RNA following the protocol provided with the reagent. The concentration and purity of RNA was determined by measuring the absorbance at 260 and 280 nm in a spectrophotometer (Ultrospec 1100 pro, Biochron, England). 1 µg of total RNA was reverse transcribed in 30 µl solution containing Moloney Mouse Leucemia Virus-Reverse Transcriptase (MMLV-RT), Random Examers (2.5 µM), Rnase OUT (1.33 U/µl), BSA (Albumin, from bovin serum 0.5 µg/µl) and dNTP (0.5 µM). RNA was incubated at 42°C for 120 minutes and then the reaction was stopped by heating at 95°C for 5 minutes. All reagents were purchased from Life Technologies.

Gene expression was analyzed by Real-Time PCR using ABI Prism 5700 sequence detection system (Applied Biosystems, Milan, Italy) or Thermal Cycler CFX96 (Bio-Rad Laboratories, USA). Initially cDNA were diluted 1: 3.2 with H₂O, then 1 µl of cDNA was amplified. For ABI Prism 5700 sequence detection system, SYBR Green Master Mix Reagent 1X (Applied Biosystems, Applied Biosystems) was employed. A specific primer forward for each gene and a common primer reverse were used (Table IV for primers sequences). The steps of amplifications were: 50°C for 2 minutes, 95°C for 10 minutes and then 40 cycles including 95°C for 15 seconds and 60°C for 1 minute. A default melting curve program was used to obtain the dissociation curve for each gene. mRNA expression levels were normalized to GAPDH (human or mouse, Table IV), as endogenous reference gene.

For Thermal Cycler CFX96, 1 µl of cDNA was amplified using SsoAdvanced SYBR Green Supermix 1X (Bio-Rad Laboratories). The steps of

Materials and methods

amplification were: 95°C for 30 seconds and then 40 cycles including 5 seconds at 95°C and 15 seconds at 60°C. A default melting curve program was used to obtain the dissociation curve for each gene. mRNA expression levels were normalized to GAPDH (human or mouse), as endogenous reference gene.

All primers were used at a final concentration of 200 nM. For relative quantification, ΔC_t method was used: $\Delta C_{t_{HER-2/\Delta 16}} = C_{t_{HER-2/\Delta 16}} - C_{t_{GAPDH}}$.

Table IV. Primers sequences for HER-2, $\Delta 16$ (Mitra *et al.*, 2009), mouse GAPDH and human GAPDH genes.

Gene	Primer	Sequence 5'-3'
HER-2	forward	GTGTGGACCTGGATGACAAGGG
$\Delta 16$	forward	CACCCACTCCCCTCTGAC
HER-2/ $\Delta 16$	reverse	GCTCCACCAGCTCCGTTTCCTG
mouse GAPDH	forward	GCTCACTGGCATGGCCTTC
	reverse	CCTTCTTGATGTCATCATACTTGGC
human GAPDH	forward	ATCAGCAATGCCTCCTGCAC
	reverse	TGGTCATGAGTCCTTCCACG

4. Sensitivity to drugs in 3-D culture

The sensitivity *in vitro* to anti HER-2 drugs was evaluated in cell lines derived from HER-2, $\Delta 16$ and F1 models and in BT-474 in 3-D culture (0.33% soft agar containing the drug). Trastuzumab, Lapatinib and Dasatinib were kindly given by Dr. Serenella Pupa, NVP-BKM120 was obtained from Novartis Institutes for BioMedical Research, Oncology (Basel, Switzerland). Drugs were used at the following concentrations: Trastuzumab 10 $\mu\text{g/ml}$, Lapatinib 1 μM , Dasatinib 1 μM , NVP-BKM120 1 μM and 0.1 μM .

Cells were suspended in MammoCult + 1% FBS containing 0.33% agar (overlayer) and layered on a base of MammoCult + 1% FBS containing 0.5% agar (underlayer) on a Costar 24-well plate (Corning Life Sciences, USA). Drugs alone or in combination were added both to underlayer and to overlayer. Plates were maintained at 37°C in a humidified 7% CO₂ atmosphere.

Colony growth was monitored weekly and determined by counting at 31.25X magnification with Diavert microscope (Leitz, Milan, Italy) after 2-3

weeks from seeding. BT-474 cells were seeded at 500 cells/well, the other cell lines at 10,000 cells/well. Drug's efficacy was assessed as percentage of colonies grown over control in 1-6 independent experiments.

5. MEK inhibition and signaling

The experiments on MEK inhibition were performed in the Laboratory of Prof. Yosef Yarden (Department of Biological Regulation, Weizmann Institute of Science, Rehovot, Israel). BT-474 and MCF-10A cell lines ($1-2 \times 10^5$ cells) were seeded on Costar 6-well plates (Corning Life Sciences) in their medium. After 24-48 hours cells were transfected with siRNA or treated with UO126.

For siRNA transfections, Oligofectamine (Life Technologies) and ON-Target SMART (Dharmacon, Lafayette, CO) oligonucleotides were used. For cell transfection, protocols suggested by the manufacturers were followed. 36-60 hours from siRNA transfection, cells were serum starved for 12 hours and then stimulated with Epidermal Growth Factor (EGF, 10 ng/ml) for 0-8 hours. Next, cell lysates were obtained by centrifugation and Western Blot was performed.

For the treatment with UO126, cells were serum starved for 12 hours and then incubated for 1 hour with UO126 5 μ M. Next, cells were stimulated for 0-8 hours with EGF, cell lysates were obtained and Western blot was performed.

For Western Blot, proteins were separated on a 8% polyacrylamide gel and then transferred to polyvinylidene difluoride membranes (Bio-Rad Laboratories). After blocking with Tris-buffered saline containing Tween-20 (TBS-T) plus 5% non-fat dry milk, membranes were incubated overnight at 4°C with primary antibodies diluted in TBS-T containing BSA 1% and NaN₃ 0.5%. The following primary antibodies were used: anti-HER2/ErbB2 (D8F12) XP rabbit monoclonal antibody (1:1,000 dilution; 4290), anti-phospho-HER2/ErbB2 (Tyr1221/1222) (6B12) rabbit monoclonal antibody (1:1,000 dilution; 2243), anti-phospho-MEK1/2 (Ser217/221) (41G9) rabbit monoclonal antibody (1:1,000 dilution, 9154), anti-MEK1 (30C8) rabbit monoclonal antibody (1:1,000 dilution, 9146), anti-MEK2 (13E3) rabbit monoclonal antibody (1:1,000 dilution, 9147) (all from Cell Signaling Technology, Danvers, MA, USA), anti-phospho-ERK1/2 clone

MAPK-YT mouse monoclonal antibody (1:20,000 dilution, M8159; Sigma-Aldrich).

Protein presence was detected through the incubation with the respective horseradish peroxidase-labeled secondary antibodies (Santa Cruz Biotechnology, Santa Cruz, CA, USA) followed by chemiluminescent reaction (ECL reagent, Amersham Pharmacia Biotech, Buckinghamshire, UK).

6. Viability tests

For the evaluation of the cytotoxic effect of R-LM249 on human cell lines, 8×10^3 cells/well were seeded in 96 well plates and treated with R-LM249 (10 pfu/cell). AlarmBlue assay was performed at 48, 96 and 144 hours from infection and plates were read at 570 and 600 nm with a Synergy HTTR-1 fluorometer (BioTek).

For Trastuzumab sensitivity, cells were seeded at $5-10 \times 10^3$ cells/well. The day after, cells were treated with 0.001-100 $\mu\text{g/ml}$ Trastuzumab and after 72-120 hours Cell Proliferation Reagent WST-1 (Roche Applied Science) was added to wells. After one hour samples absorbance at 450 nm and 630 nm was read on an ELISA plate reader (Tecan Systems, San Jose, CA, USA).

7. Preclinical models

7.1 Spontaneous carcinogenesis in transgenic models

HER-2, $\Delta 16$ and F1 female mice were inspected weekly by palpation to investigate tumor incidence, latency and number of tumors per mouse (multiplicity). During inspection, diameters of the first tumors arisen in animals were measured with caliper to evaluate tumor dimensions (progressively growing masses $\geq 50 \text{ mm}^3$ were scored as tumors). Tumor size was calculated as follows:

$$\frac{\pi}{6}(\sqrt{a \times b})^3$$

where a = maximal tumor diameter, b = maximal tumor diameter perpendicular to a .

Materials and methods

At necropsy, samples of tumor masses were collected for further analyses (immunofluorescence or Real-time PCR, see section 3). Samples for molecular analyses were frozen in liquid nitrogen and stored at -80°C .

Lungs were perfused with black India ink (15% in water, Rotring) to outline metastases and fixed in a modified-Fekete's solution (95.7% ethanol 96%, 4.3% glacial acetic acid). Autochthonous lung metastases were counted using a dissection microscope.

7.2 Syngeneic transplantation models and therapy

In HER-2 model, MAMBO 89 or MILAN 6 (10^6 cells) were injected in the mammary fat pad (intramammary, i.ma.) of 2-5 HER-2 mice per group (17-20 weeks old) in 0.1 ml of PBS to obtain the development of spontaneous metastases. For the induction of experimental metastases, HER-2 mice (7-17 weeks old) received the intravenous injection (in a lateral tail vein, i.v.) of 10^5 cells in 0.4 ml of PBS.

For the therapy with Trastuzumab and Dasatinib, lung metastases were induced with 10^5 and 10^6 MILAN 6 and MAMBO 89 cells respectively, injected i.v. in 0.4 ml of PBS in FVB non-transgenic mice. 7 days after cell injection, mice were randomized into four groups (8 mice/group) and treatments started. Treated mice (two groups) received the intraperitoneous (i.p.) injection of 4 mg/Kg Trastuzumab twice a week or the daily administration per os of 50 mg/kg Dasatinib. Control mice received the i.p. injection of diluent NaCl solution 0.9% (control group for Trastuzumab therapy) or DMSO per os (control group for Dasatinib therapy). Mice were sacrificed 11 weeks (MILAN 6) or 13 weeks (MAMBO 89) after cell injection and lungs were weighed and stained (to count metastases).

For Trastuzumab therapy of a F1 tumor, fragments of a F1 tumor were implanted in the fourth left mammary gland in 10-16 weeks old FVB non-transgenic mice (n=10). Starting 7 days after tumor implantation, 5 mice received biweekly the i.p injection of Trastuzumab (4mg/kg) for four weeks, while control group received the administration of NaCl solution 0.9%.

7.3 Xenogeneic transplantation models and therapy

7.3.1 NVP-BKM120 therapy and metastasis quantification

NVP-BKM120 was formulated in 1-methyl-2-pyrrolidone (NMP)/polyethylene glycol 300 (Fluka) (10/90, v/v). MDA-MB-453-EGFP was injected i.ma. (10^7 cells) or i.v. (2×10^6 cells) in groups of 5-9 Rag2^{-/-};Il2rg^{-/-} mice. Starting 7 days (i.ma.) or 1 day (i.v.) after cell challenge, mice were treated daily with 50 mg/kg NVP-BKM120 given per os. Control mice received vehicle alone. Mice received four drug administrations in the first week and five drug administrations in the following weeks (i.ma. injection=12 total weeks; i.v. injection=7 weeks).

Mice were sacrificed at various times, depending on tumor and metastasis growth, and an accurate necropsy was performed. To detect fluorescent metastases, whole mice and dissected organs were carefully examined using a Lighttools imaging system (Lighttools Research, Encinitas, CA, USA). Lungs were stained, then lungs and liver metastases were counted.

Brain was minced with scissors and passed through a 70 μ m cell strainer (Becton Dickinson) to obtain a homogeneous cell suspension. Bone marrow was flushed from both femurs in PBS and filtered through a 70 μ m strainer. Suspensions were observed at a fluorescent inverted microscope (Leitz, Leica Microsystem, Wetzlar, Germany). Metastatic cells in brain and bone marrow were quantified with immunofluorescence followed by cytofluorimetric analysis and by Real-time PCR.

To quantify the percentage of HER-2-positive MDA-MB-453-EGFP in brain and bone marrow, direct immunofluorescence and cytofluorimetric analysis were performed. A mouse monoclonal antibody against human HER-2 (clone Neu 24.7, Becton Dickinson) labeled with phycoerythrin was used. Fluorescence intensity was determined through flow cytometry (FACScan, Becton Dickinson).

To quantify the number of human cells in brain and bone marrow, Real-time PCR was performed. Genomic DNA was extracted with 10 mM Tris-HCl buffer pH 8.3 containing 50 mM KCl, 2.5 mM MgCl₂, 0.01% gelatin, 0.45% igepal, 0.45% tween 20 and 120 μ g/ml proteinase K. Samples were incubated overnight at 56°C and then 30 minutes at 95°C to inactivate the proteinase K. All reagents were purchased from Sigma-Aldrich. After genomic DNA quantification

by spectrophotometer, samples were diluted to a final concentration of 100 ng/ μ l and Real-time PCR was performed.

Primer and probe sequences were specific for a sequence of the α -satellite region of the human chromosome 17. They were derived from primers and probe sequences described in the study of Becker and colleagues (Becker *et al.*, 2002), with the sole alteration that the probe carried the non-fluorescent quencher dye TAMRA at the 3' end (Table V). A 100 ng aliquot of DNA per sample was amplified with 250 nM primers and 100 nM probe in a final volume of 25 μ l of TaqMan Universal PCR Master Mix (Applied Biosystems). After an initial denaturation step at 95°C for 10 minutes, 45 cycles of amplification were performed (95°C for 30 seconds and 60°C for 1 minute) using a 5700 Sequence Detection System (Applied Biosystems). Threshold cycle (Ct) values of samples were interpolated in a standard curve in each PCR. It was constructed adding scalar amounts of MDA-MB-453 human cells to cells from the mouse whole brain.

Table V. Primers and probe for the α -satellite region of the human chromosome 17 (modified from Becker *et al.*, 2002).

Primer	Sequence 5'-3'
forward	GGGATAATTTTCAGCTGACTAAACAG
reverse	AAACGTCCACTTGCAGATTCTAG
probe	6FAM-CACGTTTGAAACACTCTTTTTGCAGGATC-TAMRA

7.3.2 R-LM249 therapy and metastasis quantification

For the local therapy with R-LM249 of HER-2-positive breast cancer, MDA-MB-453 and BT-474 (10^7 cells) were injected subcutaneously (s.c.) in the right hind leg in 0.2 ml of PBS in Rag2^{-/-};Il2rg^{-/-} mice. Starting 3 days after cell injection, R-LM249 (2×10^7 or 10^8 pfu) was administered intratumorally (i.t.) once a week (for 10 weeks). Control mice received the i.t. injection of NaCl solution 0.9%. Tumor volumes were measured with caliper as described in section 7.1.

For the therapy of HER-2-positive metastatic breast cancer with R-LM249, MDA-MB-453 (2×10^6 cells) were injected i.v. in Rag2^{-/-};Il2rg^{-/-} mice. R-LM249 (10^8 pfu) was administered i.p. in 4 weekly injections. The incidence of

macroscopic metastases was determined at necropsy. Brain, lungs and ovarian metastases were quantified by Real-time PCR. Brain and lungs suspensions were obtained as previously described in section 7.3.1, while ovaries were not passed through the cell strainer. Extraction, quantification and amplification of genomic DNA was obtained as in section 7.3.1. In addition, a standard curve composed of serial amounts of MDA-MB-453 cells added to fixed amounts of mouse cells was included. Ct values were interpolated in the standard curves of each PCR, obtaining the relative amount of human to mouse cells in each sample (human DNA relative units).

For the induction of ovarian cancer peritoneal carcinomatosis, SK-OV-3 (2×10^6 cells) were injected i.p. in *nude* or *Rag2^{-/-};Il2rg^{-/-}* mice. Starting 3 days after cell administration, mice were treated with 2×10^7 or 10^8 pfu of R-LM249 once a week (for five weeks). The distribution of R-LM249 was detected using the Lighttools imaging system (Lighttools Research). Intraperitoneal metastases were collected at necropsy and weighed.

7.4 Immunoprevention

7.4.1 Vaccine schedules

HER-2-Cell vaccine was composed of human HER-2-positive ovarian cancer cells SK-OV-3 associated with exogenous administration of recombinant mouse IL-12, providing the specific (human HER-2) and the adjuvant (xenogeneic MHC and IL-12) stimuli. The proliferative ability of cells was blocked by mitomycin-C treatment ($120 \mu\text{g/ml}$, Sigma-Aldrich) for 45 minutes. Vaccine administration started when mice were 5-8 weeks old. Vaccination schedule was based on a 4-week cycle. In the first two weeks proliferation-blocked cells (2×10^6 in 0.4 ml of PBS) were injected i.p. biweekly, while in the third week IL-12 was administered i.p. daily (50 ng/mouse in the first cycle, 100 ng/mouse in the following cycles). IL-12 was diluted at a final concentration of $0.5 \mu\text{g/ml}$ in a solution of mouse serum albumin (MSA, Sigma-Aldrich) 0.01% in PBS. Control mice were untreated or treated with vehicle alone (PBS).

Materials and methods

HURT-DNA vaccine, derived from pVAX1 (Life Technologies), was developed by Quaglino and colleagues (Quaglino *et al.*, 2010) and consisted of the chimeric human/rat HER-2 plasmid, encoding for a chimeric protein in which the first 390 extracellular NH₂-terminal residues are from human HER-2 and the remaining extracellular and transmembrane residues from the rat homologue Neu. Large-scale production and purification of the plasmids were performed with EndoFree Plasmid Giga kits (QIAGEN, Valencia, CA, USA). Vaccine administration started when mice were 15-22 weeks old. Vaccination schedule was based on a 10-week schedule. In the first and third week anesthetized HER-2 mice received two intramuscular injections in the tibial muscles of 50 µg of plasmid diluted to a final volume of 40 µl (20 µl in each muscle) per mouse in final concentrations of 0.9% NaCl and 6 mg/ml polyglutamate. After the injections, electroporation of tibial muscles was performed by two square wave, 25-ms, 375 V/cm pulses generated with a T830 electroporator (BTX, San Diego, CA, USA).

In the second week and in weeks 4-10 no vaccination was performed. Control group was treated with pVax1 empty vector.

HER-2-Cell and HURT-DNA vaccinations were repeated for the entire life of mice. Mice were inspected weekly by palpation. Progressively growing masses larger than 0.3 cm in diameter were scored as tumors. Mice were killed when tumor diameter exceeded 1.7 cm.

7.4.2 ELISA (Enzyme-Linked ImmunoSorbent Assay)

For the quantification of anti-HER-2 antibodies, mice sera were collected periodically and stored frozen at -80°C. Thermo Scientific Immunoplate Nunc Maxisorp 96-well microplates (Cole-Parmer North America, Vernon Hills, CA, USA) were coated overnight with the extracellular domain of human HER-2 protein (1 µg/ml, 100 µl/well). The day after, blocking and washing of wells were performed and mice sera at 1:250 to 1:500 dilutions were added. After 2 hours of incubation and plate washing, secondary goat anti-mouse immunoglobulin G (IgG)-peroxidase conjugate antibody (1:12,000 dilution; Calbiochem, San Diego, CA, USA) was added. Then, 100 µl of 3,3',5,5'-tetramethylbenzidine peroxidase

substrate were added (Thermo Scientific). The reaction was stopped with 0.18 M sulfuric acid. The absorbance was measured at 450 and 620 nm with an ELISA microreader (Tecan Systems). In parallel, a standard curve (0.04-30ng/ml) with anti-human-HER-2 mouse monoclonal antibody clone 4D5 (Genentech) was run.

7.4.3 MLTC (Mixed Lymphocyte Tumor Cell Culture)

Evaluation of cell-mediated response after vaccination was assessed with MLTC. Mice were sacrificed after three vaccination cycles at least. Spleens were collected from control and vaccinated mice and passed through a 40 µm strainer (Falcon, Oxnard, USA) to obtain a homogeneous cell suspension. Total splenocytes were cultured for six days alone or in presence of proliferation-blocked HER-2-positive mouse (MAMBO 89) or human (SK-OV-3) cells (at a 10:1 lymphocyte/tumor cell ratio) in RPMI 1640 medium supplemented with 10% FBS and recombinant mouse IL-2 (20 U/ml). Next, culture supernatants were collected, and mouse IFN- γ was quantified by ELISA (R&D Systems, Minneapolis, MN, USA).

7.4.4 Indirect immunofluorescence and cytofluorimetric analysis

Ig isotypes analysis was performed using indirect immunofluorescence and cytofluorimetric analysis. MAMBO 89 and SK-OV-3 were incubated with sera from HURT-DNA vaccinated mice. Next, secondary fluorescein-conjugated monoclonal antibodies directed against Ig subclasses were added: anti-mouse IgG1 clone A85-1; anti-mouse IgG2a clone R19-15; anti-mouse IgG2b clone R12-3; anti-mouse IgG3 clone R4082; anti-mouse IgM clone R6-60.2. All of them were purchased from BD PharMingen. Total Ig were quantified using anti-mouse IgG AlexaFluor 488 (Life Technologies) as secondary antibody.

7.4.5 HER-2 inhibition and signaling

MAMBO 89 was treated for 5-60 minutes with a pool of sera from HURT-DNA vaccinated mice and cell pellet lysis was performed. Cell pellets were resuspended in Novagen PhosphoSafe Extraction Reagent (EMD Millipore, Milan, Italy) plus protease inhibitor cocktail 100X (Sigma-Aldrich) and incubated

Materials and methods

for 10 minutes at room temperature. To remove nuclei, samples were centrifugated for 15 minuti at 12,000 x g at 4°C. Protein concentration in the supernatants was determined by DC Protein Assay (Bio-Rad Laboratories) using BSA as standard protein and absorbance was measured at 750 nm with spectrophotometer (ULTROSPEC 1100 pro, BIOCHROM). Samples were resuspended in Laemli Sample Buffer 2x (Tris-HCl 62.5 mM pH 6.8, 25% glycerol, 2% SDS, 0.01% Bromophenol blue; Bio-Rad Laboratories) with 5% β -Mercaptoethanol (Sigma-Aldrich) and denatured at 100°C for 10 minutes.

For Western Blot, proteins were separated on a 8% polyacrylamide gel and then transferred to polyvinylidene difluoride membranes (Bio-Rad Laboratories). After blocking with PBS containing 0.1% tween 20 plus 5% non-fat dry milk for two hours at room temperature, membranes were incubated overnight at 4°C with primary antibodies diluted in blocking buffer. The following primary antibodies were used: anti-c-ErbB2/c-Neu (Ab3) mouse monoclonal antibody (3B5) (0.2 μ g/ml; Calbiochem/EMD Chemicals), anti-p-Neu (Tyr 1248)-R rabbit polyclonal antibody (0.2 μ g/ml sc-12352-R; Santa Cruz Biotechnology), anti-AKT rabbit polyclonal antibody (1:1,000 dilution; 9272), anti-phospho-AKT (Ser473) (D9E) XP rabbit monoclonal antibody (1:1,000 dilution; 4060) (all from Cell Signaling Technology) and anti-actin rabbit antibody (1 μ g/ml; Sigma Aldrich). Protein presence was detected through the incubation with the respective horseradish peroxidase-labeled secondary antibodies (Santa Cruz Biotechnology) followed by chemiluminescent reaction (LiteAbloplus, Euroclone, Milan, Italy).

7.4.6 Xenogeneic transplantation model and passive immunization

HER-2-positive cell line SK-OV-3 (2×10^6 cells) were injected i.p. in Rag2^{-/-};Il2rg^{-/-} mice. Mice were treated i.p. with 200 μ l of pooled sera from mock mice (untreated or vaccinated with pVAX1) or from mice vaccinated with HURT-DNA at day 1, 3, 7 and 14. Mice were killed 5 weeks after cell injection. An accurate necropsy was performed and tumor masses in the peritoneum were collected and weighed to quantify the therapeutic efficacy of anti-HER-2 antibodies.

8. Statistical analysis

Mantel-Haenszel's test, Student's t test, Fisher's exact test and non-parametric Wilcoxon's rank sum test were used to analyze and compare the data presented in this thesis.

RESULTS

1. F1 Model

The aim of this project was the definition of the contribute of wild-type full-length HER-2 and of the splice variant $\Delta 16$ to mammary HER-2 positive carcinogenesis. For this purpose, three mouse models that spontaneously develop mammary tumors were studied: a mouse model transgenic for the wild-type and full-length HER-2 (FVB-huHER-2 mice, here referred to as HER-2 model), a mouse model transgenic for $\Delta 16$ isoform (FVB-d16HER-2 mice, here referred to as $\Delta 16$ model) and a hybrid mouse model transgenic for both genes (F1 model). HER-2 mice were obtained from Genentech Inc., South San Francisco, CA, USA and were described for the first time by Finkle and colleagues in 2004 (Finkle *et al.*, 2004). $\Delta 16$ mice were developed and kindly provided by Prof. Augusto Amici, University of Camerino (Marchini *et al.*, 2011). F1 model was first and originally obtained in the Laboratory of Immunology and Biology of Metastasis by crossing HER-2 female mice and $\Delta 16$ male mice to better mirror the human situation, where these isoforms coexist in half HER-2-positive mammary tumors (Castiglioni *et al.*, 2006; Mitra *et al.*, 2009).

1.1 Carcinogenesis

Tumor onset in female mice carrying $\Delta 16$ was significantly faster than that of HER-2 mice (Mantel-Haenszel's test, $p < 0.001$) (Figure 1A). 100% of $\Delta 16$ and F1 mice developed tumors within 32 and 33 weeks of age, with a median tumor-free survival of 17 and 16.5 weeks respectively. Tumors in HER-2 mice started to be palpable much later, with a median tumor-free survival of 46 weeks and 12% of tumor-free mice after more than 100 weeks of age.

In addition to the earlier tumor onset, F1 and $\Delta 16$ mice showed a significantly higher number of mammary tumors per mouse if compared to HER-2 mice (Student's t test, $p < 0.01$ at least from the 4th week for F1 model, from the 5th week for $\Delta 16$ model) (Figure 1B). On average, at 26 weeks of age F1 model displayed 3.9 ± 0.6 tumors and $\Delta 16$ model 3.2 ± 0.4 tumors, while HER-2 mice were still tumor-free.

Then, the growth of first tumors arisen in the three models was evaluated

over-time (Figure 1C). Tumors of both models carrying $\Delta 16$ grew much more slowly than those of HER-2 model (Student's t test, $p < 0.05$ at least).

Taken together, data on tumor onset and multiplicity showed the aggressiveness of $\Delta 16$, if compared with HER-2, in fostering mammary carcinogenesis. Nevertheless, this anticipation seems not to be correlated with a faster tumor growth as it could be expected. In fact, looking at the kinetic of the first tumor volume, the presence of $\Delta 16$ slowed down tumor growth.

1.2 Metastasis

The autochthonous metastatic spread in the lungs of F1, $\Delta 16$ and HER-2 mice was evaluated (Figure 2). No significant differences among the models were observed: nearly half mice of each model developed metastases, with a median number of lung lesions of 1 for HER-2 and $\Delta 16$ models and of 0.5 for F1 model.

To better assess the metastatic contribution of each HER-2 isoform, we studied the metastatic ability of two cell lines previously stabilized *in vitro*: a cell line obtained from a tumor arisen in a HER-2 mouse in the Laboratory of Immunology and Biology of Metastasis (MAMBO 89) and a cell line derived from a $\Delta 16$ tumor (MILAN 6, obtained in the Laboratory of Dr. Serenella Pupa, Istituto Tumori, Milan, Italy). Table 1 shows the expression of plasmatic HER-2 protein and the expression of HER-2 and $\Delta 16$ transcripts in these cell lines (see section 1.3). MAMBO 89 and MILAN 6 were injected orthotopically (i.e. intramammary, i.ma) or intravenously (i.v.) in HER-2 mice (Table 2). After i.ma. injection of MAMBO 89, half mice developed spontaneous metastases in the lungs, with a median of 2 lesions. Lung metastases were observed in all mice treated with MILAN 6 (median=6). 80% of HER-2 mice that had received the i.v. injection of MAMBO 89 developed induced metastases (median=2), while MILAN 6 i.v. injection caused a metastatic spread in the lungs of all animals (median=58). Globally, a higher metastatic spread was detected after the injection of $\Delta 16$ -expressing MILAN 6.

Induced metastatic spread in the lungs was evaluated also in non-tolerant syngeneic FVB mice (Table 3). Both cell lines i.v. injected determined the

development of lung metastases in 100% of mice. The median number of lung lesions was 64 after the injection of MAMBO 89 and 211 after MILAN 6 administration.

1.3 HER-2 and $\Delta 16$ expression

Protein expression level of total HER-2 was evaluated in HER-2, $\Delta 16$ and F1 tumors by Cytofluorimetry (Fig. 3A). A primary antibody that binds both HER-2 isoforms was used, because specific antibodies for each isoform have not been developed yet. HER-2 tumors displayed a significantly higher HER-2 level than those of models carrying $\Delta 16$ (Student's t test, $p < 0.0001$). Tumors of HER-2 mice had a median fluorescence intensity of 698 (range 120-2054), while $\Delta 16$ and F1 tumors showed a median expression of HER-2 of 233 (range 107-422) and 221 (range 27-2053).

The expression/coexistence of HER-2 and $\Delta 16$ transcripts in 41 F1 tumors was analysed by Real-time PCR, using specific primers for each isoform (Figure 3B). 83% of F1 tumors (34/41) presented a high level of $\Delta 16$ and a low level of HER-2 as those of $\Delta 16$ mice, while only 5% of tumors (2/41) showed an expression of the isoforms that was comparable to that of HER-2 tumors (high HER-2, low $\Delta 16$). A high level of both isoforms (high HER-2, high $\Delta 16$) was observed in 7% of analysed tumors (3/41). Finally, 2 F1 tumors expressed a high level of HER-2 and an intermediate level of $\Delta 16$.

Analysis of HER-2 and $\Delta 16$ expression was extended to cell lines derived from the three models (Table 1). MAMBO 89 and MILAN 6 were previously described in section 1.2. Among cell lines that were obtained and *in vitro* stabilized from F1 tumors, 4 cell lines were chosen for drugs experiments (see section 2) because they were representative of the different expression levels of HER-2 and $\Delta 16$ observed in F1 tumors. One of these cell lines (143-VS) showed a high expression of HER-2 and a low expression of $\Delta 16$, while an opposite expression profile was observed in 156-VS and 156-IS (high $\Delta 16$, low HER-2). The last chosen cell line was representative of the group of F1 tumors with a high expression of both isoforms.

2. Anti-cancer strategies against HER-2

The main aim of this project was the evaluation of innovative anti-cancer strategies against HER-2-positive breast cancer. This kind of cancer has a bad prognosis if compared with other types of breast cancer. In addition, despite the therapeutic revolution after the development of Trastuzumab, nearly 70% of patients with metastatic breast cancer have intrinsic resistance to this HER-2 targeted therapy and almost all of them become resistant over-time (Brufsky, 2014). In light of that, new and efficacious treatments targeting HER-2, its isoforms and its signaling pathways are required.

2.1 Drugs

The therapeutic efficacy of already clinically approved or under experimentation drugs was studied *in vitro* and *in vivo* in HER-2-positive breast cancer models. Susceptibility to the following drugs was analysed:

- Trastuzumab (recombinant humanized monoclonal antibody that target the extracellular domain of HER-2);
- Lapatinib (reversible kinase inhibitor that blocks the catalytic domain of HER-2 and EGFR);
- Dasatinib (kinase inhibitor directed against Src kinase);
- NVP-BKM120 (PI3K inhibitor);
- UO126 (dual MEK1/MEK2 inhibitor).

2.1.1 Trastuzumab

In vitro sensitivity to Trastuzumab (10 µg/ml) was evaluated in cell lines derived from HER-2, Δ16 and F1 mice as percentage of grown colonies compared to the control in a 3-D culture (0.33% soft agar containing the drug) (Figure 4A). F1 cell lines with a high level of Δ16 were the most sensitive to Trastuzumab (156-VS=24% growth over control; 156-IS=46%), followed by MILAN 6 (57%). All cell lines with high HER-2 (MAMBO 89, 143-VS and 302-IVD) were resistant to Trastuzumab.

The efficacy of Trastuzumab on high Δ16 tumors was confirmed *in vivo* on

Results

a F1 tumor model (Figure 4B-C). Fragments of a F1-derived mammary tumor with a high expression of $\Delta 16$ were implanted in immunocompetent non-tolerant syngeneic mice (FVB mice). After 24 weeks of intraperitoneal (i.p.) treatment with Trastuzumab (4 mg/kg), tumor growth was not detectable in any treated mouse, while in 80% of untreated mice the tumor had significantly grown (Fisher's exact test, $p < 0.05$).

Therapeutic effectiveness of the humanized monoclonal antibody was also studied in a metastatic setting (Table 4). To better define the roles of HER-2 and $\Delta 16$ in conditioning the drug response, MAMBO 89 and MILAN 6 were injected i.v. in FVB mice. The i.p. treatment with the drug (4 mg/kg) highly inhibited the growth of induced metastases expressing $\Delta 16$ (Student's t test, $p < 0.001$). The inhibition was evident as reduction of lung weight (Table 4A) and as decreased median number of lung metastases (Table 4B). The treatment was significantly effective also in reducing HER-2 metastases, but in a lower extent (Student's t test, $p < 0.05$).

2.1.2 Lapatinib

Lapatinib (1 μM) effectively reduced the number of grown colonies of all cell lines analysed in 3-D experiments (Figure 5A). However, cell lines expressing $\Delta 16$ were more sensitive to Lapatinib than those expressing HER-2 alone (Student's t test, $p < 0.05$). In fact, in MILAN 6, 302-IVD, 156-VS and 156-IS a complete growth inhibition was observed, while in MAMBO 89 and 143-VS the percentages of grown colonies were 64% and 33% respectively.

The activity of Lapatinib was tested also in combination with Trastuzumab (Figure 5B). The rationale of combining these anti-HER-2 drugs is the fact that they target different portions of HER-2 protein: Lapatinib is directed against the intracellular domain of HER-2, while Trastuzumab targets the extracellular domain of the protein. No additional inhibition was found comparing the effect of the combination Lapatinib-Trastuzumab with that of Lapatinib alone.

2.1.3 Dasatinib

Sensitivity to Dasatinib (1 μM) alone or in combination with anti-HER-2

Results

drugs (Trastuzumab and Lapatinib) was studied *in vitro* and *in vivo*.

In 3-D culture all cell lines derived from HER-2, $\Delta 16$ and F1 models were sensitive to Dasatinib, but the effect of treatment was significantly higher in cell lines carrying $\Delta 16$ gene (MILAN 6, 143-VS and 302-IVD) than in MAMBO 89 (Student's t test, $p < 0.001$) (Figure 6). In detail, after treatment with the drug the percentage of growth in MAMBO 89 was 53% , while in 302-IVD grown colonies were only 17%. MILAN 6 and 143-VS were completely inhibited by Dasatinib.

Nearly the same significant differences among cell lines were obtained combining Dasatinib with Lapatinib or Trastuzumab (Student's t test, $p < 0.01$ at least). The triple combination (Dasatinib+Lapatinib+Trastuzumab) confirmed what previously described (Student's t test, $p < 0.05$ at least).

Focusing on the different treatments in each cell line, in MILAN 6 and 143-VS no additional effect was seen after combining drugs with Dasatinib compared to Dasatinib alone. In 302-IVD all combinations were significantly more effective than Dasatinib alone (Student's t test, $p < 0.05$ at least). In MAMBO 89, additional effects were observed combining Dasatinib with Lapatinib and in the triple combination of drugs (Student's t test, $p < 0.001$).

As partially described before for Trastuzumab (see section 2.1.1), inhibition of HER-2 and $\Delta 16$ metastases by Trastuzumab (4 mg/kg) and/or Dasatinib (50 mg/kg) was evaluated (Table 4). Therapeutic efficacy of Trastuzumab was already discussed (section 2.1.1). *In vitro* efficacy of Dasatinib was not confirmed *in vivo*. Treatment with Dasatinib did not reduce the quantity of lung metastases expressed both as lung weight (Table 4A) and as number of counted metastases (Table 4B). Focusing on the combination of Dasatinib with Trastuzumab, a significant additional effect of Dasatinib in the reduction of $\Delta 16$ metastases was noted if compared with the efficacy of Trastuzumab alone (Student's t test, $p < 0.01$).

2.1.4 NVP-BKM120

In vitro sensitivity to NVP-BKM120 was studied in cell lines derived from HER-2, $\Delta 16$ and F1 tumors. All cell lines in 3-D culture showed a 100% growth inhibition when treated with NVP-BKM120 at the concentration of 1 μM . After

Results

treatment with a lower concentration (0.1 μM), only MAMBO 89, 156-VS and 156-IS were sensitive to NVP-BKM120 (Figure 7).

Brain metastases have a high incidence in patients with HER-2-positive breast cancer. Hence, due to the demonstrated ability of NVP-BKM120 to penetrate the blood-brain barrier, drug's activity on human HER-2-positive metastases in the brain and other organs was tested (Nanni *et al.*, 2012). For this purpose a mouse model of multiorgan metastatic dissemination, previously developed in the Laboratory of Immunology and Biology of Metastasis, was employed. It consists of the orthotopic (i.ma.) or i.v. administration of human HER-2-positive cell lines in immunodeficient Rag2^{-/-};Il2rg^{-/-} mice. These mice have a dramatically impaired immune system because of the absence of mature T, B and NK cells. The metastatic pattern in Rag2^{-/-};Il2rg^{-/-} mice well reproduces the multiorgan metastatic situation displayed by advanced HER-2-positive breast cancer patients. In particular, the high incidence of brain metastases makes this model the perfect target for new therapeutic approaches. Human HER-2 positive breast cancer cell line MDA-MB-453 was injected i.ma. or i.v. in Rag2^{-/-};Il2rg^{-/-} mice. To better detect and quantify the metastatic burden in mice, MDA-MB-453 was transfected with Enhanced Green Fluorescent Protein (EGFP). Figure 8 shows EGFP and HER-2 expression profiles of this cell line at cytofluorimetric analysis. Both routes (i.ma, 10⁷ cells; i.v., 2x10⁶ cells) determined a wide multiorgan metastatic pattern. Starting seven days (i.ma.) or one day (i.v.) after cell injection, mice were treated per os with NVP-BKM120 (50 mg/kg) for 7-12 weeks. The therapeutic activity of the drug was evident in multiple organs, where a sizeable proportion of mice were noted to be metastasis-free (Figure 9). In the group of mice injected i.v., a strong and significant reduction in the incidence of metastases was observed in brain, femoral bone marrow and liver (Fisher's exact test, p<0.05 at least). Figure 10 shows representative pictures of the therapeutic effect of NVP-BKM120 in brain and lungs after exposure of organs to the fluorescent Lighttools imaging system.

Reduction of brain macro-metastases at necropsy was confirmed after quantification of induced metastatic cells by Real-time PCR and Cytofluorimetry. These technologies were specifically developed to detect and quantify micro-

Results

metastases not visible at fluorescent observation. Real-time was performed to measure the number of human cells using primers and probe specific for a α -satellite region on the human chromosome 17, while Cytofluorimetry was able to quantify the percentage of HER-2-positive cells in brain. Both analyses confirmed the strong reduction in the amount of brain metastases (more than 90%) after treatment with NVP-BKM120 (Student's t test, $p < 0.05$) (Figure 11A-B). The metastatic pattern was quantified by Cytofluorimetry also in femoral bone marrow samples. In the group of mice treated with the drug, a 71% metastatic reduction was observed (Figure 11C). Quantification by visual count showed a significant decreased number of involved bones per mouse after treatment (inhibition of 67%) (Student's t test, $p < 0.05$) (Figure 11 D). A reduction was observed also in kidney and adrenal glands (Figure 11E). Globally, NVP-BKM120 was able to significantly reduce the number of metastatic sites per mouse, with an inhibition percentage of 54% (Student's t test, $p < 0.05$) (Figure 11F).

2.1.5 MEK inhibition

The inhibition of MEK (Ras/Raf/MEK/ERK cascade) was studied in collaboration with the Laboratory of Prof. Yosef Yarden (Department of Biological Regulation, Weizmann Institute of Science, Rehovot, Israel). The aim of the study was the detection of modifications at protein level of EGFR family receptors and their intracellular effectors after inhibiting MEK by siRNA or by treatment with UO126. A time course with Epidermal Growth Factor (EGF) was included in all the experiments.

To detect possible differences between non-neoplastic and cancer cells, the study was conducted on a non-tumorigenic cell line (MCF-10A, derived from epithelial breast tissue of a woman with fibrocystic disease) and on a HER-2-positive breast cancer cell line (BT-474).

Knockdown of MEK was achieved by transfecting siRNA oligonucleotides against MEK1, MEK2 or both isoforms simultaneously in these cell lines. The main result after silencing MEK was an increase in HER-2 activation both in non-neoplastic and in HER-2-positive breast cancer cells if compared with controls (Figure 12). In detail, an increase in p-HER-2 expression

Results

was observed after transfection of MCF-10A with siRNA MEK2 and with the combination siRNA MEK1 + siRNA MEK2 (Figure 12A). An higher amount of activated HER-2 was detected in BT-474 lysates after combining siRNA MEK1 and siRNA MEK2 at the same time (Figure 12B). The similar function of MEK1 and MEK2 may explain the fact that only the inhibition of both isoforms was able to effectively increase p-HER-2 expression in both cell lines. Furthermore, the absence of increase in activated HER-2 after knocking down MEK2 alone in BT-474 could be caused by the more active signaling cascades in cancer cells if compared with non-neoplastic cells.

Similarly to transfection, treatment of cell lines with UO126 increased HER-2 activation (Figure 13). Both cell lines, after dual MEK1/MEK2 inhibition, displayed a higher expression of p-HER-2 compared to controls. In addition to that, an increase in p-MEK1/2 was detected in cells treated for 1 hour with the drug if compared with control cells. UO126 inhibition of MEK1/MEK2 is noncompetitive with respect to ATP (Duncia *et al.*, 1998), allowing MEK activation but blocking MEK-mediated ERK activation.

2.2 Oncolytic virus R-LM249

Oncolytic virotherapy exploits the ability of viruses to target and kill cells. HER-2 overexpression on breast cancer cells makes HER-2-positive mammary tumor the perfect target for anti-HER-2 viruses. In 2009 the group directed by Prof. Campadelli-Fiume (University of Bologna) retargeted a herpes simplex virus 1 to HER-2, obtaining R-LM249 (Menotti *et al.*, 2009). Susceptibility to this oncolytic virus was evaluated on breast and ovarian HER-2-positive models in the Laboratory of Immunology and Biology of Metastasis (Nanni *et al.*, 2013).

2.2.1 *In vitro* sensitivity

Cytotoxicity to R-LM249 was firstly evaluated *in vitro* on three HER-2-positive cancer cell lines: MDA-MB-453 and BT-474, that are breast cancer cell lines, and SK-OV-3, that is an ovary cancer cell line. As negative control, MDA-MB-231 (low/negative HER-2 expression) was included in the experiment. After six days of treatment, all cell lines with high HER-2 expression were killed by R-

Results

LM249 (Figure 14A). Only a residual 10% viability was detected in BT-474 and SK-OV-3, but when these cells were cultured again they were unable to proliferate. R-LM249 effectiveness was compared to that of Trastuzumab (Figure 14B). Among HER-2-positive cell lines, only BT-474 was sensitive to the 72 hours-treatment with the monoclonal antibody, while MDA-MB-453 and SK-OV-3 displayed resistance to the drug. Therefore R-LM249, but not Trastuzumab, was able to target and kill all HER-2-positive cell lines analysed. These data are even more relevant if we consider the high incidence of patients with Trastuzumab-resistant HER-2-positive tumors.

2.2.2 Therapy of localized HER-2-positive breast cancer

After demonstrating the cytotoxic activity of R-LM249 on BT-474 and MDA-MB-453, *in vivo* therapy of localized disease was assessed after the subcutaneous (s.c.) injection of these cell lines (10^7 cells) in Rag2^{-/-};Il2rg^{-/-} mice (Figure 15). Tumor growth was inhibited by both chosen doses of R-LM249 (2×10^7 and 10^8 pfu). In detail, in groups of BT-474-injected mice intratumoral administration of the retargeted virus strongly reduced tumor volume (Student's t test, $p < 0.05$ at least from day 20 at the lower dose, from day 13 at the higher dose of R-LM249) (Figure 15A). 59 days after challenge with BT-474, the control group reached a mean tumor volume of $2.6 \pm 0.2 \text{ cm}^3$, while mice treated with 2×10^7 pfu of R-LM249 showed a mean tumor volume of $0.5 \pm 0.2 \text{ cm}^3$. The higher dose administration of the oncolytic virus almost avoided tumor growth ($0.08 \pm 0.05 \text{ cm}^3$). Also the s.c. injection of MDA-MB-453 significantly reduced tumor volume of R-LM249-treated mice (Student's t test, $p < 0.05$ at least from day 13 for both doses) (Figure 15B). In these mice the mean tumor volumes at 59 days from challenge with cells were $0.2 \pm 0.1 \text{ cm}^3$ (2×10^7 pfu) and $0.1 \pm 0.05 \text{ cm}^3$ (10^8 pfu). Focusing on mice survival (Figure 15C-D), R-LM249 was able to significantly prolong mice lifetime (Mantel-Haenszel's test, $p < 0.01$ for both cell lines and both doses of virus). After BT-474 challenge and 10 weeks of virus administration, treated mice had a median survival time of 139 (lower dose) and 146 (higher dose) days, while control mice had a much shorter life expectancy (73 days after cell injection) (Figure 15C). For MDA-MB-453 groups, mice receiving

Results

the treatment survived nearly a month more than mice treated with vehicle (median survival days: Vehicle=98, R-LM249 2×10^7 =125, R-LM249 10^8 =132) (Figure 15D). Furthermore, at more than 150 days after challenge with cells, 20% of treated mice were still alive (apart from the group injected with BT-474 and treated with 2×10^7 pfu of R-LM249).

2.2.3 Therapy of disseminated HER-2-positive breast cancer

To mimic the wide metastatic pattern in clinic, the multiorgan metastatic model of breast cancer (see section 2.1.4) was employed. MDA-MB-453 was preferred to BT-474 for its Trastuzumab resistance, as previously shown (see section 2.2.1). 2×10^6 cells were injected i.v. in Rag2^{-/-};Il2rg^{-/-} mice. The i.p. treatment for 4 weeks with R-LM249 (10^8 pfu) determined the complete absence of ovarian macro-metastases (Fisher's exact test, $p < 0.0001$) (Figure 16A). On the contrary, in all mice receiving the PBS-treatment ovarian lesions were found, showing the high efficacy of R-LM249 in inhibiting peritoneal HER-2 positive macroscopic metastases. These data were confirmed after quantification of human cells in mice ovaries by Real-time PCR (Figure 16B). As already described, this molecular assay consists of the amplification of α -satellite sequences on human chromosome 17 if human metastatic cells are present. Confirming what detected at necropsy, the micro-metastatic burden was widely reduced by the administration of the oncolytic virus (Student's t and non-parametric Wilcoxon's rank sum tests, $p < 0.0005$). R-LM249 activity was not experimented only on peritoneal metastases, but also on brain lesions, often found in patients with HER-2-positive breast cancer and connected with Trastuzumab incapability to cross the blood-brain barrier. The oncolytic virus was effectively able to target and destroy HER-2-positive cells in the brain (Figure 16C-D). MDA-MB-453 i.v. injected in Rag2^{-/-};Il2rg^{-/-} mice gave rise to brain metastases in 78% of non-treated animals, while after administration of R-LM249 only 30% of mice presented brain metastases (Figure 16C). A significant reduction was observed by Real-time quantification: only 1.9 ± 0.8 human DNA relative units were detected in the brain of treated mice, while a metastatic brain burden of 4.1 ± 1.3 human DNA relative units was quantified in the control group (Wilcoxon's non-parametric rank sum

Results

test, $p < 0.05$) (Figure 16D). These data highlight the potential high therapeutic ability of R-LM249 to fight brain metastases, that is currently the most problematic challenge in HER-2-positive breast cancer patients' treatment.

Despite the high effectiveness on ovarian and brain metastases, R-LM249 was not able to reduce the incidence of lung metastases (Figure 16E). Furthermore, only a small reduction of human cells in the lungs of treated mice was found after molecular quantification (Figure 16F).

2.2.4 Therapy of disseminated HER-2-positive ovarian cancer

Intraperitoneal metastases are commonly found in patients with disseminated HER-2-positive ovarian cancer. For this reason, two models of peritoneal carcinosis were developed in the Laboratory of Immunology and Biology of Metastasis. The first model consisted of HER-2-positive ovarian cancer cell line SK-OV-3 injected i.p. (2×10^6 cells) in athymic *nude* mice, while in the second one $Rag2^{-/-}; Il2rg^{-/-}$ mice were employed.

Figure 17 shows the therapeutic ability of R-LM249 i.p. administered in *nude* mice (2×10^7 pfu) after the i.p. challenge with SK-OV-3. Mice lifetime was widely prolonged by the treatment, with a median survival time that moved from 103 (control group) to 440 days (R-LM249 group) (Mantel-Haenszel's test, $p < 0.05$). Due to the slow growth of cells in *nude* mice, the experiment required a long observation period and most of treated mice died not because of peritoneal metastases, but when they reached their expected lifetime.

To better assess the actual efficacy of R-LM249 on disseminated ovarian cancer, the second model that employ $Rag2^{-/-}; Il2rg^{-/-}$ mice was developed (Figure 18). After i.p. injection of SK-OV-3, all control mice rapidly developed peritoneal carcinosis, allowing a precise quantification of metastases after only six weeks from challenge with cells. Furthermore, in most of control animals ascitic fluid in the peritoneum was present (71%). Hence, $Rag2^{-/-}; Il2rg^{-/-}$ mice confirmed their superiority in miming the clinic situation of patients if compared with *nude* mice. The i.p. administration of R-LM249 (10^8 pfu) started 3 days after cells injection and determined a 40% reduction in the incidence of peritoneal masses (Figure 18A). A high and significant decrease in tumor burden in the peritoneum was

Results

observed (Figure 18B): the mean cumulative weight of peritoneal metastases in the group treated with the oncolytic virus was 60 ± 38 mg, much lighter than that of control group (1164 ± 284 mg) (Student's t test, $p<0.01$). In mice treated with the virus peritoneal ascites was not found (Fisher's exact test, $p<0.05$) (Figure 18C).

To underline the efficacy of R-LM249 on peritoneal metastases, representative pictures of control and treated mice were taken at necropsy (Figure 19A-B). R-LM249 was engineered by Prof. Campadelli-Fiume and colleagues with the insertion of EGFP sequence, allowing the monitoring of intraperitoneal spread of the virus. With this purpose, SK-OV-3 was injected i.p. in $Rag2^{-/-};Il2rg^{-/-}$ mice and after 9 weeks mice were treated with the virus. R-LM249 was able to target and reach all visible human HER-2-positive intraperitoneal masses, while surrounding human HER-2-negative tissue was green fluorescence-free (Figure 19C).

2.3 Anti-HER-2 vaccines

HER-2 is a tumor-associated antigen (oncoantigen) and an ideal immunotherapeutic target (Lollini *et al.*, 2006). Therefore, among investigational options for HER-2-positive breast cancer, anti-HER-2 vaccines are currently studied. The immunopreventive activity of two vaccines was assessed in the Laboratory of Immunology and Biology of Metastasis: a xenogeneic whole-cell vaccine (called HER-2-Cell vaccine) and a DNA human/rat chimeric vaccine (called HURT-DNA vaccine) (De Giovanni *et al.*, 2014).

2.3.1 Immunoprevention of HER-2-positive breast cancer

Both vaccines successfully delayed tumor onset in immunocompetent HER-2 mice (Mantel-Haenszel's test, $p<0.05$) (Figure 20A). At 60 weeks of age, 57% of mice vaccinated with HER-2-Cell and 64% of mice that were receiving HURT-DNA were still tumor-free, while 87% of mock animals had already developed at least a mammary tumor. In HURT-DNA group this percentage was still stable after more than 80 weeks of age.

Vaccinations were able to postpone not only tumor onset, but also the death of mice with tumors. Median latency from tumor onset to death was 16 and

Results

14.5 weeks for HER-2-Cell and HURT-DNA vaccinated mice, while this range of time was nearly a month shorter for not vaccinated mice (11.5 weeks).

Focusing on tumor multiplicity, at 70 weeks of age the mean number of tumors per mouse was 2.4 ± 0.3 for mock group, whereas only 0.4 ± 0.3 and 1.0 ± 0.4 tumors were arisen in HER-2-Cell and HURT-DNA groups respectively (Figure 20B). Hence, the number of tumors per mouse was significantly reduced by vaccinations (Student's t test, $p < 0.05$ at least from the 50th week in HER-2-Cell vaccinated group and from the 54th week for HURT-DNA group). Globally, HER-2-Cell and HURT-DNA vaccines were both able to delay tumor onset, prolong life expectancy and reduce the growth of multiple tumors in HER-2 mice.

2.3.2 Immune responses to anti-HER-2 vaccines

To understand the effect of vaccinations on the immune system, sera from mock and vaccinated groups were collected at different times and analysed by ELISA (Figure 21A). Both vaccines were able to break the tolerance towards HER-2 and induce the humoral response in HER-2 mice. However, HURT-DNA vaccine caused a stably higher production of anti-HER-2 antibodies if compared with HER-2-Cell vaccine (Wilcoxon's non-parametric test, $p < 0.05$ at least at 4th, 24th and 40th weeks of treatment). Specifically, at 4 and 12 weeks of vaccination the mean concentration of anti-HER-2 antibodies in sera of HURT-DNA group was nearly 20 $\mu\text{g/ml}$ (week 4, $26.1 \pm 22.4 \mu\text{g/ml}$; week 12, $19.0 \pm 14.5 \mu\text{g/ml}$). At the following time points the antibodies level increased even more, reaching a mean concentration of 57.4 ± 23.0 and $59.2 \pm 41.8 \mu\text{g/ml}$ at 24 and 40 weeks respectively. Focusing on the humoral response elicited by HER-2-Cell vaccine, anti-HER-2 antibodies reached the concentration peak of $4.5 \pm 1.1 \mu\text{g/ml}$ after 12 weeks of vaccination, while nearly 1 $\mu\text{g/ml}$ of anti-HER-2 antibodies was detected in sera of vaccinated mice at 4th, 24th and 40th weeks of treatment (week 4, $1.4 \pm 0.5 \mu\text{g/ml}$; week 24, $1.1 \pm 0.4 \mu\text{g/ml}$; week 40, $0.9 \pm 0.3 \mu\text{g/ml}$).

Cell-mediated immune response was evaluated as murine Interferon- γ (IFN- γ) production by spleen cells of control and vaccinated mice (Figure 21B). Spleen cells were collected and cultured for six days alone (spontaneous release) or in co-culture with two HER-2-positive cell lines to foster the cytokine

Results

production (MAMBO 89 and SK-OV-3). MAMBO 89 derived, as previously described (see section 1.2), from a mammary tumor of a HER-2 mouse and was employed as syngeneic cell line (syn-HER-2). SK-OV-3 (xenogeneic, xeno-HER-2) was the main component of HER-2-Cell vaccine. After culture, supernatants were collected and ELISA was performed. Spleen cells of HER-2-Cell vaccinated mice spontaneously produced IFN- γ . The presence of MAMBO 89 determined an increase in the amount of this cytokine, and a high peak level was detected after incubation of spleen cells with SK-OV-3. The release of IFN- γ by splenocytes from HURT-DNA vaccinated mice was comparable to that of mock group: no production was observed after co-culture with syngeneic cells, while in the supernatants of spleen cells and SK-OV-3 co-culture a low production was detected.

Overall, these data suggest that after HURT-DNA vaccination, unlike cell vaccination, the high humoral response was sufficient to prevent and delay tumor onset in HER-2 mice.

2.3.3 Anti-HER-2 antibodies

To further study the effectiveness of anti-HER-2 antibodies, we chose to focus on sera from HURT-DNA vaccinated mice because of the high humoral response in this group of animals and for the absence of xenogeneic stimuli that could affect the response. With this purpose, *in vitro* and *in vivo* experiments were performed to characterize anti-HER-2 antibodies.

First, isotypes expressed in sera of HURT-DNA vaccinated animals were evaluated by indirect immunofluorescence (Figure 22A). MAMBO 89 and SK-OV-3 were employed as substrate for anti-HER-2 antibodies. Among expressed isotypes, IgG1, IgG2a and IgG2b were well-represented and they were able to recognize both syngeneic and xenogeneic cell lines.

HER-2 signaling activation was also evaluated (Figure 22B). MAMBO 89 was incubated for 5 to 60 minutes with HURT-DNA sera and the expression of HER-2, AKT and the corresponding phosphorylated proteins was evaluated by Western Blot. An inhibitory effect mediated by antibodies was detected on analysed proteins. In detail, after 1 hour of treatment, anti-HER-2 antibodies,

Results

compared with control mice sera, determined in cells a 57% decrease in the expression of activated p-HER-2 and a reduction was observed also on plasmatic HER-2 (38%). Focusing on the cytoplasmatic signaling effector AKT, in cells treated with antibodies the lowest expression was observed after 30 minutes of treatment (20%), while the most dramatic reduction in activated AKT was detected after 5 minutes of treatment with anti-HER-2 antibodies (36%).

To assess the *in vivo* ability of anti-HER-2 antibodies to target and delay HER-2 carcinosis, the peritoneal metastatic model already described in section 2.2.4 was employed. Immunodeficient mice were chosen to avoid any possible additive immunologic anti-tumor activity by the host, in order to evaluate the real contribution of anti-HER-2 antibodies alone. SK-OV-3 was injected in Rag2^{-/-};Il2rg^{-/-} mice and animals were treated for two weeks with pools of sera from mock- or HURT-DNA-vaccinated mice. After 5 weeks from challenge, total tumor weight in each mouse was evaluated (Figure 23). Mice treated with HURT-DNA group sera displayed a median tumor weight of 42 mg, much lower than that of animals treated with sera from mock-vaccinated mice (297 mg) (Wilcoxon's non-parametric test, p=0.05). Hence, the passive immunization by anti-HER-2 antibodies produced by HURT-DNA vaccinated mice was effective in inhibiting HER-2-positive tumor growth in immunodeficient Rag2^{-/-};Il2rg^{-/-}, despite the absence of most cellular and cytokine responses.

FIGURES AND TABLES

Table 1. HER-2 and $\Delta 16$ expression in cell lines derived from HER-2, $\Delta 16$ and F1 tumors. MAMBO 89 derived from a HER-2 tumor; 143-VS, 302-IVD, 156-VS and 156-IS derived from tumors arisen in F1 mice. All these cell lines were stabilized *in vitro* in the Laboratory of Immunology and Biology of Metastasis. MILAN 6 was obtained from a $\Delta 16$ tumor in the Laboratory of Dr. Serenella Pupa. The human HER-2-positive breast cancer cell line BT-474 was included in this analysis. Transcripts expression of HER-2 and $\Delta 16$ was calculated as $\Delta Ct = Ct_{HER-2/\Delta 16} - Ct_{GAPDH}$. Abbreviations: MFI, Median Fluorescence Intensity.

Cell line	Transcripts expression		Protein expression
	ΔCt HER2	ΔCt $\Delta 16$	Total HER2 (MFI)
MAMBO 89	0.7	17.4	1592
MILAN 6	19.7	1.4	301
143-VS	0.7	13.0	284
302-IVD	-2.1	-2.7	1433
156-VS	11.6	-0.2	673
156-IS	11.4	0.8	392
BT-474	0.1	3.9	999

Table 2. Spontaneous and induced metastatic spread in HER-2 mice.

MAMBO 89 and MILAN 6 were injected intramammary (i.ma., spontaneous metastases) and intravenously (i.v., induced metastases) in HER-2 mice.

Cell line	Route	Dose	Median week after cell injection	Lung metastases		
				Incidence (%)	Median	Range
MAMBO 89	i.ma.	10 ⁶	14	1/2 (50%)	2	0-4
MILAN 6	i.ma.	10 ⁶	13	5/5 (100%)	6	1-16
MAMBO 89	i.v.	10 ⁵	18	4/5 (80%)	2	0-4
MILAN 6	i.v.	10 ⁵	13	5/5 (100%)	58	39-101

Table 3. Induced metastatic spread in FVB non-transgenic mice.

MAMBO 89 and MILAN 6 were injected intravenously (i.v) in immunocompetent non-tolerant syngeneic mice (FVB mice).

Cell line	Route	Dose	Median week after cell injection	Lung metastases		
				Incidence (%)	Median	Range
MAMBO 89	i.v.	10 ⁶	13	8/8 (100%)	64	4-223
MILAN 6	i.v.	10 ⁵	11	8/8 (100%)	211	104-257

Table 4. Treatment of induced HER-2 and Δ16 metastases with Trastuzumab and/or Dasatinib. MAMBO 89 (10^6 cells) and MILAN 6 (10^5 cells) were injected i.v. in immunocompetent non-tolerant syngeneic mice (FVB mice). Mice were treated with Trastuzumab (4 mg/kg, i.p.) and/or with Dasatinib (50 mg/kg, per os). **(A)** Weight of the lungs minus the weight of metastases-free lungs. Median lung weight and range are shown. Statistical significances (Student's t test): for MILAN 6, Control vs Trastuzumab/ Trastuzumab+Dasatinib $p < 0.001$. **(B)** Number of lung metastases. Incidence, median and range are shown. Statistical significances (Student's t test): MAMBO 89, Control vs Trastuzumab/ Trastuzumab+Dasatinib $p < 0.05$; MILAN 6, Control vs Trastuzumab/ Trastuzumab+Dasatinib $p < 0.001$, Trastuzumab vs Trastuzumab+Dasatinib $p < 0.01$.

A

Treatment	Lung weight (mg)	
	MAMBO 89	MILAN 6
Control	62 ± 23	121 ± 15
Trastuzumab	50 ± 9	7 ± 7
Dasatinib	97 ± 33	138 ± 31
Trast+Das	63 ± 14	1 ± 8

B

Treatment	MAMBO 89			MILAN 6		
	Incidence	Median	Range	Incidence	Median	Range
Control	8/8	64	4-223	8/8	211	104-257
Trastuzumab	7/8	16	0-43	7/8	24	0-49
Dasatinib	7/8	90	0-169	8/8	172	65-256
Trast+Das	7/8	22	0-61	6/8	3	0-11

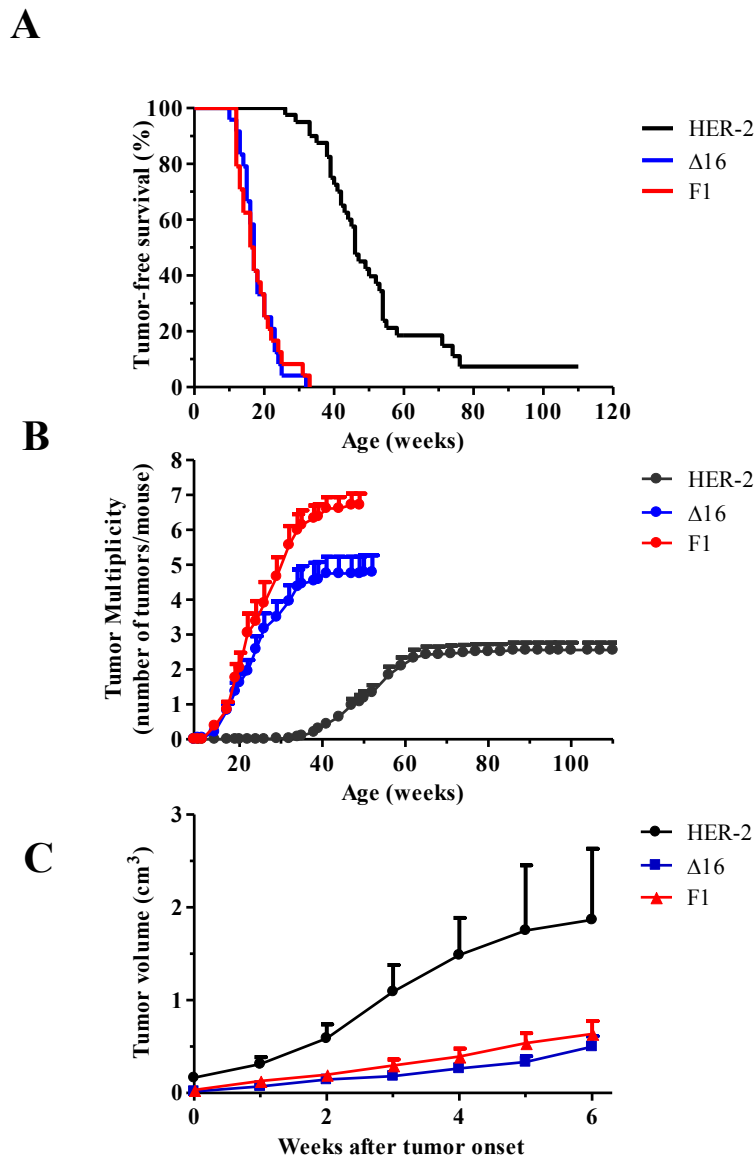


Figure 1. Spontaneous mammary carcinogenesis in F1 model compared to HER-2 and $\Delta 16$ models. (A) Kaplan-Meier analysis. HER-2 mice n=40, $\Delta 16$ mice n=24, F1 mice n=24. Incidence of mammary tumors in mice: HER-2 model 35/40 (88%); $\Delta 16$ model 24/24 (100%); F1 model 24/24 (100%). Statistical significances (Mantel-Haenszel's test): HER-2 vs $\Delta 16$ and HER-2 vs F1 $p < 0.001$. **(B)** Tumor multiplicity. Each point represents the mean number of tumors/mouse \pm standard error at death. HER-2 mice n=39, $\Delta 16$ mice n=24, F1 mice n=21. Statistical significances (Student's t test): HER-2 vs $\Delta 16$ $p < 0.01$ at least from the 5th week; HER-2 vs F1 $p < 0.01$ at least from the 4th week; F1 vs $\Delta 16$ vs $p < 0.05$ at least from the 22nd week. **(C)** Kinetic of the growth of the first tumor. Each point

Figures and tables

is the mean tumor volume \pm standard error. HER-2 tumors n=23, Δ 16 tumors n=30, F1 tumors n=23. Statistical significances (Student's t test): HER-2 vs Δ 16 p< 0.05 at least; HER-2 vs F1 p< 0.05 at least between 1st and 5th weeks.

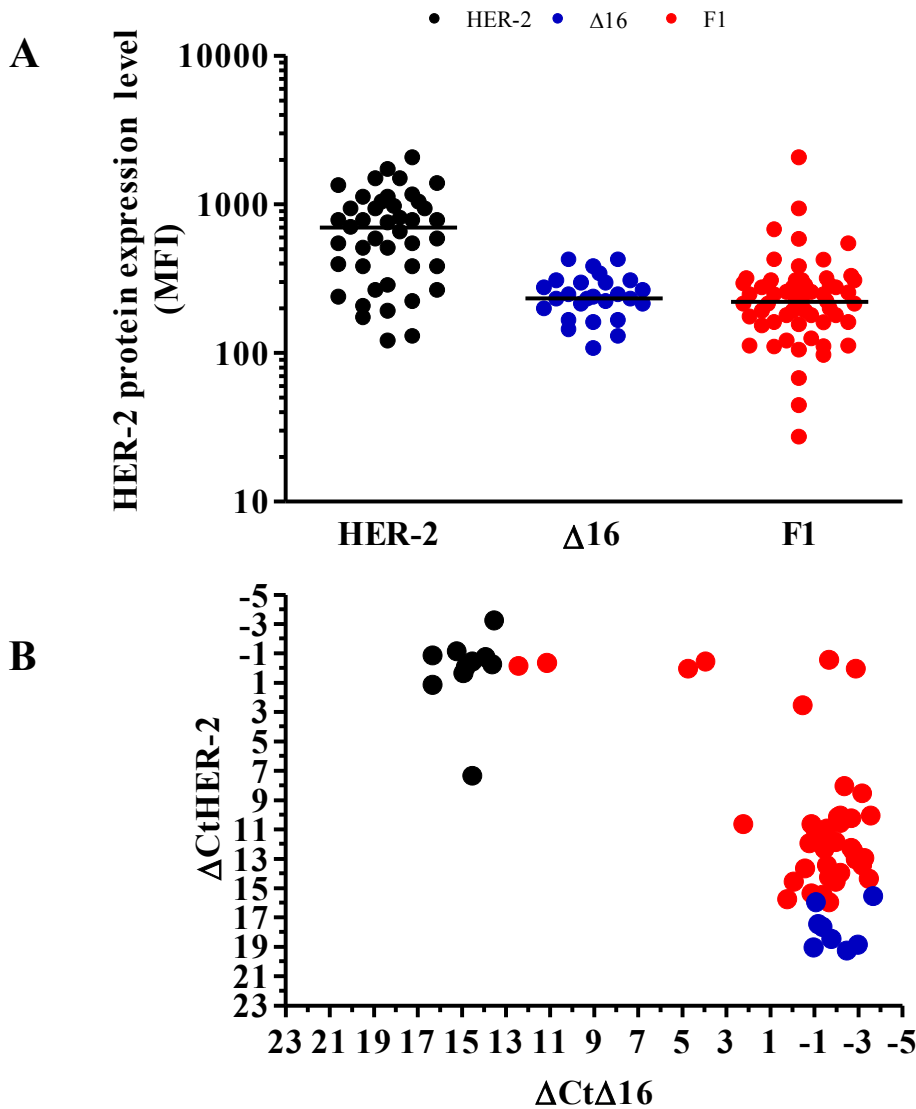


Figure 3. HER-2 expression in tumors. (A) Expression of total HER-2 protein on cell membrane by Cytofluorimetry. Each point represents a tumor. HER-2 tumors n=43, Δ16 tumors n=26, F1 tumors n=59. Median expression of HER-2 protein: HER-2 model median=698; Δ16 model median=233; F1 model median=221. Statistical significances (Student's t test): HER-2 vs Δ16 and HER-2 vs F1 $p < 0.0001$. (B) Expression of HER-2 and Δ16 transcripts. Each point represents a tumor. HER-2 tumors n=10, Δ16 tumors n=8, F1 tumors n=41. GAPDH was employed as house-keeping gene. Transcripts expression was calculated as follows: $\Delta Ct_{HER-2/\Delta 16} = Ct_{HER-2/\Delta 16} - Ct_{GAPDH}$.

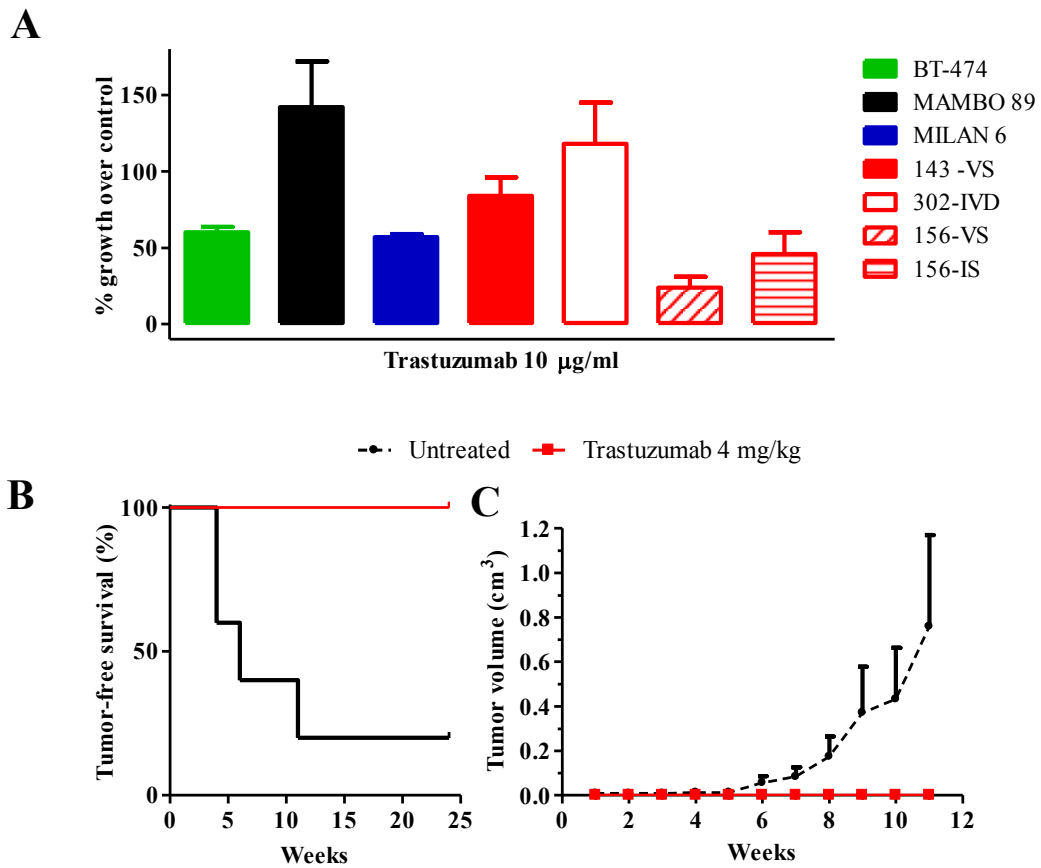


Figure 4. Sensitivity to Trastuzumab.

(A) *In vitro* (3-D culture) sensitivity to Trastuzumab (10 µg/ml). Cell lines derived from HER-2, Δ16 and F1 mammary tumors. Each bar represents the mean ± standard error percentage of colonies grown in 2-4 independent experiments. BT-474, MILAN 6, 156-VS and 156-IS were sensitive to Trastuzumab. (B,C) *In vivo* sensitivity to Trastuzumab in immunocompetent non-tolerant syngeneic mice (FVB mice) implanted with a F1-derived mammary tumor. Trastuzumab (4 mg/Kg) was administered i.p. twice a week for four weeks. (B) Kaplan-Meier analysis. Incidence of mammary tumor in mice: untreated mice 4/5 (80%); treated mice 0/5 (0%). (C) Kinetic of the growth of F1 tumor. Each point represents the mean tumor volume ± standard error. Statistical significances (Fisher's exact test): $p < 0.05$.

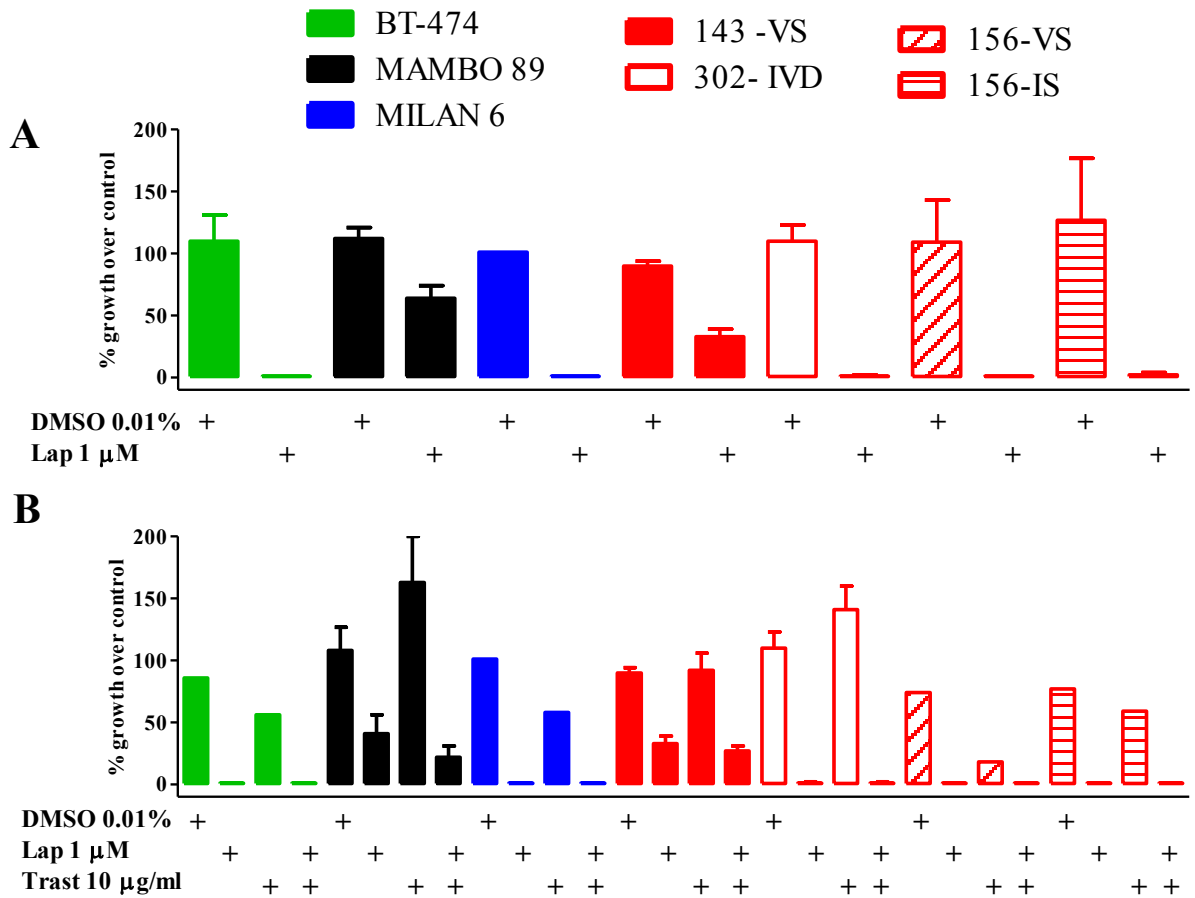


Figure 5. Sensitivity to Lapatinib (alone or in combination with Trastuzumab).

(A) *In vitro* (3-D culture) sensitivity to Lapatinib (1 μM). Each bar represents the mean ± standard error percentage of colonies grown in 2-6 independent experiments. Statistical significances (Student's t test): for Lapatinib MAMBO 89/143-VS vs BT-474/MILAN 6/ 302-IVD/156-VS/156-IS $p < 0.05$ (B) *In vitro* sensitivity to Lapatinib and/or Trastuzumab. Each bar represents the mean ± standard error in 1-3 independent experiments. Statistical significances when $n > 1$ (Student's t test): for Lapatinib + Trastuzumab MAMBO 89 vs 302-IVD $p = 0.054$; 143-VS vs 302-IVD $p < 0.005$.

Figures and tables

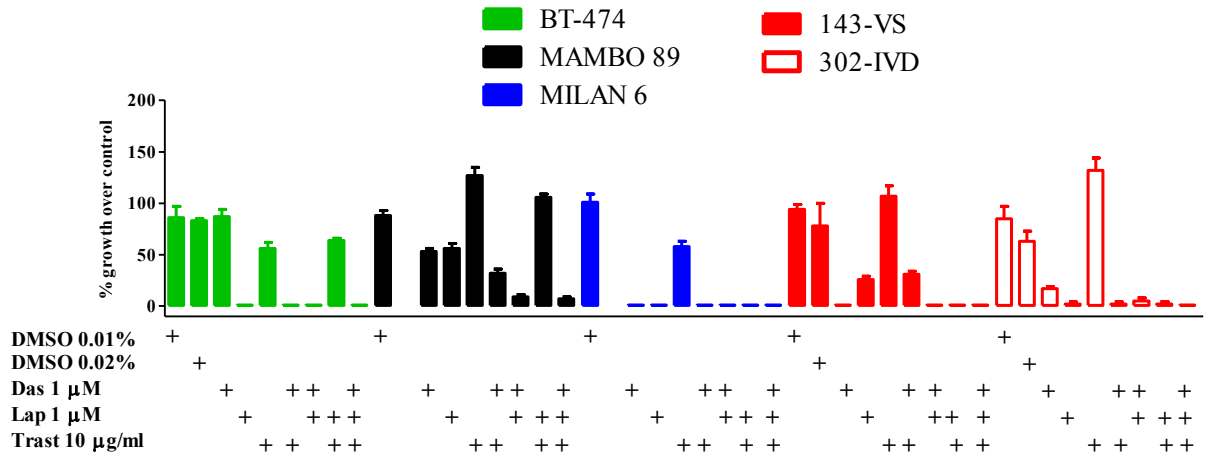


Figure 6. Sensitivity to Dasatinib (alone or in combination with Trastuzumab and/or Lapatinib).

(A) *In vitro* (3-D culture) sensitivity to Dasatinib (1 μ M) alone or in combination with Trastuzumab (10 μ g/ml) and/or Lapatinib (1 μ M). Each bar represents the mean \pm standard error of 4-6 counts of the same experiment. Statistical significances among cell lines (Student's t test): for Dasatinib MAMBO 89 vs MILAN 6/143-VS/302-IVD $p < 0.001$, 302-IVD vs MILAN 6/143-VS $p < 0.001$; for Dasatinib+Lapatinib MAMBO 89 vs MILAN 6/143-VS $p < 0.01$; for Dasatinib+Trastuzumab MAMBO 89 vs MILAN 6/143-VS/302-IVD $p < 0.001$; for Dasatinib+Lapatinib+Trastuzumab MAMBO 89 vs MILAN 6/143-VS/302-IVD $p < 0.05$. Statistical significances among treatments (Student's t test): for MAMBO 89 Dasatinib vs Dasatinib+Lapatinib/Dasatinib+Lapatinib+Trastuzumab $p < 0.001$; for 302-IVD Dasatinib vs Dasatinib+Lapatinib $p < 0.05$, Dasatinib vs Dasatinib+Trastuzumab $p < 0.005$, Dasatinib vs Dasatinib+Lapatinib+Trastuzumab $p < 0.001$.

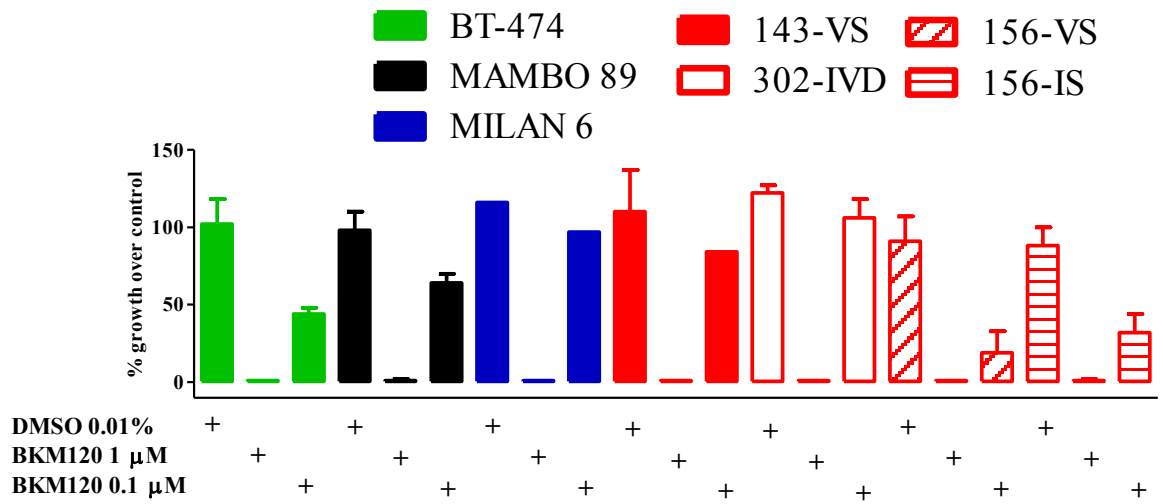


Figure 7. Sensitivity to NVP-BKM120.

In vitro (3-D culture) sensitivity to NVP-BKM120 (1 μM and 0.1 μM). Each bar represents the mean ± standard error percentage of colonies grown in 1-2 independent experiments. Statistical significances (Student's t test) when n>1: for BKM120 0.1 μM 302-IVD vs 156-VS/156-IS p<0.05.

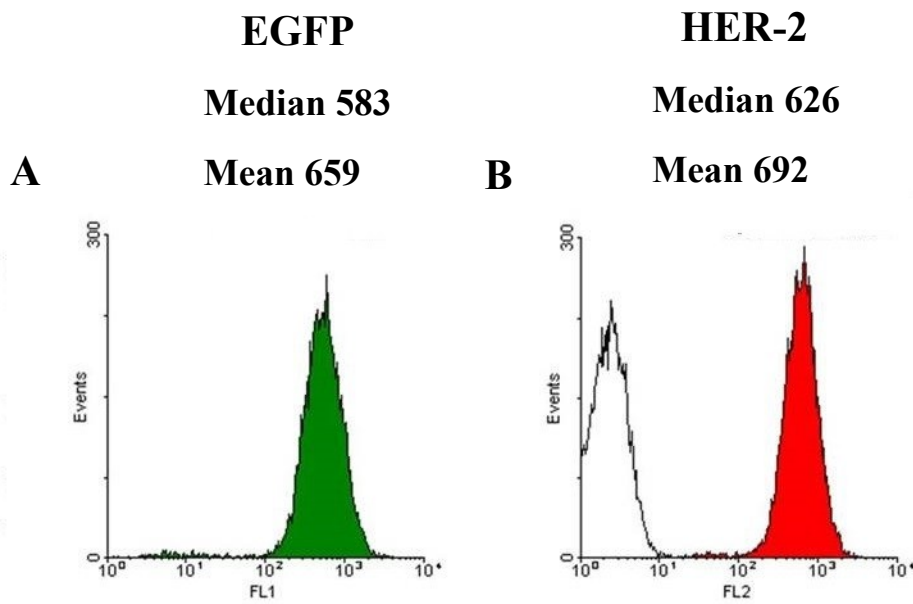


Figure 8. Cytofluorimetric expression of *Enhanced Green Fluorescent Protein (EGFP)* and *HER-2* in MDA-MB-453-EGFP.

(A) In green EGFP expression in MDA-MB-453 transduced with EGFP (MDA-MB-453-EGFP) is shown. (B) In red HER-2 expression in MDA-MB-453-EGFP. Empty profile shows basal fluorescence of MDA-MB-453-EGFP after incubation only with the secondary antibody. X axis reports fluorescent intensity in arbitrary units, y axis reports the number of events.

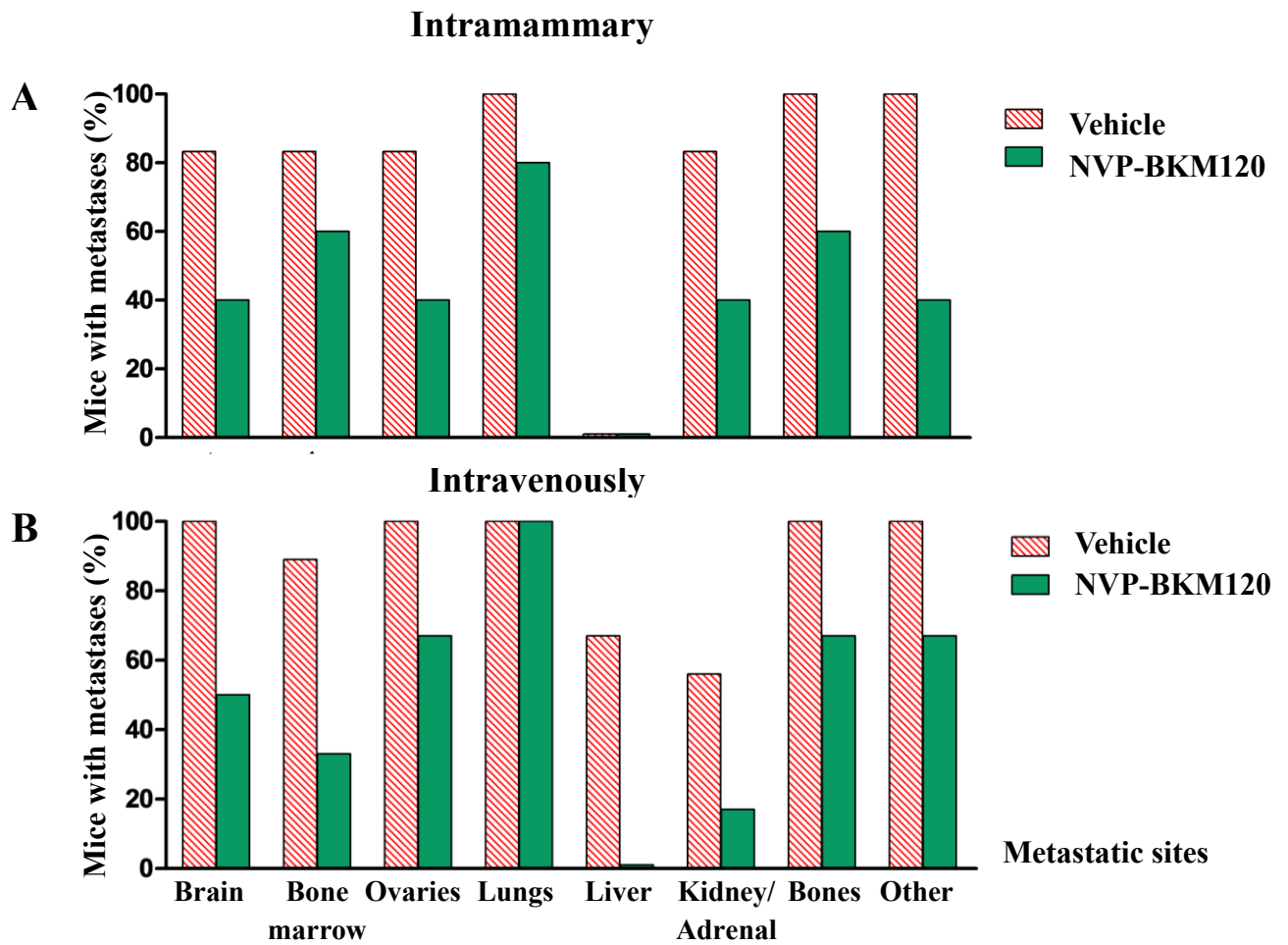


Figure 9. Treatment of spontaneous and induced HER-2 positive human metastases with NVP-BKM120.

(A) Incidence of spontaneous metastases in different sites after intramammary injection of MDA-MB-453-EGFP (10^7 cells) in $Rag2^{-/-};Il2rg^{-/-}$ mice. Mice were treated with NVP-BKM120 (50 mg/kg, per os) starting seven days after cell injection. Vehicle n=6, NVP-BKM120 n=5. (B) Incidence of induced metastases in different sites after intravenous injection of MDA-MB-453-EGFP (2×10^6 cells). Mice were treated with NVP-BKM120 (50 mg/kg, per os) starting one day after cell injection. Vehicle n=9, NVP-BKM120 n=6. Statistical significances (Fisher's exact test): Vehicle vs NVP-BKM120 in brain, bone marrow and liver $p < 0.05$ at least.

BRAIN

LUNGS

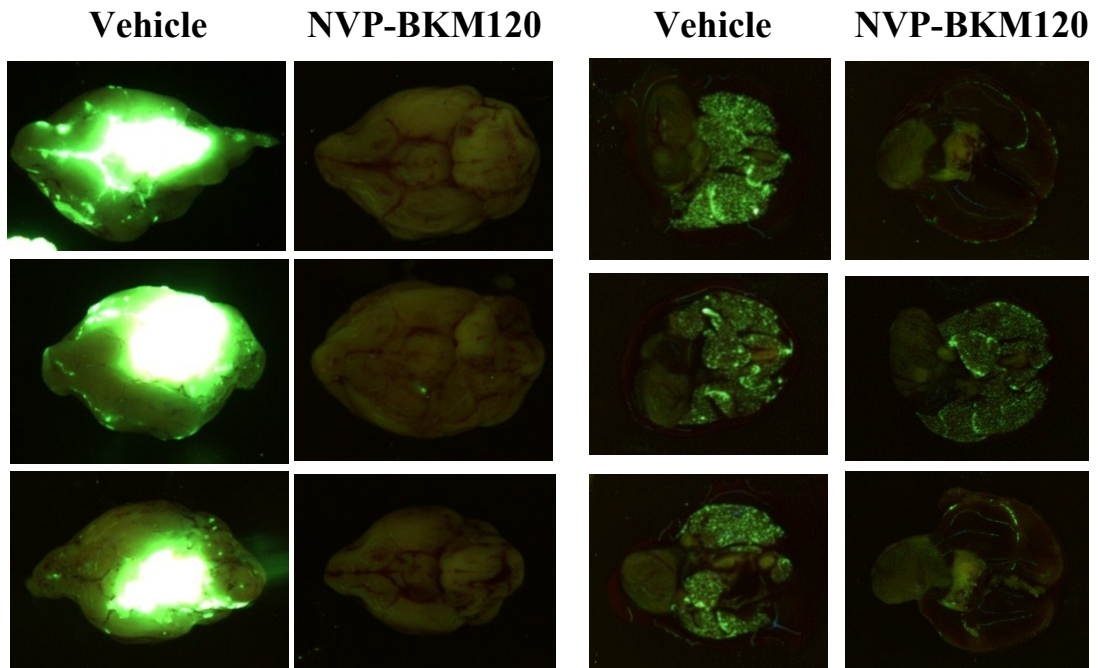


Figure 10. Inhibition of HER-2-positive metastatic growth by NVP-BKM120 in brain and lungs.

Representative pictures of dissected control and treated mouse brains (ventral view) and lungs. Lighttools imaging system was used to detect fluorescent metastatic deposits.

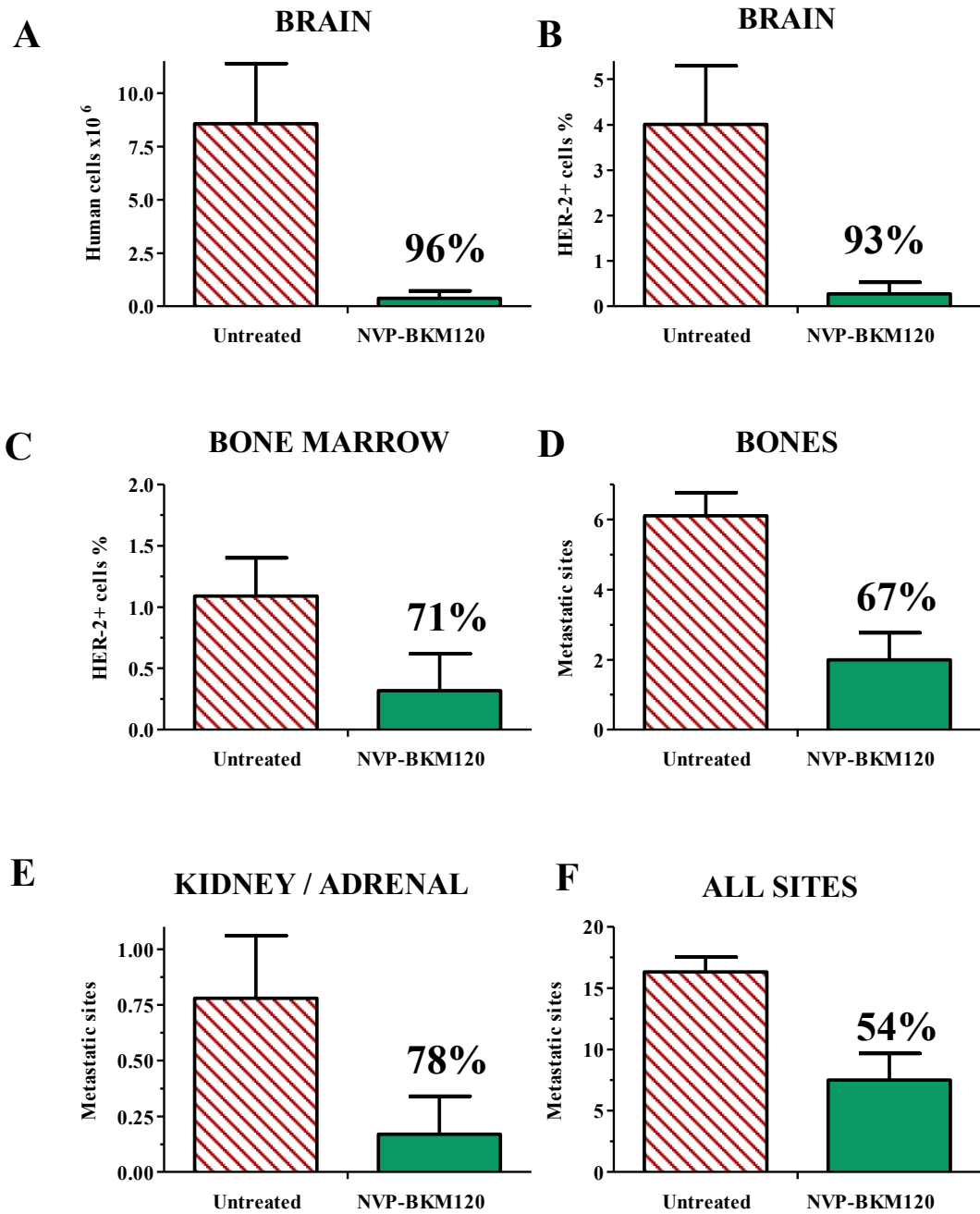


Figure 11. Quantification of HER-2-positive induced metastases after treatment with NVP-BKM120.

The mean metastatic burden \pm standard error was evaluated in mice treated i.v. with MDA-MB-453-EGFP. Untreated mice n=9, NVP-BKM120 n=6. Percentage inhibition is shown in each graph above NVP-BKM120 bar. **(A)** Quantitative analysis of brain metastases in Real-time PCR calculated as number of human cells in mouse brain. **(B,C)** Cytofluorimetric quantification of HER-2-positive

Figures and tables

cells in brain (B) and femoral bone marrow (C). **(D,E,F)** Visual count of metastatic sites per mouse. Statistical significances (Student's t test): panel A, B, D and F untreated vs NVP-BKM120 $p < 0.05$.

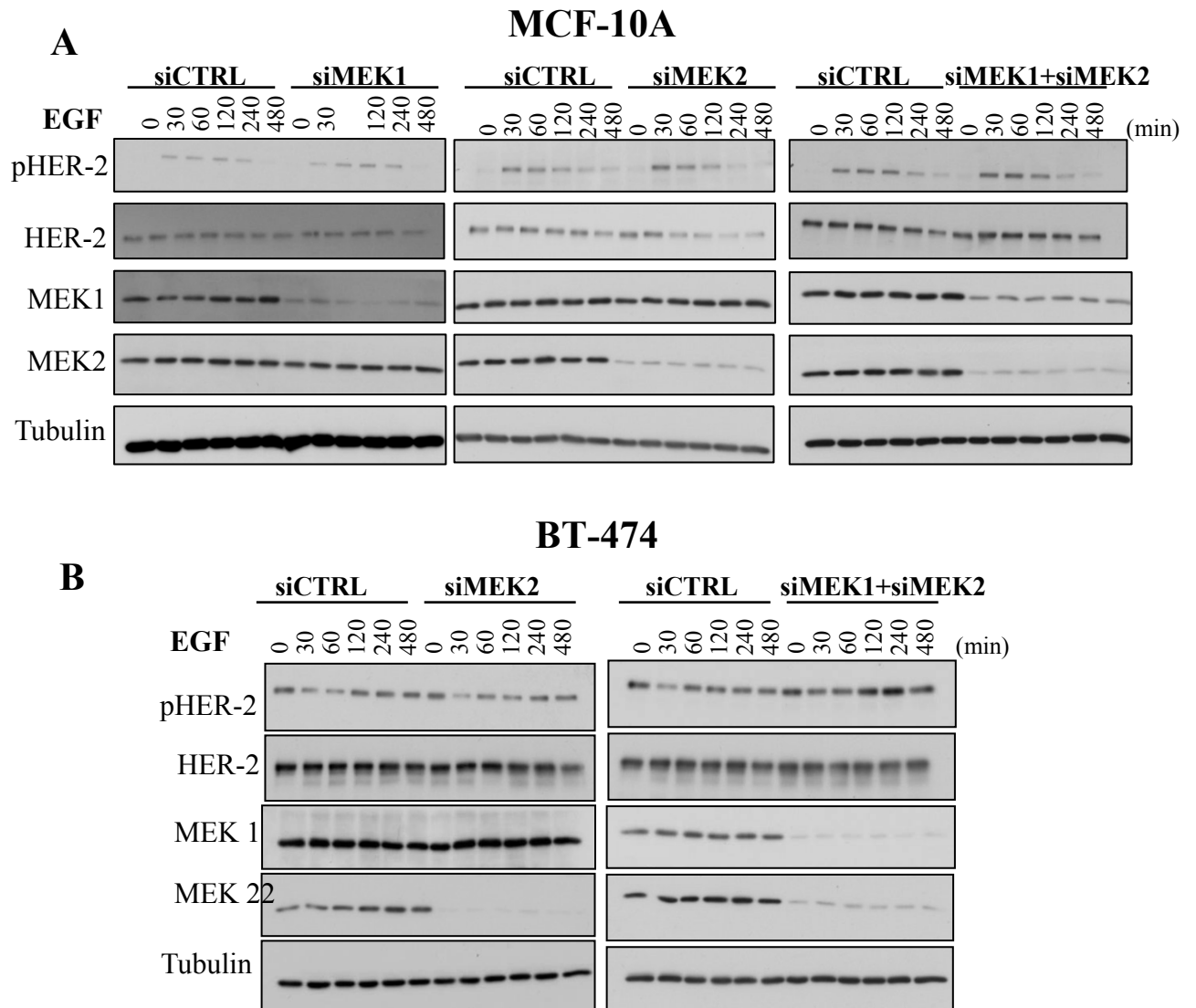


Figure 12. MEK inhibition by siRNA in MCF-10A and BT-474.

MCF-10A and BT-474 were transfected with siRNA Control, siRNA MEK1, siRNA MEK2 and siRNA MEK1 + siRNA MEK2 (Dharmacon) at a final concentration of 50 nM. An EGF time course was included. Tubulin was employed as house-keeping protein. **(A)** Western blots on MCF-10A lysates; **(B)** Western blots on BT-474 lysates.

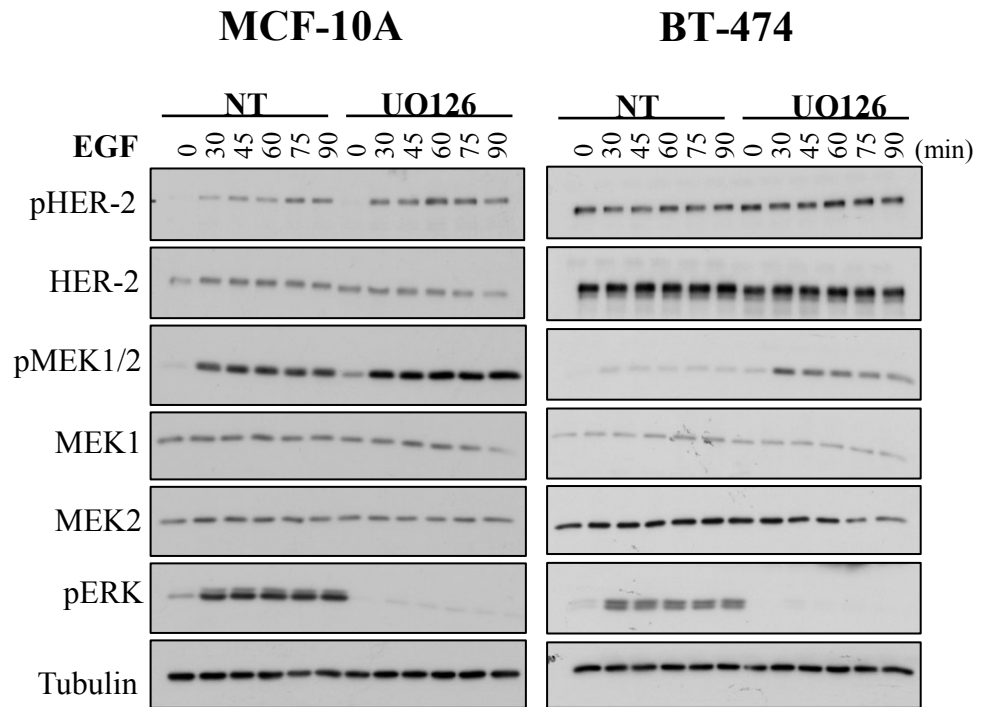


Figure 13. MEK inhibition by treatment with UO126 of MCF-10A and BT-474.

MCF-10A and BT-474 were treated for 1 hour with UO126 5 μM. Western blots were performed on cell lysates. An EGF time course was included. Tubulin was employed as house-keeping protein.

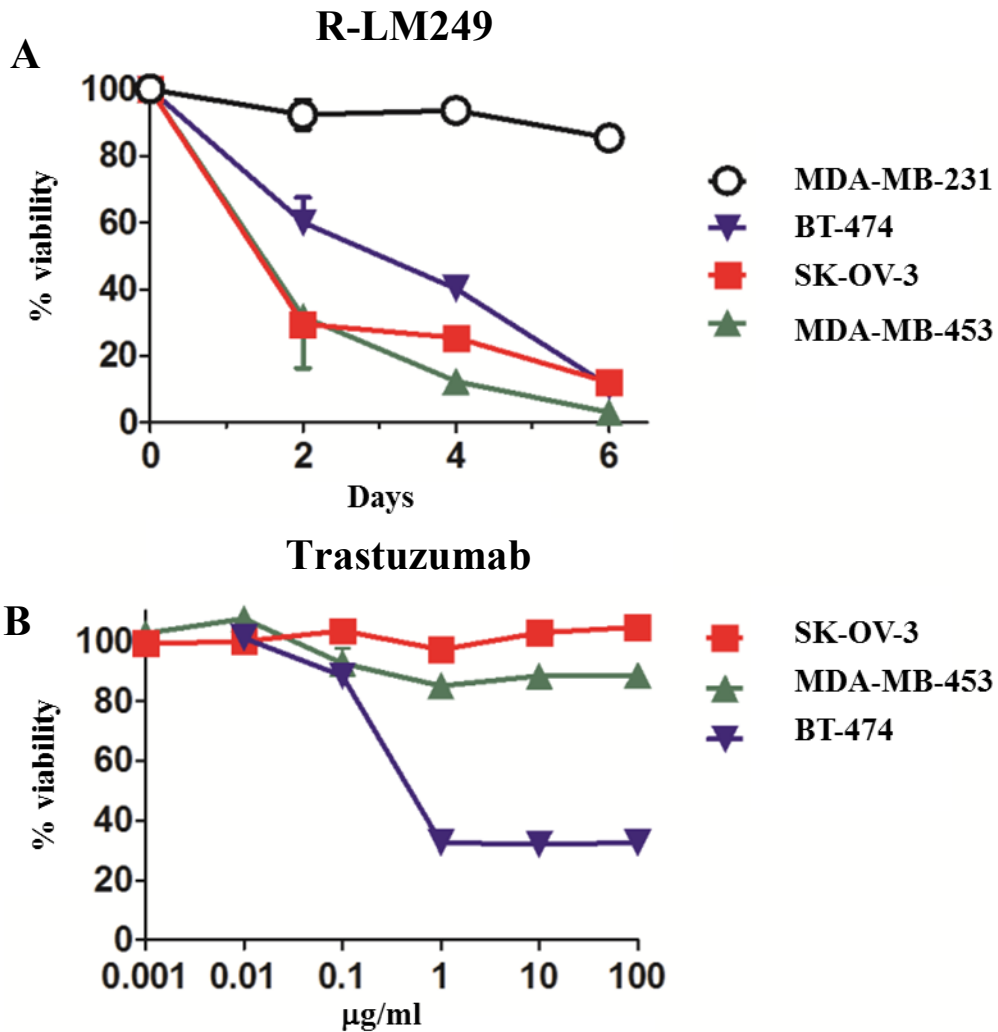
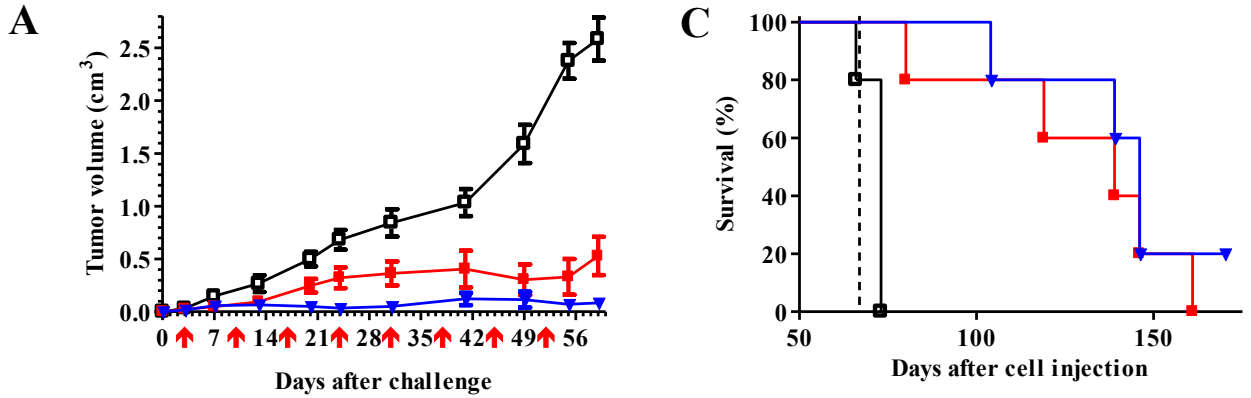


Figure 14. *In vitro* sensitivity to R-LM249 and Trastuzumab.

(A) Cytotoxicity of R-LM249 (10 pfu/cell) in three HER-2-positive cancer cell lines (BT-474 and MDA-MB-453, breast cancer; SK-OV-3, ovarian cancer). HER-2-low/negative breast cancer cell line MDA-MB-231 was included as negative control. Cell viability was measured by alarmBlue assay. Each point represents the mean of quadruplicates + standard deviation expressed as percentage with respect to uninfected cells. (B) Sensitivity to Trastuzumab after 72 hours culture. Mean \pm standard error from 3-5 independent experiments is shown. Abbreviations: pfu, plaque-forming units.

BT-474



MDA-MB-453

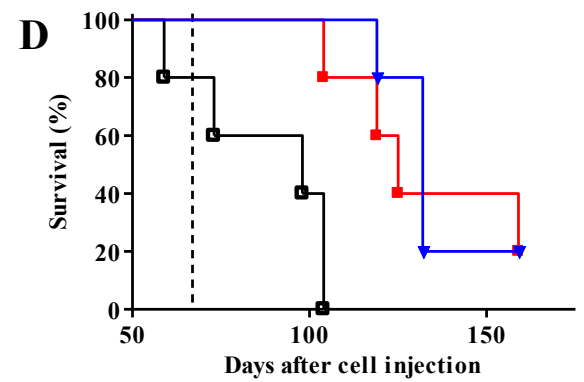
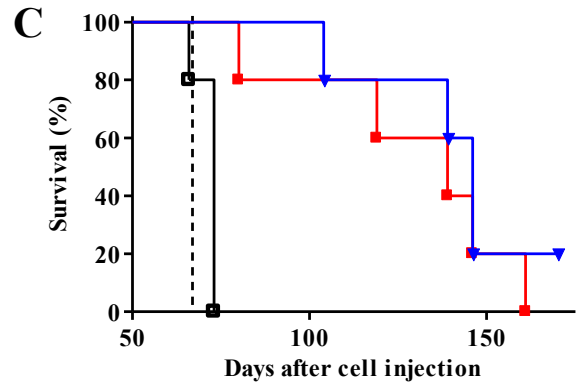
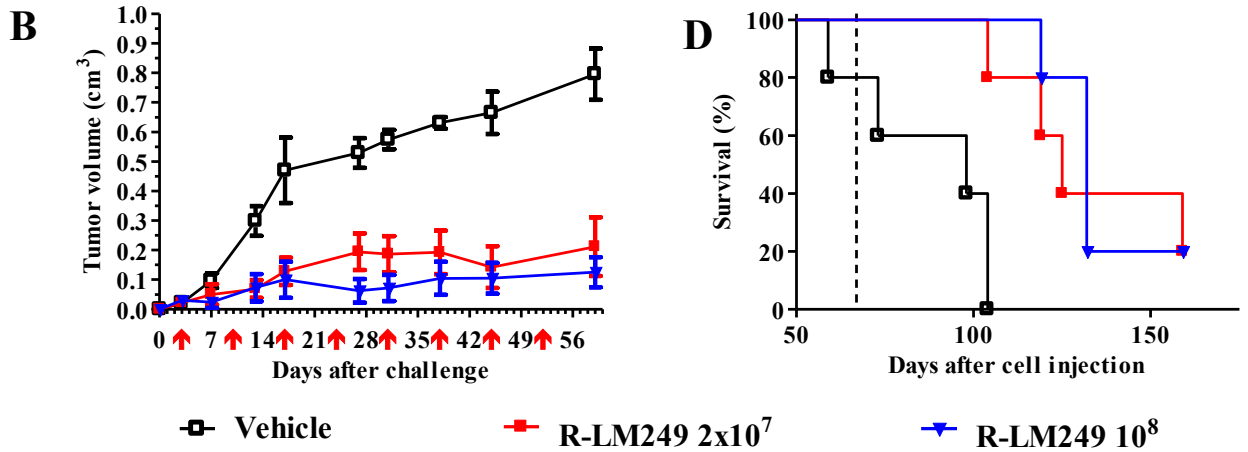


Figure 15. Therapy of localized HER-2-positive human breast cancer with R-LM249.

(A,B) Tumor growth inhibition by R-LM249. BT-474 and MDA-MB-453 (10^7 cells) were injected s.c. in Rag2^{-/-};Il2rg^{-/-} mice. R-LM249 (2×10^7 or 10^8 pfu) was administered intratumorally at the indicated days (red arrows below x axis). Each point represents the mean tumor volume \pm standard error until all mice per group are alive (in each group n=5). Statistical significances (Student's t test): for BT-474, Vehicle vs R-LM249 2×10^7 p<0.05 at least from 20th day, Vehicle vs R-LM249 10^8 p<0.05 at least from 13th day; for MDA-MB-453, Vehicle vs R-LM249 $2 \times 10^7/10^8$ p<0.05 at least from 13th day. (C,D) Kaplan-Meier analyses. A vertical dashed line shows the end of treatment with R-LM249 (67 days). (C) Median survival days: Vehicle=73, R-LM249 2×10^7 =139, R-LM249 10^8 =146. (D) Median survival days: Vehicle=98, R-LM249 2×10^7 =125, R-LM249 10^8 =132.

Figures and tables

Statistical significances (Mantel-Haenszel's test): for BT-474 and MDA-MB-453, Vehicle vs R-LM249 $2 \times 10^7 / 10^8$ $p < 0.01$ at least.

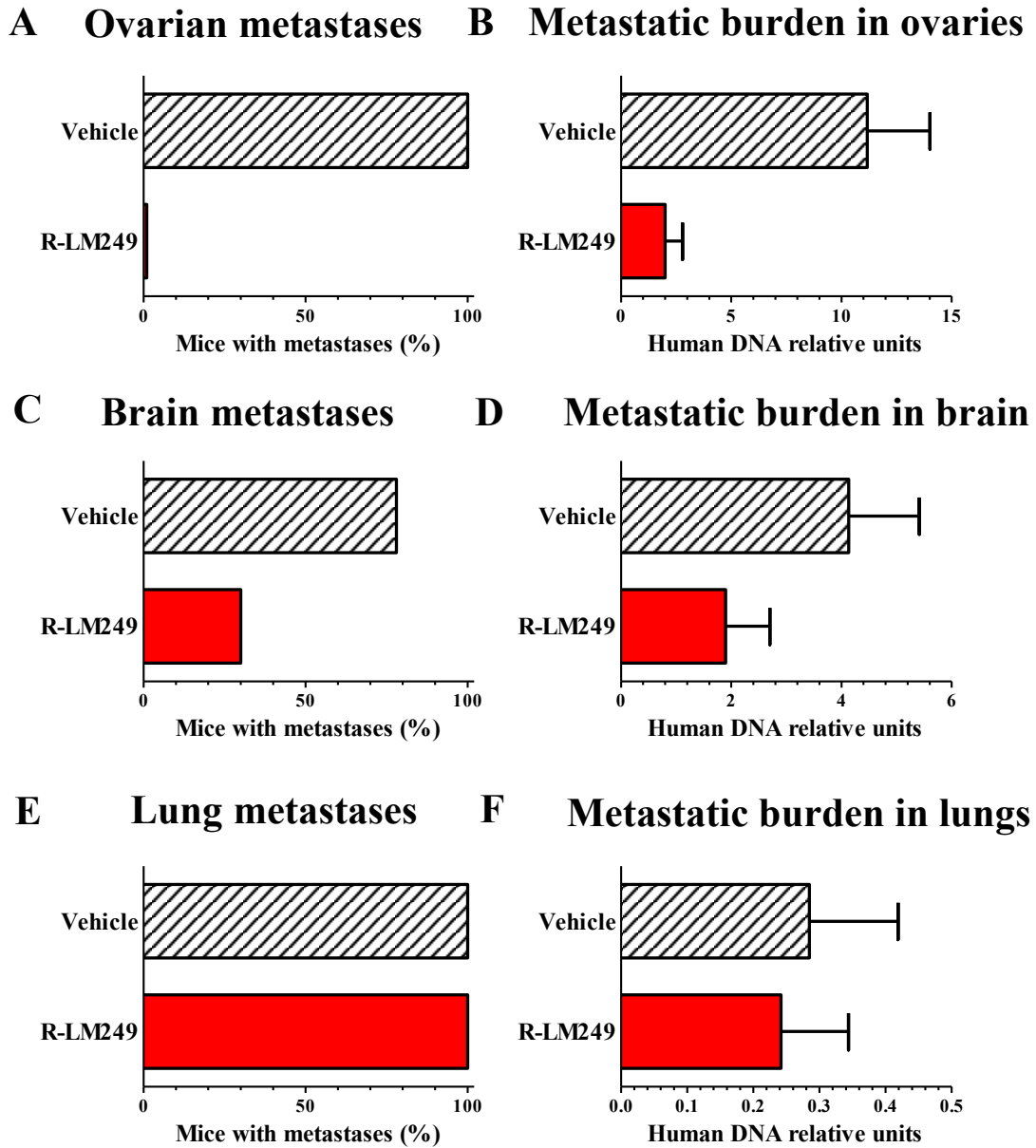


Figure 16. Therapy of metastatic HER-2-positive human breast cancer with R-LM249. MDA-MB-453 (2×10^6 cells) were injected i.v. in $Rag2^{-/-}; Il2rg^{-/-}$ mice. R-LM249 (10^8 pfu) was administered i.p. in 4 weekly injections. Vehicle $n=9$, R-LM249 $n=10$. **(A, C, E)** Incidence of macroscopic metastases in organs at necropsy. **(B, D, F)** Quantification of metastatic burden in organs by Real-time PCR. Each bar represents the mean \pm standard error in each group. Statistical significances: (A), $p < 0.0001$ (Fisher's exact test); (B), $p = 0.0004$ (Student's t test and non-parametric Wilcoxon's rank sum test); (C), $p = 0.07$ (Fisher's exact test); (D), $p = 0.056$ (Student's t test), $p = 0.03$ (non-parametric Wilcoxon's rank sum test).

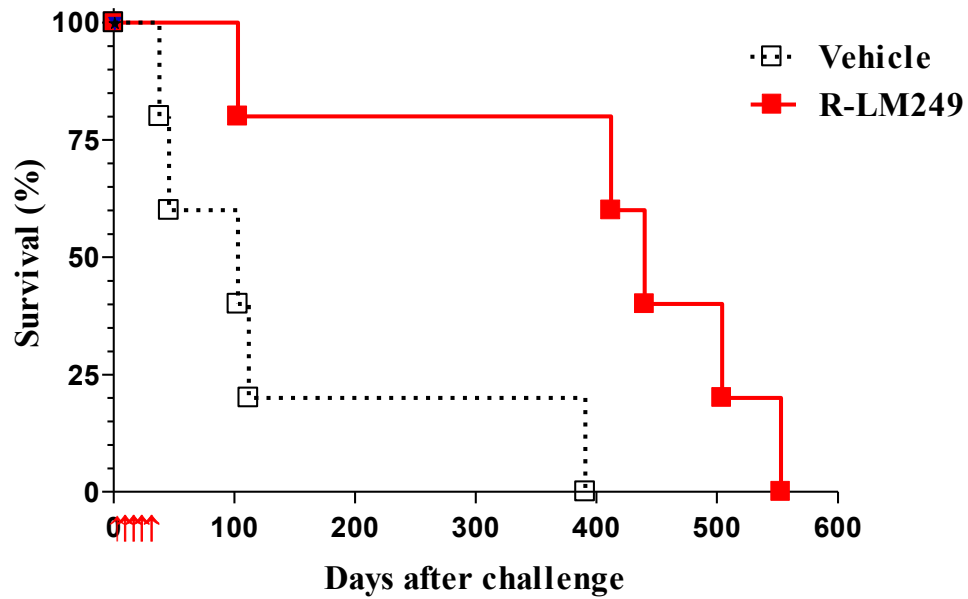


Figure 17. Therapy with R-LM249 of peritoneal carcinosis of HER-2-positive ovarian carcinoma in *nude* mice.

Kaplan-Meier analysis. SK-OV-3 (2×10^6 cells) were injected i.p. in *nude* mice. R-LM249 (2×10^7 pfu) was administered i.p. weekly at the indicated days (red arrows below x axis), starting 3 days after cell injection. In each group $n=5$. Median survival days: Vehicle=103, R-LM249=440. Statistical significances (Mantel-Haenszel's test): $p=0.02$.

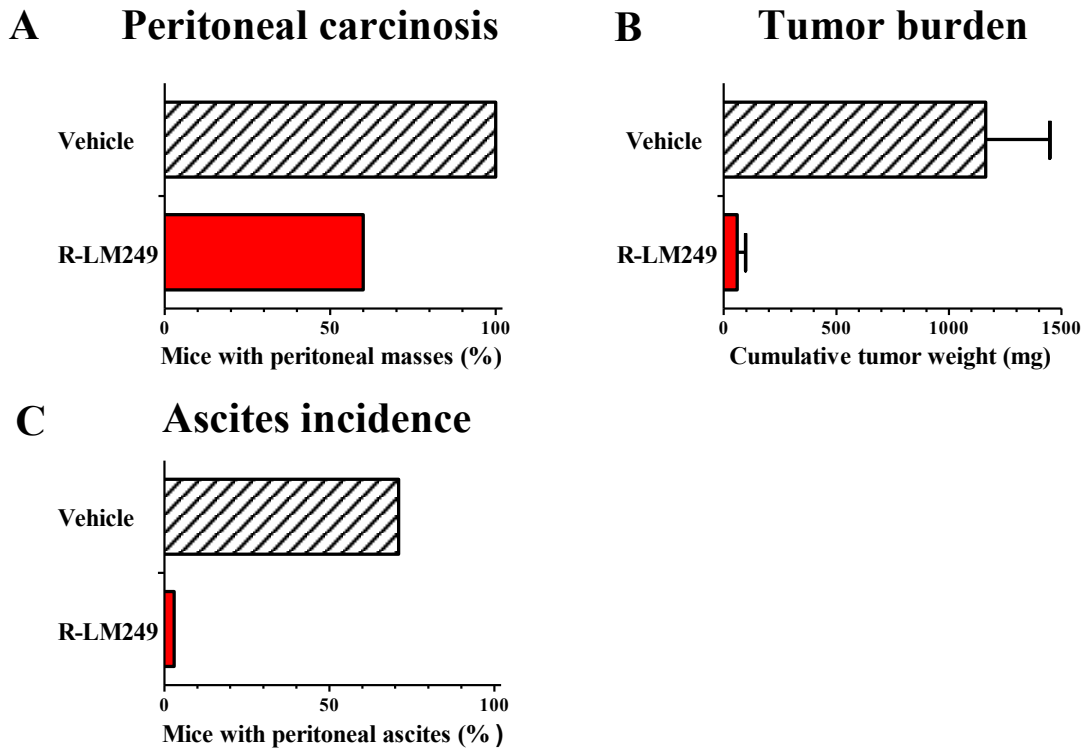


Figure 18. Therapy with R-LM249 of peritoneal metastatic HER-2-positive ovarian cancer in $Rag2^{-/-};Il2rg^{-/-}$ mice.

SK-OV-3 (2×10^6 cells) were injected i.p. in $Rag2^{-/-};Il2rg^{-/-}$ mice. R-LM249 (10^8 pfu) was administered i.p. weekly for 5 weeks, starting 3 days after cell injection. Vehicle n=5, R-LM249 n=7. **(A)** Incidence of peritoneal carcinosis **(B)** Mean cumulative weight of peritoneal metastases \pm standard error. Statistical significances (Student's t test): p=0.007. **(C)** Incidence of peritoneal ascites. Statistical significances (Fisher's exact test): p=0.027.

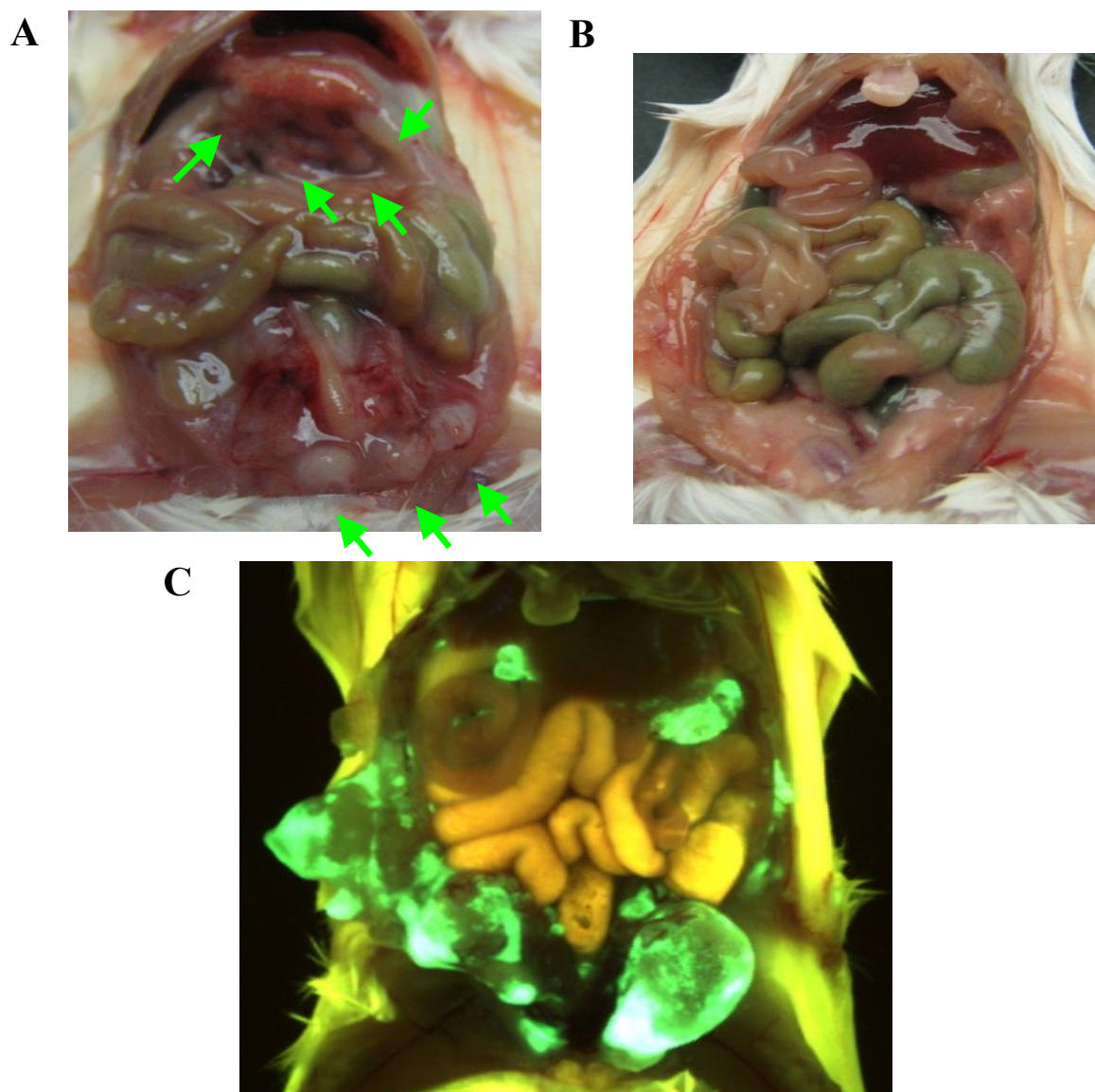


Figure 19. R-LM249 efficacy in targeting and inhibiting HER-2-positive ovarian cancer metastases.

Representative pictures of $Rag2^{-/-};Il2rg^{-/-}$ mice after the i.p. injection of SK-OV-3 and i.p. treatment with R-LM249. **(A)** Control mouse (treated with PBS). Green arrows show multiple peritoneal metastases. **(B)** Metastases-free mouse treated with R-LM249. **(C)** Distribution of R-LM249 transfected with EGFP in a mouse with multiple peritoneal metastases. Yellow-brown fluorescence: autofluorescence of mouse fur and visceral organs.

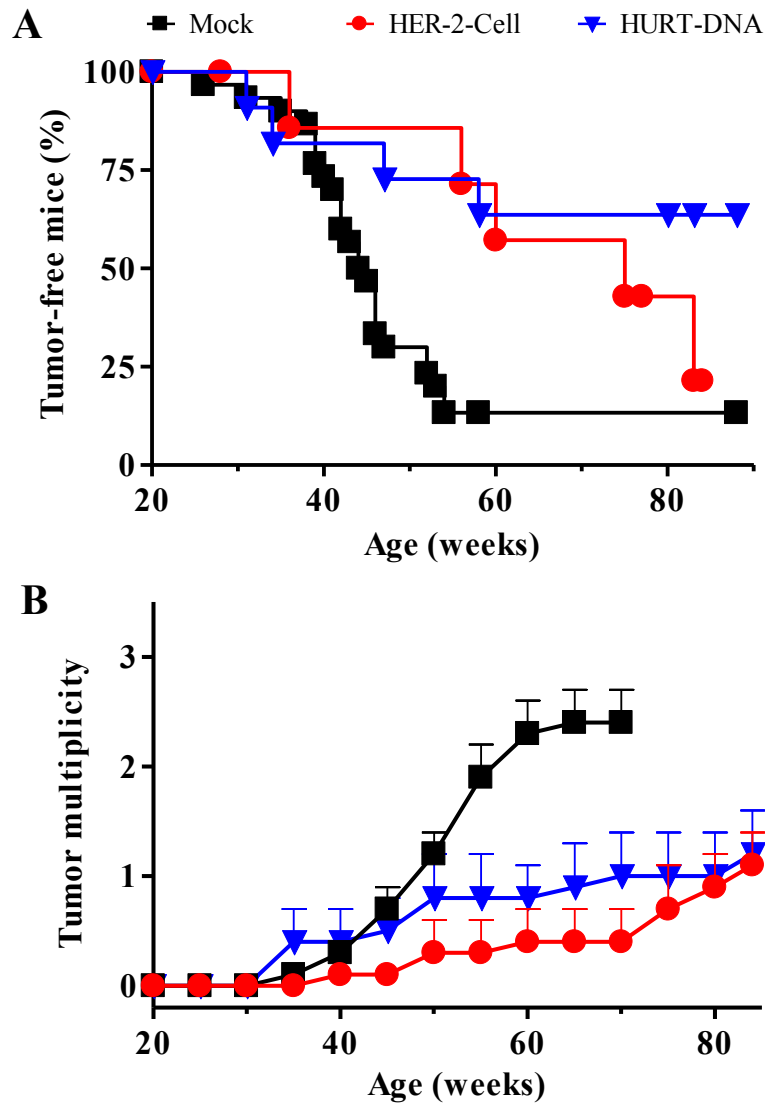
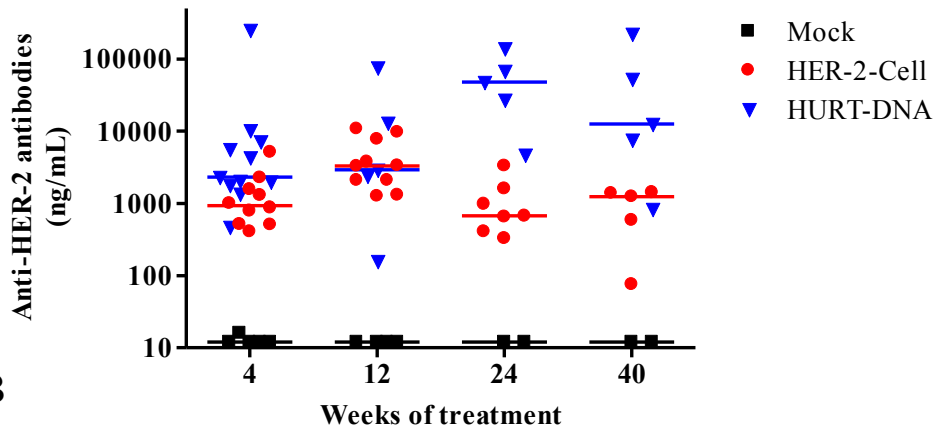


Figure 20. Immunopreventive efficacy of anti-HER-2 vaccines on HER-2 model.

Mock group (untreated, vehicle and pVAX1) n=31, HER-2-Cell vaccine n=8, HURT-DNA vaccine n=12. **(A)** Kaplan-Meier analysis. Incidence of mammary tumors in HER-2 mice: Mock 87%; HER-2-Cell vaccine 79%; HURT-DNA vaccine 36%. Statistical significances (Mantel-Haenszel's test): Mock vs HER-2-Cell/HURT-DNA vaccines p<0.05. **(B)** Tumor multiplicity. Each point represents the mean number of tumors/mouse \pm standard error at death. Statistical significances (Student's t test): Mock vs HER-2-Cell vaccine p<0.05 at least from 50th week; Mock vs HURT-DNA p<0.05 at least from 54th week.

A



B

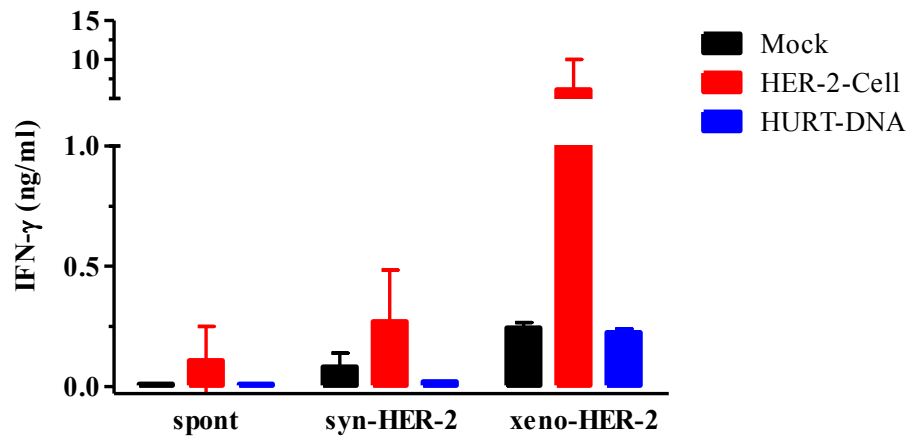
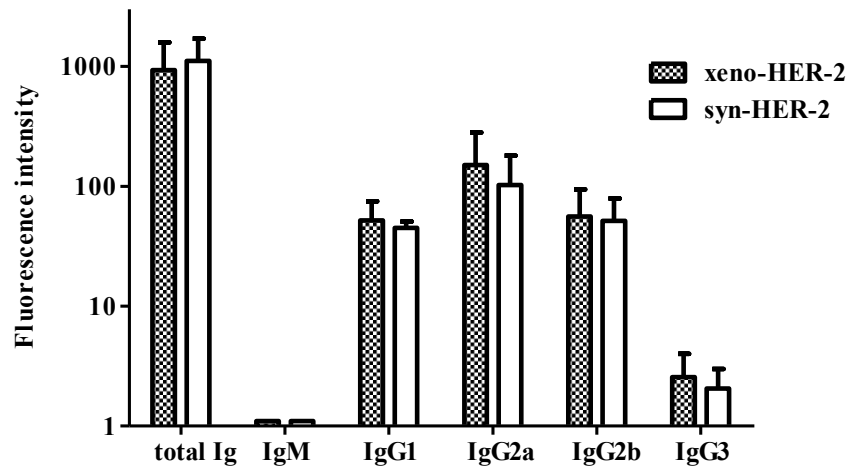


Figure 21. Humoral and cell-mediated immune responses to anti-HER-2 vaccines in HER-2 model.

(A) Serum anti-HER-2 antibodies after vaccination with HER-2-Cell or HURT-DNA vaccines. Median value of each group is shown as a horizontal bar. Mock n=2-5, HER-2-Cell n=5-10, HURT-DNA n=5-11. Statistical significances (Wilcoxon's non-parametric test): HURT-DNA vs HER-2-Cell $p < 0.05$ at least at 4th, 24th and 40th weeks of treatment. (B) Interferon γ (IFN- γ) production by spleen cells after vaccination. Mock n=6, HER-2-Cell n=4, HURT-DNA n=3. Each bar represents the mean \pm standard error of each group. Spleen cells were cultured alone (spont) or in the presence of HER-2-positive syngeneic (syn-HER-2, MAMBO 89) or xenogeneic (xeno-HER-2, SK-OV-3) cancer. Statistical significances: for syn-HER-2 and xeno-HER-2, HER-2-Cell vs Mock/HURT-DNA $p < 0.05$.

A



B

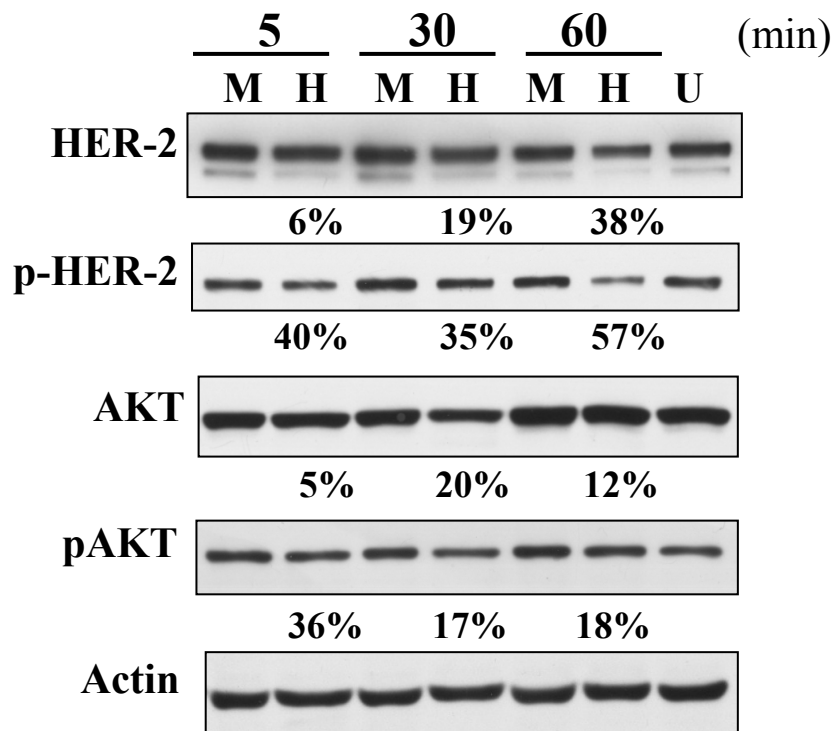


Figure 22. Anti-HER-2 antibodies produced by HER-2 mice vaccinated with HURT-DNA.

(A) Isotypes expression of anti-HER-2 antibodies by indirect immunofluorescence after incubation of sera with HER-2-positive syngeneic (syn-HER-2, MAMBO 89) or xenogeneic (xeno-HER-2, SK-OV-3) cancer cells. (B) Activation of HER-2 signaling in syngeneic HER-2 positive cell line (MAMBO 89) after treatment with anti-HER-2 antibodies. Time of exposure to antibodies is shown. Band

Figures and tables

intensity was detected by densitometric analysis and normalized over actin. The percentage decrease between M and H is shown. Abbreviations: U, untreated cells; M, cells treated with sera from Mock-vaccinated mice; H, cells treated with sera from mice vaccinated with HURT-DNA.

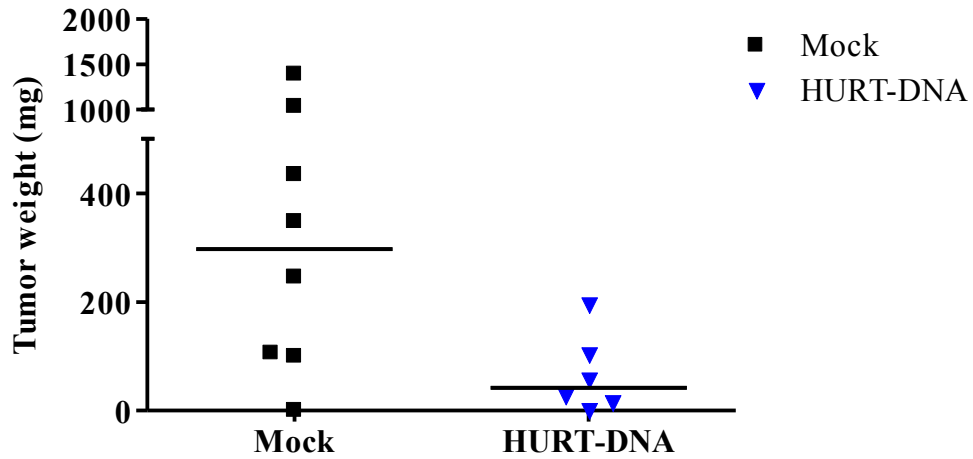


Figure 23. Tumor growth inhibition by anti-HER-2 antibodies.

HER-2-positive cell line SK-OV-3 (2×10^6) was injected i.p. in Rag2^{-/-};Il2rg^{-/-} mice. Mice were treated i.p. with sera from Mock mice (untreated or pVAX1-treated) or from mice vaccinated with HURT-DNA at day 1, 3, 7 and 14. Each point represents the weight of all tumors grown intraperitoneally in each mouse. Mock n=8, HURT-DNA n=6. Median tumor weight is shown as horizontal bar. Statistical significances (Wilcoxon's non-parametric test): p=0.05.

DISCUSSION

Discussion

The project described in this thesis had two aims: the study of the contribute of wild-type full-length HER-2 and of its splice variant $\Delta 16$ to mammary HER-2-positive carcinogenesis and the evaluation of innovative anti-HER-2 strategies against HER-2-positive breast cancer.

Besides the 185kDa protein, over the years other isoforms of HER-2 were found in HER-2-positive breast cancers, including C- and N-terminal fragments of the protein (p95HER-2 and H2NTF) and the splice variant $\Delta 16$ (Kwong and Hung, 1998; Arribas *et al.*, 2011; Morancho *et al.*, 2013). In $\Delta 16$ isoform, the in-frame deletion of exon 16 (48 bp) determines the lack of 16 aminoacids, including two cysteines, in the juxtamembrane region (Kwong and Hung, 1998). Due to the loss of these cysteine residues, intermolecular disulfide bonds with other monomers are promoted, triggering a stronger signal transduction in respect to HER-2 (Castiglioni *et al.*, 2006).

The transforming ability of wild-type HER-2 has been widely investigated since the discovery of its connection to cancer in 1984 by Schechter and colleagues (Schechter *et al.*, 1984) and led to the development of revolutionary anti-HER-2 agents. Due to their relatively recent detection, more studies on HER-2 isoforms are required to shed light into their role in HER-2 carcinogenesis and in the development of resistance to current anti-HER-2 agents.

With this purpose, in this thesis the comparative study of mammary carcinogenesis in three mouse models transgenic for different forms of HER-2 is reported: two mouse strains that carry HER-2 proto-oncogene (HER-2 model; Finkle *et al.*, 2004) or $\Delta 16$ variant gene ($\Delta 16$ model; Marchini *et al.*, 2011) respectively, and a hybrid model transgenic for both genes (F1 model).

Confirming the findings of Marchini and co-workers (Marchini *et al.*, 2011), the presence of $\Delta 16$ caused the anticipation of tumor onset in mice. Furthermore, mammary carcinogenesis was observed in all $\Delta 16$ -expressing mice, while 12% of HER-2 mice were still tumor free at 100 weeks of age. The simultaneous expression of $\Delta 16$ and HER-2 did not determine any difference in F1 tumor latency compared to that of $\Delta 16$ mice, suggesting a dominant role of the splice variant in F1 phenotype.

Discussion

The evaluation of tumor multiplicity, i.e. the number of tumors per mouse, showed once again the aggressiveness of $\Delta 16$ isoform in respect to HER-2. Models carrying $\Delta 16$ shared a dramatic increase in tumor multiplicity in respect to HER-2 mice, even though a significant higher number of tumors per mouse was observed in F1 mice if compared to $\Delta 16$ mice starting from the 22nd week of age.

In light of these findings, $\Delta 16$ isoform appears to be a more aggressive oncogene in respect to wild-type HER-2, in which additional genetic events, besides amplification, are required to trigger mammary carcinogenesis. Supporting these conclusions, Marchini and colleagues proposed the candidacy of $\Delta 16$ as the transforming form of HER-2, showing that its specific expression by mammary tumor cells was sufficient to induce tumor onset in $\Delta 16$ mice. Notably, the splice variant was not expressed in non-neoplastic mammary glands or other tissues (Marchini *et al.*, 2011). On the contrary, in HER-2 model developed by Finkle and co-workers wild-type HER-2 was detected in mammary tumors as well as in normal mammary glands and several other tissues. Furthermore, analyzing mammary tumors arisen in HER-2 mice, the group led by Finkle found sequence anomalies, e.g. deletions, in the same region that is deleted in $\Delta 16$ isoform, suggesting the need for a “second hit” in mice transgenic for wild-type HER-2 to trigger carcinogenesis (Finkle *et al.*, 2004). Previously, studies on the rat homologue of HER-2 (Neu) and on its mutated (i.e. activated) isoform NeuT highlighted the necessity of additional mutations, beside Neu amplification, to foster mammary carcinogenesis. The delayed tumor onset in Neu mice in respect to NeuT mice was attributed to the acquisition of genetic abnormalities. In particular, somatic mutations, including deletions, were found in tumors arisen in Neu mice (Guy *et al.*, 1992; Siegel *et al.*, 1994) in the same region of exon 16 deletion and of HER-2 genetic mutations observed in HER-2 mice (Finkle *et al.*, 2004). Discordant findings have been achieved so far in humans, where HER-2-amplified breast cancers do not display genetic mutations as those observed in preclinical models (Moasser, 2007; Arteaga and Engelman, 2014).

Despite the enhanced transforming ability of $\Delta 16$, tumors in $\Delta 16$ and F1 mice grew slower than those of HER-2-expressing mice. Furthermore, no differences in autochthonous metastatic spread were found among the three

Discussion

models. Thus, the expression of the splice variant seems significant for early carcinogenic events, but it may not be so relevant for later stages as progression and metastasis development.

However, transgenic mice are, in general, inappropriate for the study of late stages of breast cancer, i.e. the metastatic spread, because of the low incidence of metastases (Ottewell *et al.*, 2006; Saxena and Christofori, 2013). To overcome this issue, as well as to better define the role of HER-2 and $\Delta 16$ in advanced disease, syngeneic transplantation models were employed in this project. The injection of MAMBO 89 (derived from a tumor of a HER-2 mouse) or MILAN 6 (obtained from a tumor arisen in a $\Delta 16$ transgenic mouse) allowed to compare HER-2- and $\Delta 16$ -driven metastasis formation in HER-2-tolerant or non-tolerant mice. Both strains were permissive to the metastatic growth of cell lines in the lungs, but MILAN 6 transplantation models were more prone to the development of lung metastases. Using a xenotransplantation model, Alajati and colleagues previously showed the metastatic ability of $\Delta 16$, although they did not compare it with that of HER-2 (as done in this thesis) (Alajati *et al.*, 2014). Scientists observed a high incidence of induced and spontaneous lung metastases in immunodeficient mice (SCID/Beige) that had previously received the i.v. or i.m.a. injection of the human cell line MCF-10A transfected with $\Delta 16$. However, compared with the findings of this thesis, metastases were not found in all animals, likely because of the choice of the transplantation model. Indeed, the immunodeficient mouse strain that they employed is characterized by reduction, but not complete absence, of NK cells and phagocytes activity that could prevent the growth of human cells (Thomsen *et al.*, 2008). Furthermore, MCF-10A is an immortalized cell line (i.e. not prone to terminal differentiation or senescence), but with a non-neoplastic origin (it derives from epithelial breast tissue of a woman with fibrocystic disease).

The expression of total plasmatic HER-2 protein was assessed in F1 tumors and compared to that of HER-2- and $\Delta 16$ -driven tumors. The differential evaluation of wild-type HER-2 and $\Delta 16$ protein levels on tumor cells surface was hampered by the lack of antibodies that specifically target each isoform. Models carrying $\Delta 16$ gene showed similar HER-2 levels in tumors, significantly lower

Discussion

than those displayed by HER-2 transgenic mice. Three main reasons can be mentioned to clarify these observations. First, the model transgenic for wild-type HER-2 alone could have a real higher expression of the cell membrane receptor. Secondly, an impaired Ig binding to $\Delta 16$ protein might cause its lower detection on tumor cells. Finally, these findings could be attributed to the different number of transgene copies inserted in HER-2 (30-50 copies) and $\Delta 16$ (5 copies) models (Finkle *et al.*, 2004; Marchini *et al.*, 2011).

The coexistence of HER-2 and $\Delta 16$ in mammary tumors arisen in the hybrid model was shown by the presence of the transcripts of both isoforms. In humans, HER-2 and $\Delta 16$ transcripts coexist in nearly half HER-2-positive breast cancers and in 90% of patients with locally advanced disease, i.e. with invasive cancer cells in the lymph nodes (Castiglioni *et al.*, 2006; Mitra *et al.*, 2009). Thus, if compared with HER-2 and $\Delta 16$ models, F1 mice represent a further step in the attempt to mimic the human situation in preclinical models. According to the expression of HER-2 and $\Delta 16$, F1 mammary tumors were classified in three groups: the majority displayed expression levels comparable to $\Delta 16$ tumors (low HER-2, high $\Delta 16$), while just a couple of tumors were similar to HER-2 tumors (high HER-2, low $\Delta 16$). Finally, 12% of tumors coexpressed HER-2 and $\Delta 16$ at high/intermediate levels (high HER-2, high/intermediate $\Delta 16$). In general, the heterogeneity found in F1 tumors reflects what happens in human breast cancers, whose HER-2 expression in different patients, as well as in different portions of a single tumor, show peculiar characteristics (Arteaga and Engelman, 2014).

Hence, the heterogeneous expression of HER-2 and $\Delta 16$ enhances the preclinical value of F1 model, that appears even more suitable for investigational studies on new therapeutic strategies against HER-2. With this purpose, four cell lines were obtained from F1 tumors with different expression levels of HER-2 and $\Delta 16$ transcripts and *in vitro* stabilized: 143-VS (high HER-2, low $\Delta 16$), 156-VS and 156-IS (low HER-2, high $\Delta 16$), 302-IVD (high HER-2, high $\Delta 16$). As described below, in this project the susceptibility of these cell lines to anti-HER-2 drugs was tested in a 3-D culture, but they will be employed in future therapeutic studies on HER-2-positive syngeneic models.

Discussion

Since the development of Trastuzumab, a new era for the treatment of HER-2-positive breast cancer began. However, despite an initial drug response, many patients finally become resistant to anti-HER-2 agents that have been already approved by FDA (Arteaga and Engelman, 2014). Early studies on $\Delta 16$ splice variant reported that Trastuzumab is ineffective when applied to $\Delta 16$ -expressing cells *in vitro* (Castiglioni *et al.*, 2006; Mitra *et al.*, 2009). In contrast, in the current study a high susceptibility to the humanized monoclonal antibody was shown in all cell lines with a high expression of $\Delta 16$ (156-IS, 156-VS and MILAN 6), while cell lines expressing HER-2 at high levels (MAMBO 89, 143-VS and 302-IVD) were resistant to the drug. The effectiveness of Trastuzumab on high- $\Delta 16$ tumor cells was confirmed *in vivo* by the inhibition of F1 tumor growth in a syngeneic model. Supporting these findings, Alajati and co-workers previously showed that Trastuzumab was able to block the growth of MCF-10A transfected with $\Delta 16$ and injected orthotopically in SCID/Beige mice (Alajati *et al.*, 2013). Notably, the lower administration dose of Trastuzumab in the syngeneic model (4 mg/kg instead of 10 mg/kg delivered to xenotransplanted animals) was balanced by the compromised immune system of SCID/Beige mice, that were therefore unlikely to trigger ADCC after Trastuzumab treatment because of the absence of the most active ADCC effectors.

The resistant phenotype shown *in vitro* by F1 cell lines expressing HER-2 at a high level and, above all, by MAMBO 89 could be attributed to the presence of additional HER-2 transforming mutations on HER-2 gene in the original tumors (Finkle *et al.*, 2004). In contrast with these *in vitro* findings, treatment with Trastuzumab was able to significantly reduce the development of both HER-2 and $\Delta 16$ induced metastases in a syngeneic model. However, the reduction in the HER-2 metastatic burden was observed in a lower extent if compared with that of treated $\Delta 16$ mice. The efficacy of monoclonal antibodies in overcoming *in vitro* resistance of MAMBO 89 may be due to the triggering of Trastuzumab-mediated ADCC.

Overall, the presence of $\Delta 16$ correlated with a better response to Trastuzumab. Supporting the role of HER-2 isoforms in Trastuzumab-positive response, two recent studies reversed the notion that CTF cause resistance to the

Discussion

drug. In fact, despite the intrinsic resistant phenotype of p95HER-2 because of the lack of Trastuzumab binding site (Arribas *et al.*, 2011), the studies conducted by Parra-Palau and Scaltriti associated the expression of CTF in human samples of HER-2-positive breast cancer to high levels of HER-2 and, unexpectedly, to sensitivity to Trastuzumab (Parra-Palau *et al.*, 2014; Scaltriti *et al.*, 2014). In particular, Parra-Palau and colleagues suggested that the accumulation of HER-2 at the cell surface was caused by p95HER-2-driven inhibition of phospho-HER-2 and stabilization of HER-2 (Parra-Palau *et al.*, 2014). Indeed, the study conducted by Gosh and colleagues previously demonstrated that high levels of HER-2 homodimers, which correlated with HER-2 expression, were related to increased Trastuzumab activity (Ghosh *et al.*, 2011). In light of these findings, the enhanced susceptibility to Trastuzumab here displayed by $\Delta 16$ -expressing tumor cells could be explained by the demonstrated formation of stable and constitutive active $\Delta 16$ homodimers (Castiglioni *et al.*, 2006). Conversely, *in vitro* resistance and lower *in vivo* sensitivity to Trastuzumab of cell lines with high HER-2 might be caused, besides genetic mutations of HER-2, by the presence of less stable HER-2 homodimers and/or by a larger amount of HER-2-containing heterodimers.

All HER-2, $\Delta 16$ and F1 cell lines were susceptible *in vitro* to the treatment with another anti-HER-2 agent, the tyrosine kinase inhibitor Lapatinib. However, the drug was more effective on $\Delta 16$ -expressing cells, where a complete inhibition of cell growth was observed. This evidence could be explained, similarly to Trastuzumab sensitivity, by the high dependence of cell signaling on stable $\Delta 16$ homodimers, whose constitutive catalytic activity may be highly hampered by the drug. No additional effect was observed *in vitro* after combining Lapatinib with Trastuzumab in HER-2-expressing cell lines (MAMBO 89 and 143-VS). In the other cell lines the statistical evaluation of the combinatorial-regimen efficacy could not be investigated because of their complete growth inhibition after treatment with Lapatinib alone and/or because no replicates of the experiments were performed. However, Scaltriti and colleagues (Scaltriti *et al.*, 2014), showed that the benefit for the combination of Lapatinib with Trastuzumab could be predicted by total levels of HER-2 that, as suggested by Gosh and co-

Discussion

workers, correlate with high levels of HER-2 homodimers (Ghosh *et al.*, 2011), including $\Delta 16$ homodimers.

A wide signaling network is triggered by HER-2 and the other ErbB members after dimers formation. In particular, MAPK and PI3K-AKT are the most activated cascades downstream to HER-2 (Yarden and Sliwkowski, 2001; Arteaga and Engelman, 2014). In addition, Src kinase activation has been correlated to HER-2- and $\Delta 16$ -dependent signal transduction. In particular, phospho-Src was connected to HER-2/HER-3 interaction and it was suggested as convergent point of multiple upstream signals, thus conferring resistance to anti-HER-2 agents (Tan *et al.*, 2005; Zhang *et al.*, 2011; Rexer *et al.*, 2011). Furthermore, Src activation was specifically related to $\Delta 16$ -driven signal transduction (Mitra *et al.*, 2009; Marchini *et al.*, 2011; Castagnoli *et al.*, 2014). Thus, besides HER-2 receptor, these intracellular effectors represent valuable targets for new anti-HER-2 strategies (Arteaga and Engelman, 2014).

Indeed, in this thesis the activity of three intracellular inhibitors was investigated: the Src inhibitor Dasatinib, the PI3K inhibitor NVP-BKM120 and MEK dual inhibitor UO126. Susceptibility to Dasatinib was evaluated both *in vitro* and *in vivo*. In 3-D culture the drug was effective on all cell lines derived from HER-2, $\Delta 16$ and F1 models. Nevertheless, the presence, even at very low levels, of $\Delta 16$ determined a much more evident therapeutic effect, thus supporting the $\Delta 16$ /Src correlation suggested in previous studies (Mitra *et al.*, 2009; Marchini *et al.*, 2011; Castagnoli *et al.*, 2014). *In vivo*, when combined with Trastuzumab, Dasatinib was able to inhibit the growth of $\Delta 16$ metastases in a higher extent in respect to Trastuzumab alone, suggesting the potential efficacy of Src inhibitor also in a preclinical setting, besides in *in vitro* experiments. Combining Dasatinib with HER-2 targeted agents showed additional effect also *in vitro*, thus supporting the notion that combinatorial regimens targeting different “layers” of HER-2 signaling may be more effective than single-agent treatments (Yarden and Pines, 2012; Arteaga and Engelman, 2014). For example, Trastuzumab resistance displayed by MAMBO 89 was overcome by the independent administration of both Dasatinib and Lapatinib, but their combination caused a more potent inhibition of tumor cell growth.

Discussion

The rationale of targeting PI3K with NVP-BKM120 was the hyper-activation of PI3K-AKT pathway in HER-2-positive breast tumors, connected to the formation of the highly active HER-2/HER-3 heterodimer (Lee-Hoeflich *et al.*, 2008; Chakrabarty *et al.*, 2013). All HER-2, Δ16 and F1 cell lines were strongly inhibited by the drug at the higher concentration chosen for *in vitro* experiments (1 μM), highlighting the importance of targeting effectors belonging to PI3K-AKT signaling cascade.

However, targeting only a signaling pathway is thought to be a frequent cause for acquired resistance to single-agent treatment, because of the feedback activation of other cascades (Arteaga and Engelman, 2014). In this thesis, MEK1/MEK2 inhibition in MCF-10A and BT-474 by siRNA or UO126 determined an increase in HER-2 activation, confirming the findings of earlier studies. In particular, Turke and colleagues demonstrated that the treatment of BT-474 with a MEK inhibitor (AZD6244) was able to activate ErbB receptors (including HER-2) by releasing a negative feedback on ErbB dimerization. As a consequence, the impaired MAPK cascade was compensated by the strong activation of PI3K-AKT pathway (Turke *et al.*, 2012). Similarly, two studies showed that the inhibition of PI3K-AKT cascade in the same cell line caused the potent activation of HER receptors and of MAPK pathway (Chandarlapaty *et al.*, 2011; Serra *et al.*, 2011).

The importance of HER-2/MAPK pathway correlation was underlined also in a therapeutic setting. Gayle and co-workers observed a sustained MAPK activation in HER-2-positive cancer cell lines resistant to Lapatinib. Therefore, combining the drug with MEK suppression (by drugs-mediated inhibition as well as by dual silencing of MEK1/MEK2) they succeeded in blocking the growth of resistant cancer cells (Gayle *et al.*, 2013). Almost symmetrically, Chandarlapaty and colleagues showed that the combinatorial regimen of a AKT inhibitor and Lapatinib determined the reduction of ErbB receptors activation (Chandarlapaty *et al.*, 2011).

Besides the increase in phospho-HER-2, cells treated with UO126 displayed high levels of phospho-MEK1/2. Notably, no increase of constitutive MEK 1 and MEK 2 was observed. UO126 inhibition of MEK1/MEK2 is non-competitive with

Discussion

respect to ATP (Duncia *et al.*, 1998), allowing MEK activation but blocking MEK-mediated ERK activation. Consequently, phospho-MEK1/2 accumulation could be attributed to its inability to phosphorylate the downstream effector ERK. Otherwise, lower levels of phospho-ERK could relieve a negative feedback on upstream signaling effectors of the pathway (e.g. Raf or Ras) or directly on ErbB receptors. In light of this explanation, the accumulation of activated MEK1/2 could be the direct consequence of the increase in phospho-HER-2. The knockdown of MEK 1 and MEK2 by siRNA did not allow to detect this increase, likely because of the low/absent expression of constitutive MEK isoforms.

Importantly, BT-474 is known to coexpress HER-2 and $\Delta 16$. In *in vitro* therapeutical experiments its sensitivity to anti-HER-2 agents was comparable to that of F1 cell lines. Hence, cells derived from the hybrid model can successfully predict the response of human HER-2-positive cancer cells to treatments. In addition, in the attempt to find correlations between drug-resistant feedback cascades and heterogeneous levels of HER-2 and $\Delta 16$, F1 cell lines could be employed besides BT-474.

Xenotransplantation models have been widely used for the study of HER-2-positive breast cancer and for the development of new anti-tumor and anti-metastatic approaches targeting HER-2. In the Laboratory of Immunology and Biology of Metastasis a multiorgan metastatic model of HER-2-positive breast cancer was developed. It consists of the i.m. or i.v. injection of human HER-2-positive breast cancer cell lines in immunodeficient $Rag2^{-/-}; Il2rg^{-/-}$ mice, that lack mature T, B and NK cells. The metastatic pattern in $Rag2^{-/-}; Il2rg^{-/-}$ mice well reproduces the multiorgan metastatic situation displayed by advanced HER-2-positive breast cancer patients. In particular, the high incidence of brain metastases makes this model the perfect target for new therapeutic approaches. In this thesis, $Rag2^{-/-}; Il2rg^{-/-}$ mice were employed to study the efficacy of NVP-BKM120 in inhibiting metastases to brain and other organs and of an oncolytic virus retargeted against HER-2 (Nanni *et al.*, 2012; Nanni *et al.*, 2013).

NVP-BKM120 was effective in reducing the incidence of metastatic spread in many organs, especially brain, femoral bone marrow and liver. Using a specific quantitative analysis, a more than 90% reduction in the brain metastatic

Discussion

burden was detected after treatment with the drug, underlining its ability to cross the blood-brain barrier and stop the growth of HER-2-positive tumor cells. In addition, NVP-BKM120 was able to efficiently inhibit metastases to the bones and, in general, to all sites (Nanni *et al.*, 2012). Notably, the model here described was obtained by the injection of MDA-MB-453, that is a Trastuzumab-resistant cell line. Hence, its current usefulness is undeniable.

The high clinical impact of brain metastases in HER-2-positive breast cancer patients (Singh *et al.*, 2014) enhances the potential role of some small molecule inhibitors that, in contrast with Trastuzumab, display the ability to reach the brain. As described above, Src family is critical in HER-2- and $\Delta 16$ -driven signal transduction. Recently, Zhang and co-workers suggested a Src role in promoting brain metastases in breast cancer and they showed that the therapeutic combination of Src inhibitor Saracatinib and HER-2/EGFR inhibitor Lapatinib was effective in inhibiting experimental HER-2-positive brain metastases in a preclinical model (Zhang *et al.*, 2013). Similarly to Saracatinib, other combinatorial regimens targeting both HER-2 receptor and signaling effectors, including PI3K, could be equally effective and need to be investigated. To address this issue, the multiorgan metastatic model described in this thesis seems particularly suitable.

Since the pioneering study of Martuza and colleagues (Martuza *et al.*, 1991), the therapeutic ability of oncolytic HSV has been evaluated in preclinical and clinical studies. For example, NV1020, an attenuated recombinant HSV with wild-type tropism, was effective in treating colorectal cancer metastatic to liver in a phase II clinical trial (Geevarghese *et al.*, 2010). However, virus attenuation generally interferes with its therapeutic potential, and the development of engineered viruses with high specificity for tumor cells allows to preserve their wild-type replicative activity (Miest and Cattaneo, 2014). Here, the efficacy of a HER-2-retargeted HSV (R-LM249) was assessed in $Rag2^{-/-};Il2rg^{-/-}$ mice (Nanni *et al.*, 2013). All HER-2-positive human cell lines tested *in vitro*, including Trastuzumab-resistant cells, were sensitive to R-LM249. After the s.c. injection of HER-2-positive human breast cancer cells, the virus was able to inhibit tumor growth and prolong the life expectancy of mice. Finally, treatment of HER-2-

Discussion

positive breast and ovarian advanced cancers in Trastuzumab-resistant models successfully inhibited the growth of metastases in the peritoneum and in the brain of animals.

In contrast with other anti-HER-2 agents (i.e. monoclonal antibodies and tyrosine kinases inhibitors), R-LM249 efficacy lies on its combined abilities to specifically target HER-2 (as well as other agents targeting HER-2 receptor do) and kill tumor cells (cytotoxic activity that belongs to viruses). Furthermore, contrary to HER-2 inhibitors and monoclonal antibodies, the retargeted virus is not dependent on HER-2 signaling and on host's immune responses (e.g. Trastuzumab-triggered ADCC). In addition, it is able to amplify its cytotoxic effect replicating into cancer cells, but it exhausts itself when HER-2-positive tumor cells are no longer available.

If compared to oncolytic HSV previously investigated, R-LM249 was designed to target a specific antigen overexpressed only by tumor cells (oncoantigen, see below in the Discussion). As a result, it exploits its activity only when it reaches HER-2-positive cancer cells, without infecting other sites.

Due to its systemic delivery route (i.p.), a high safety profile of R-LM249 was required. In preliminary *in vivo* experiments conducted by Menotti and colleagues the virus did not kill any mouse, even at doses that were much higher than those required by wild-type HSV to kill all mice (Menotti *et al.*, 2009). Furthermore, the retargeted virus was specific for tumor cells that highly expressed HER-2 on plasmatic membrane and it could not revert to the wild-type form because of the deletion of a large portion of gD gene (Menotti *et al.*, 2009). Nevertheless, specific therapy with acyclovir is available in a worst case scenario (Campadelli-Fiume *et al.*, 2011).

The reduction in the incidence and in the quantity of brain metastatic HER-2-positive cells in Rag^{-/-}; Il2rg^{-/-} mice treated with R-LM249 can be attributed to its ability to cross the blood-brain barrier. In light of these findings, this retargeted virus should be further investigated for anti-HER-2 regimens targeting brain metastases in addition to small molecule inhibitors. Furthermore, the high-potential use of R-LM249 is even enhanced by the possibility to re-engineer it in order to target other oncoantigens.

Discussion

In addition to novel anti-HER-2 therapeutic agents, HER-2-targeting active immune approaches are under evaluation, exploiting the notion that HER-2 is a cell surface antigen specifically overexpressed by tumor cells (Lollini *et al.*, 2013). E75 NeuVax is a nonapeptide derived from the extracellular domain of HER-2 protein. As reported by Mittendorf and colleagues (Mittendorf *et al.*, 2012), the s.c. injection of E75 may stimulate CD8⁺ cytotoxic T cells and drive them to kill HER-2-positive tumor cells. This peptide-based vaccine is currently studied in a phase III clinical trial for the adjuvant therapy of HER-2 low-expressing breast cancers to prevent disease recurrence (Yan *et al.*, 2014).

In this thesis a whole tumor cell- and a DNA-based vaccine were described for the immunoprevention of HER-2-positive breast cancer in a HER-2-tolerant model (De Giovanni *et al.*, 2014). The whole-cell vaccine (called HER-2-Cell) was developed in the Laboratory of Immunology and Biology of Metastasis according to previous studies conducted by the same group of scientists for the prevention of Neu-driven carcinogenesis in BalbNeuT mice (Nanni *et al.*, 2001; De Giovanni *et al.*, 2004). HER-2-Cell vaccine is composed of three stimuli: a human HER-2-positive cell line with blocked proliferative ability (SK-OV-3, specific stimulus), the xenogeneic class I molecules of this cell line and murine recombinant IL-12 (adjuvant stimuli). HURT-DNA vaccine was developed by Quaglino and co-workers and its administration is combined with electroporation as adjuvant stimulus (Quaglino *et al.*, 2010).

As widely described, HER-2 model develops autochthonous mammary tumors due to the presence in its genome of 30-50 copies of human HER-2 gene and, therefore, HER-2 mice are tolerant towards HER-2. Both vaccines here investigated were able to break this tolerance, delaying tumor onset and prolonging the life of vaccinated mice. Thus, HER-2-Cell vaccine efficacy is an advance of the results obtained by Nanni and co-workers in 2001 (Nanni *et al.*, 2001), because it allows to resemble a more realistic immunological approach targeting the human proto-oncogene HER-2, instead of its mutated rat orthologue NeuT. Notably, vaccination schedules were repeated all-life long and after more than 80 weeks of age, more than 60% of HURT-DNA vaccinated mice were still tumor-free. Focusing on tumor multiplicity, vaccinations were able to reduce the

Discussion

growth of multiple tumors. Conversely, in control mice the number of tumors was more than doubled if compared to that of vaccinated animals.

The anti-tumor activity of anti-HER-2 vaccination lies on both humoral and cell-mediated responses. Nanni and co-workers showed that the production of anti-HER-2 antibodies (by B cells) and IFN- γ release (by T helper cells) were able to prevent mammary carcinogenesis in vaccinated BalbNeuT mice (Nanni *et al.*, 2001). In a further study, they crossed BalbNeuT mice with a knockout strain lacking IFN- γ production or with B cells-deficient mice, showing that vaccination was not able to protect these animals from the development of mammary tumors. Thus, they demonstrated that tumor prevention was dependent on cytokines and specific antibodies induction (Nanni *et al.*, 2004). Here, both vaccines elicited in general a strong humoral response. However, higher and more stable levels of anti-HER-2 antibodies were detected in sera from HURT-DNA vaccinated mice. In these animals, most represented isotypes were IgG1, IgG2a and IgG2b, whose production by B cells is mediated by T helper cells. The inhibitory effect of anti-HER-2 antibodies on HER-2-positive mammary tumor cells was confirmed by their ability to suppress the activation of HER-2 receptor and of PI3K-AKT pathway in MAMBO 89. *In vivo*, the passive immunization by anti-HER-2 antibodies produced by HURT-DNA vaccinated mice was effective in inhibiting the growth of HER-2-positive peritoneal masses in Rag2^{-/-};Il2rg^{-/-} mice, despite the absence of most cellular and cytokine responses. Immunodeficient mice were chosen to avoid any possible additive immunologic anti-tumor activity by the host and, thus, to evaluate the real contribution of anti-HER-2 antibodies alone.

Focusing on cell-mediated response, only HER-2-Cell vaccine determined the production of IFN- γ in HER-2 mice, confirming the results obtained with the cell vaccine developed by Nanni and colleagues in 2001. IFN- γ release by T helper cells was suggested to mediate anti-tumor efficacy and IgG2a production in BalbNeuT mice (Nanni *et al.*, 2001). Thus, the low levels of IFN- γ released in HURT-DNA vaccinated mice suggested that the high humoral response induced by HURT plasmid was sufficient to prevent and delay tumor onset in HER-2 mice.

CONCLUSIONS

Conclusions

In this thesis the contribution of HER-2 and $\Delta 16$ to mammary carcinogenesis was investigated in a model transgenic for both genes (F1 model). A dominant role of $\Delta 16$, especially in early stages of tumorigenesis, was suggested and the coexistence of heterogeneous levels of HER-2 and $\Delta 16$ in F1 tumors revealed the undeniable value of F1 strain as preclinical model of HER-2-positive breast cancer, closer resembling the human situation in respect to previous models.

The therapeutical efficacy of anti-HER-2 agents, targeting HER-2 receptor (Trastuzumab, Lapatinib, R-LM249) or signaling effectors (Dasatinib, UO126, NVP-BKM120), was investigated in models of local or advanced HER-2-positive breast cancer. In contrast with early studies, data herein collected suggested that the presence of $\Delta 16$ can predict a better response to Trastuzumab and other agents targeting HER-2 receptor or Src activity. Using a multiorgan HER-2-positive metastatic model, the efficacy of NVP-BKM120 (PI3K inhibitor) in blocking the growth of brain metastases and the oncolytic ability of R-LM249 (HER-2-retargeted HSV) to reach and destroy metastatic HER-2-positive cancer cells were shown.

Finally, exploiting the definition of “oncoantigen” given to HER-2, the immunopreventive activity of two vaccines on HER-2-positive mammary tumorigenesis was demonstrated.

SCIENTIFIC PUBLICATIONS DURING PHD PERIOD

Related to the PhD project

Nanni P, Gatta V, Menotti L, De Giovanni C, Ianzano M, Palladini A, Grosso V, **Dall'Ora M**, Croci S, Nicoletti G, Landuzzi L, Iezzi M, Campadelli-Fiume G and Lollini PL. (2013) *Preclinical therapy of disseminated HER-2(+) ovarian and breast carcinomas with a HER-2-retargeted oncolytic herpesvirus*. PLoS Pathog; 9: e1003155.

De Giovanni C, Nicoletti G, Quaglino E, Landuzzi L, Palladini A, Ianzano ML, **Dall'Ora M**, Grosso V, Ranieri D, Laranga R, Croci S, Amici A, Penichet ML, Iezzi M, Cavallo F, Nanni P and Lollini PL. (2014) *Vaccines against human HER2 prevent mammary carcinoma in mice transgenic for human HER2*. Breast Cancer Res; 16: R10.

Other

Ianzano ML, Croci S, Nicoletti G, Palladini A, Landuzzi L, Grosso V, Ranieri D, **Dall'Ora M**, Santeramo I, Urbini I, De Giovanni C, Lollini P-L, Nanni P. (2014) *Tumor suppressor genes promote rhabdomyosarcoma progression in p53 heterozygous, HER-2/neu transgenic mice*. Oncotarget; 5: 108-119

Landuzzi L, Ianzano ML, Nicoletti G, Palladini A, Grosso V, Ranieri D, **Dall'Ora M**, Raschi E, Laranga R, Gambarotti M, Picci P, De Giovanni C, Nanni P, Lollini P-L. (2014) *Genetic prevention of lymphoma in p53 knockout mice allows the early development of p53 related sarcomas*. Oncotarget; 5(23):11924-38.

Croci S, Nanni P, Nicoletti G, Grosso V, Benegiamo G, Palladini A, Landuzzi L, Iezzi M, Ianzano ML, Ranieri D, **Dall'Ora M**, De Giovanni C and Lollini P-L. *IL-15 is required for immunosurveillance and immunoprevention of HER2/neu-driven mammary carcinogenesis*. Breast Cancer Research, under revision.

Mancini M, Gaborit N, Lindzen M, **Dall'Ora M**, Sevilla M, Hai A, Downward J and Yarden Y. *Combining three antibodies nullifies feedback and inhibits Erlotinib resistant lung cancer*. Submitted.

REFERENCES

References

- Alajati A, Sausgruber N, Aceto N, Duss S, Sarret S, Voshol H, Bonenfant D and Bentires-Alj M. (2013) *Mammary tumor formation and metastasis evoked by a HER2 splice variant*. *Cancer Res*; 73: 5320-5327.
- Arribas J, Baselga J, Pedersen K and Parra-Palau JL. (2011) *p95HER2 and breast cancer*. *Cancer Res*; 71: 1515-1519.
- Arteaga CL and Engelman JA. (2014) *ERBB receptors: from oncogene discovery to basic science to mechanism-based cancer therapeutics*. *Cancer Cell*; 25: 282-303.
- Becker M, Nitsche A, Neumann C, Aumann J, Junghahn I and Fichtner I. (2002) *Sensitive PCR method for the detection and real-time quantification of human cells in xenotransplantation systems*. *Br J Cancer*; 87: 1328-1335.
- Boggio K, Nicoletti G, Di CE, Cavallo F, Landuzzi L, Melani C, Giovarelli M, Rossi I, Nanni P, De Giovanni C, Bouchard P, Wolf S, Modesti A, Musiani P, Lollini PL, Colombo MP and Forni G. (1998) *Interleukin 12-mediated prevention of spontaneous mammary adenocarcinomas in two lines of Her-2/neu transgenic mice*. *J Exp Med*; 188: 589-596.
- Bos PD, Zhang XH, Nadal C, Shu W, Gomis RR, Nguyen DX, Minn AJ, van de Vijver MJ, Gerald WL, Foekens JA and Massague J. (2009) *Genes that mediate breast cancer metastasis to the brain*. *Nature*; 459: 1005-1009.
- Bose R, Kavuri SM, Searleman AC, Shen W, Shen D, Koboldt DC, Monsey J, Goel N, Aronson AB, Li S, Ma CX, Ding L, Mardis ER and Ellis MJ. (2013) *Activating HER2 mutations in HER2 gene amplification negative breast cancer*. *Cancer Discov*; 3: 224-237.
- Brufsky AM. (2014) *Current Approaches and Emerging Directions in HER2-resistant Breast Cancer*. *Breast Cancer (Auckl)*; 8: 109-118.
- Cadoo KA, Fornier MN and Morris PG. (2013) *Biological subtypes of breast cancer: current concepts and implications for recurrence patterns*. *Q J Nucl Med Mol Imaging*; 57: 312-321.
- Campadelli-Fiume G, De Giovanni C, Gatta V, Nanni P, Lollini PL and Menotti L. (2011) *Rethinking herpes simplex virus: the way to oncolytic agents*. *Rev Med Virol*; 21: 213-226.
- Cao X, Shores EW, Hu-Li J, Anver MR, Kelsall BL, Russell SM, Drago J, Noguchi M, Grinberg A, Bloom ET and . (1995) *Defective lymphoid development in mice lacking expression of the common cytokine receptor gamma chain*. *Immunity*; 2: 223-238.
- Castagnoli L, Iezzi M, Ghedini GC, Ciravolo V, Marzano G, Lamolinara A, Zappasodi R, Gasparini P, Campiglio M, Amici A, Chiodoni C, Palladini A, Lollini PL, Triulzi T, Menard S, Nanni P, Tagliabue E and Pupa SM. (2014)

References

Activated d16HER2 homodimers and SRC kinase mediate optimal efficacy for trastuzumab. Cancer Res; 74: 6248-6259.

Castiglioni F, Tagliabue E, Campiglio M, Pupa SM, Balsari A and Menard S. (2006) *Role of exon-16-deleted HER2 in breast carcinomas.* Endocr Relat Cancer; 13: 221-232.

Chakrabarty A, Bhola NE, Sutton C, Ghosh R, Kuba MG, Dave B, Chang JC and Arteaga CL. (2013) *Trastuzumab-resistant cells rely on a HER2-PI3K-FoxO-survivin axis and are sensitive to PI3K inhibitors.* Cancer Res; 73: 1190-1200.

Chandarlapaty S, Sawai A, Scaltriti M, Rodrik-Outmezguine V, Grbovic-Huezo O, Serra V, Majumder PK, Baselga J and Rosen N. (2011) *AKT inhibition relieves feedback suppression of receptor tyrosine kinase expression and activity.* Cancer Cell; 19: 58-71.

Chappell WH, Steelman LS, Long JM, Kempf RC, Abrams SL, Franklin RA, Basecke J, Stivala F, Donia M, Fagone P, Malaponte G, Mazzarino MC, Nicoletti F, Libra M, Maksimovic-Ivanic D, Mijatovic S, Montalto G, Cervello M, Laidler P, Milella M, Tafuri A, Bonati A, Evangelisti C, Cocco L, Martelli AM and McCubrey JA. (2011) *Ras/Raf/MEK/ERK and PI3K/PTEN/Akt/mTOR inhibitors: rationale and importance to inhibiting these pathways in human health.* Oncotarget; 2: 135-164.

Daphu I, Sundstrom T, Horn S, Huszthy PC, Niclou SP, Sakariassen PO, Immervoll H, Miletic H, Bjerkvig R and Thorsen F. (2013) *In vivo animal models for studying brain metastasis: value and limitations.* Clin Exp Metastasis; 30: 695-710.

De Giovanni C, Nicoletti G, Landuzzi L, Astolfi A, Croci S, Comes A, Ferrini S, Meazza R, Iezzi M, Di Carlo E, Musiani P, Cavallo F, Nanni p and Lollini PL. (2004) *Immunoprevention of HER-2/Neu transgenic mammary carcinoma through an interleukin 12-engineered allogeneic cell vaccine.* Cancer Res; 64: 4001-4009.

De Giovanni C, Nicoletti G, Palladini A, Croci S, Landuzzi L, Antognoli A, Murgio A, Astolfi A, Ferrini S, Fabbi M, Orengo AM, Amici A, Penichet ML, Aurisicchio L, Iezzi M, Musiani P, Nanni P and Lollini PL. (2009) *A multi-DNA preventive vaccine for p53/Neu-driven cancer syndrome.* Hum Gene Ther; 20:453-464.

De Giovanni C, Nicoletti G, Quaglino E, Landuzzi L, Palladini A, Ianzano ML, Dall'Ora M, Grosso V, Ranieri D, Laranga R, Croci S, Amici A, Penichet ML, Iezzi M; Cavallo F, Nanni P and Lollini PL. (2014) *Vaccines against human HER2 prevent mammary carcinoma in mice transgenic for human HER2.* Breast Cancer Res; 16: R10.

Duncia JV, Santella JB, III, Higley CA, Pitts WJ, Wityak J, Frieze WE, Rankin FW, Sun JH, Earl RA, Tabaka AC, Teleha CA, Blom KF, Favata MF, Manos EJ,

References

Daulerio AJ, Stradley DA, Horiuchi K, Copeland RA, Scherle PA, Trzaskos JM, Magolda RL, Trainor GL, Wexler RR, Hobbs FW and Olson RE. (1998) *MEK inhibitors: the chemistry and biological activity of U0126, its analogs, and cyclization products*. Bioorg Med Chem Lett; 8: 2839-2844.

Emde A, Kostler WJ and Yarden Y. (2012) *Therapeutic strategies and mechanisms of tumorigenesis of HER2-overexpressing breast cancer*. Crit Rev Oncol Hematol; 84 Suppl 1: e49-e57.

Finkle D, Quan ZR, Asghari V, Kloss J, Ghaboosi N, Mai E, Wong WL, Hollingshead P, Schwall R, Koeppen H and Erickson S. (2004) *HER2-targeted therapy reduces incidence and progression of midlife mammary tumors in female murine mammary tumor virus huHER2-transgenic mice*. Clin Cancer Res; 10: 2499-2511.

Francia G, Cruz-Munoz W, Man S, Xu P and Kerbel RS. (2011) *Mouse models of advanced spontaneous metastasis for experimental therapeutics*. Nat Rev Cancer; 11: 135-141.

Gayle SS, Castellino RC, Buss MC and Nahta R. (2013) *MEK inhibition increases lapatinib sensitivity via modulation of FOXM1*. Curr Med Chem; 20: 2486-2499.

Geevarghese SK, Geller DA, de Haan HA, Horer M, Knoll AE, Mescheder A, Nemunaitis J, Reid TR, Sze DY, Tanabe KK and Tawfik H. (2010) *Phase I/II study of oncolytic herpes simplex virus NV1020 in patients with extensively pretreated refractory colorectal cancer metastatic to the liver*. Hum Gene Ther; 21: 1119-1128.

Ghosh R, Narasanna A, Wang SE, Liu S, Chakrabarty A, Balko JM, Gonzalez-Angulo AM, Mills GB, Penuel E, Winslow J, Sperinde J, Dua R, Pidaparathi S, Mukherjee A, Leitzel K, Kostler WJ, Lipton A, Bates M and Arteaga CL. (2011) *Trastuzumab has preferential activity against breast cancers driven by HER2 homodimers*. Cancer Res; 71: 1871-1882.

Giordano SH, Temin S, Kirshner JJ, Chandarlapaty S, Crews JR, Davidson NE, Esteva FJ, Gonzalez-Angulo AM, Krop I, Levinson J, Lin NU, Modi S, Patt DA, Perez EA, Perlmutter J, Ramakrishna N and Winer EP. (2014) *Systemic therapy for patients with advanced human epidermal growth factor receptor 2-positive breast cancer: American Society of Clinical Oncology clinical practice guideline*. J Clin Oncol; 32: 2078-2099.

Goldman JP, Blundell MP, Lopes L, Kinnon C, Di Santo JP and Thrasher AJ. (1998) *Enhanced human cell engraftment in mice deficient in RAG2 and the common cytokine receptor gamma chain*. Br J Haematol; 103: 335-342.

Gril B, Palmieri D, Qian Y, Smart D, Ileva L, Liewehr DJ, Steinberg SM and Steeg PS. (2011) *Pazopanib reveals a role for tumor cell B-Raf in the prevention of HER2+ breast cancer brain metastasis*. Clin Cancer Res; 17: 142-153.

References

- Guy CT, Webster MA, Schaller M, Parsons TJ, Cardiff RD and Muller WJ. (1992) *Expression of the neu protooncogene in the mammary epithelium of transgenic mice induces metastatic disease*. Proc Natl Acad Sci U S A; 89: 10578-10582.
- Hirasawa T, Yamashita H and Makino S. (1998) *Genetic typing of the mouse and rat nude mutations by PCR and restriction enzyme analysis*. Exp Anim; 47: 63-67.
- Huang X, Gao L, Wang S, McManaman JL, Thor AD, Yang X, Esteva FJ and Liu B. (2010) *Heterotrimerization of the growth factor receptors erbB2, erbB3, and insulin-like growth factor-1 receptor in breast cancer cells resistant to herceptin*. Cancer Res; 70: 1204-1214.
- Hurvitz SA, Hu Y, O'Brien N and Finn RS. (2013) *Current approaches and future directions in the treatment of HER2-positive breast cancer*. Cancer Treat Rev; 39: 219-229.
- Jonkers J and Derksen PW. (2007) *Modeling metastatic breast cancer in mice*. J Mammary Gland Biol Neoplasia; 12: 191-203.
- Khanna C and Hunter K. (2005) *Modeling metastasis in vivo*. Carcinogenesis; 26: 513-523.
- Kovanen PE and Leonard WJ. (2004) *Cytokines and immunodeficiency diseases: critical roles of the gamma(c)-dependent cytokines interleukins 2, 4, 7, 9, 15, and 21, and their signaling pathways*. Immunol Rev; 202: 67-83.
- Kwong KY and Hung MC. (1998) *A novel splice variant of HER2 with increased transformation activity*. Mol Carcinog; 23: 62-68.
- Lee-Hoeflich ST, Crocker L, Yao E, Pham T, Munroe X, Hoeflich KP, Sliwkowski MX and Stern HM. (2008) *A central role for HER3 in HER2-amplified breast cancer: implications for targeted therapy*. Cancer Res; 68: 5878-5887.
- Lollini PL, Cavallo F, Nanni P and Forni G. (2006) *Vaccines for tumour prevention*. Nat Rev Cancer; 6: 204-216.
- Lollini PL, Menotti L, De Giovanni C, Campadelli-Fiume G and Nanni P. (2009) *Oncolytic herpes virus retargeted to HER-2*. Cell Cycle; 8: 2859-2860.
- Lollini PL, Nicoletti G, Landuzzi L, Cavallo F, Forni G, De Giovanni C and Nanni P. (2011) *Vaccines and other immunological approaches for cancer immunoprevention*. Curr Drug Targets; 12: 1957-1973.
- Lollini PL, De Giovanni C and Nanni P. (2013) *Preclinical HER-2 Vaccines: From Rodent to Human HER-2*. Front Oncol; 3: 151.

References

- Maira SM, Pecchi S, Huang A, Burger M, Knapp M, Sterker D, Schnell C, Guthy D, Nagel T, Wiesmann M, Brachmann S, Fritsch C, Dorsch M, Chene P, Shoemaker K, De PA, Menezes D, Martiny-Baron G, Fabbro D, Wilson CJ, Schlegel R, Hofmann F, Garcia-Echeverria C, Sellers WR and Voliva CF. (2012) *Identification and characterization of NVP-BKM120, an orally available pan-class I PI3-kinase inhibitor*. *Mol Cancer Ther*; 11: 317-328.
- Marchini C, Gabrielli F, Iezzi M, Zenobi S, Montani M, Pietrella L, Kalogris C, Rossini A, Ciravolo V, Castagnoli L, Tagliabue E, Pupa SM, Musiani P, Monaci P, Menard S and Amici A. (2011) *The human splice variant Delta16HER2 induces rapid tumor onset in a reporter transgenic mouse*. *PLoS One*; 6: e18727.
- Martuza RL, Malick A, Markert JM, Ruffner KL and Coen DM. (1991) *Experimental therapy of human glioma by means of a genetically engineered virus mutant*. *Science*; 252: 854-856.
- Menotti L, Nicoletti G, Gatta V, Croci S, Landuzzi L, De Giovanni C, Nanni P, Lollini PL and Campadelli-Fiume G. (2009) *Inhibition of human tumor growth in mice by an oncolytic herpes simplex virus designed to target solely HER-2-positive cells*. *Proc Natl Acad Sci U S A*; 106: 9039-9044.
- Miest TS and Cattaneo R. (2014) *New viruses for cancer therapy: meeting clinical needs*. *Nat Rev Microbiol*; 12: 23-34.
- Milani A, Sangiolo D, Montemurro F, Aglietta M and Valabrega G. (2013) *Active immunotherapy in HER2 overexpressing breast cancer: current status and future perspectives*. *Ann Oncol*; 24: 1740-1748.
- Mitra D, Brumlik MJ, Okamgba SU, Zhu Y, Duplessis TT, Parvani JG, Lesko SM, Brogi E and Jones FE. (2009) *An oncogenic isoform of HER2 associated with locally disseminated breast cancer and trastuzumab resistance*. *Mol Cancer Ther*; 8: 2152-2162.
- Mittendorf EA, Wu Y, Scaltriti M, Meric-Bernstam F, Hunt KK, Dawood S, Esteva FJ, Buzdar AU, Chen H, Eksambi S, Hortobagyi GN, Baselga J and Gonzalez-Angulo AM. (2009) *Loss of HER2 amplification following trastuzumab-based neoadjuvant systemic therapy and survival outcomes*. *Clin Cancer Res*; 15: 7381-7388.
- Mittendorf EA, Clifton GT, Holmes JP, Clive KS, Patil R, Benavides LC, Gates JD, Sears AK, Stojadinovic A, Ponniah S and Peoples GE. (2012) *Clinical trial results of the HER-2/neu (E75) vaccine to prevent breast cancer recurrence in high-risk patients: from US Military Cancer Institute Clinical Trials Group Study I-01 and I-02*. *Cancer*; 118: 2594-2602.
- Moasser MM. (2007) *The oncogene HER2: its signaling and transforming functions and its role in human cancer pathogenesis*. *Oncogene*; 26: 6469-6487.

References

Morancho B, Parra-Palau JL, Ibrahim YH, Bernado MC, Peg V, Bech-Serra JJ, Pandiella A, Canals F, Baselga J, Rubio I and Arribas J. (2013) *A dominant-negative N-terminal fragment of HER2 frequently expressed in breast cancers*. *Oncogene*; 32: 1452-1459.

Muller WJ, Sinn E, Pattengale PK, Wallace R and Leder P. (1988) *Single-step induction of mammary adenocarcinoma in transgenic mice bearing the activated c-neu oncogene*. *Cell*; 54: 105-115.

Naito S, Giavazzi R, Walker SM, Itoh K, Mayo J and Fidler IJ. (1987) *Growth and metastatic behavior of human tumor cells implanted into nude and beige nude mice*. *Clin Exp Metastasis*; 5: 135-146.

Nanni P, Nicoletti G, De Giovanni C, Landuzzi L, Di Carlo E, Cavallo F, Pupa SM, Rossi I, Colombo MP, Ricci C, Astolfi A, Musiani P, Forni G and Lollini PL. (2001) *Combined allogeneic tumor cell vaccination and systemic interleukin 12 prevents mammary carcinogenesis in HER-2/neu transgenic mice*. *J Exp Med*; 194: 1195-1205.

Nanni P, Landuzzi L, Nicoletti G, De Giovanni C, Rossi I, Croci S, Astolfi A, Iezzi M, Di CE, Musiani P, Forni G and Lollini PL. (2004) *Immunoprevention of mammary carcinoma in HER-2/neu transgenic mice is IFN-gamma and B cell dependent*. *J Immunol*; 173: 2288-2296.

Nanni P, Nicoletti G, Landuzzi L, Croci S, Murgo A, Palladini A, Antognoli A, Ianzano ML, Stivani V, Grosso V, Maira SM, Garcia-Echeverria C, Scotlandi K, De Giovanni C and Lollini PL. (2010) *High metastatic efficiency of human sarcoma cells in Rag2/gammac double knockout mice provides a powerful test system for antimetastatic targeted therapy*. *Eur J Cancer*; 46: 659-668.

Nanni P, Nicoletti G, Palladini A, Croci S, Murgo A, Ianzano ML, Grosso V, Stivani V, Antognoli A, Lamolinara A, Landuzzi L, di TE, Iezzi M, De Giovanni C and Lollini PL. (2012) *Multiorgan metastasis of human HER-2+ breast cancer in Rag2-/-;Il2rg-/- mice and treatment with PI3K inhibitor*. *PLoS One*; 7: e39626.

Nanni P, Gatta V, Menotti L, De Giovanni C, Ianzano M, Palladini A, Grosso V, Dall'Ora M, Croci S, Nicoletti G, Landuzzi L, Iezzi M, Campadelli-Fiume G and Lollini PL. (2013) *Preclinical therapy of disseminated HER-2(+) ovarian and breast carcinomas with a HER-2-retargeted oncolytic herpesvirus*. *PLoS Pathog*; 9: e1003155.

Oettinger MA, Schatz DG, Gorka C and Baltimore D. (1990) *RAG-1 and RAG-2, adjacent genes that synergistically activate V(D)J recombination*. *Science*; 248: 1517-1523.

Ottewell PD, Coleman RE and Holen I. (2006) *From genetic abnormality to metastases: murine models of breast cancer and their use in the development of anticancer therapies*. *Breast Cancer Res Treat*; 96: 101-113.

References

Palmieri D, Bronder JL, Herring JM, Yoneda T, Weil RJ, Stark AM, Kurek R, Vega-Valle E, Feigenbaum L, Halverson D, Vortmeyer AO, Steinberg SM, Aldape K and Steeg PS. (2007) *Her-2 overexpression increases the metastatic outgrowth of breast cancer cells in the brain*. *Cancer Res*; 67: 4190-4198.

Parra-Palau JL, Morancho B, Peg V, Escorihuela M, Scaltriti M, Vicario R, Zacarias-Fluck M, Pedersen K, Pandiella A, Nuciforo P, Serra V, Cortes J, Baselga J, Perou CM, Prat A, Rubio IT and Arribas J. (2014) *Effect of p95HER2/611CTF on the response to trastuzumab and chemotherapy*. *J Natl Cancer Inst*; 106:

Quaglino E, Mastini C, Amici A, Marchini C, Iezzi M, Lanzardo S, De Giovanni C, Montani M, Lollini PL, Masucci G, Forni G and Cavallo F. (2010) *A better immune reaction to Erbb-2 tumors is elicited in mice by DNA vaccines encoding rat/human chimeric proteins*. *Cancer Res*; 70: 2604-2612.

Rexer BN, Ham AJ, Rinehart C, Hill S, Granja-Ingram NM, Gonzalez-Angulo AM, Mills GB, Dave B, Chang JC, Liebler DC and Arteaga CL. (2011) *Phosphoproteomic mass spectrometry profiling links Src family kinases to escape from HER2 tyrosine kinase inhibition*. *Oncogene*; 30: 4163-4174.

Ritter CA, Perez-Torres M, Rinehart C, Guix M, Dugger T, Engelman JA and Arteaga CL. (2007) *Human breast cancer cells selected for resistance to trastuzumab in vivo overexpress epidermal growth factor receptor and ErbB ligands and remain dependent on the ErbB receptor network*. *Clin Cancer Res*; 13: 4909-4919.

Saini KS, Loi S, De AE, Metzger-Filho O, Saini ML, Ignatiadis M, Dancey JE and Piccart-Gebhart MJ. (2013) *Targeting the PI3K/AKT/mTOR and Raf/MEK/ERK pathways in the treatment of breast cancer*. *Cancer Treat Rev*; 39: 935-946.

Saxena M and Christofori G. (2013) *Rebuilding cancer metastasis in the mouse*. *Mol Oncol*; 7: 283-296.

Scaltriti M, Nuciforo P, Bradbury I, Sperinde J, Agbor-Tarh D, Campbell C, Chenna A, Winslow J, Serra V, Parra JL, Prudkin L, Jimenez J, Aura C, Harbeck N, Pusztai L, Ellis CE, Eidtmann H, Arribas J, Cortes J, De AE, Piccart M and Baselga J. (2014) *High HER2 expression correlates with response to the combination of lapatinib and trastuzumab*. *Clin Cancer Res*;

Schechter AL, Stern DF, Vaidyanathan L, Decker SJ, Drebin JA, Greene MI and Weinberg RA. (1984) *The neu oncogene: an erb-B-related gene encoding a 185,000-Mr tumour antigen*. *Nature*; 312: 513-516.

Serra V, Scaltriti M, Prudkin L, Eichhorn PJ, Ibrahim YH, Chandarlapaty S, Markman B, Rodriguez O, Guzman M, Rodriguez S, Gili M, Russillo M, Parra JL, Singh S, Arribas J, Rosen N and Baselga J. (2011) *PI3K inhibition results in*

References

enhanced HER signaling and acquired ERK dependency in HER2-overexpressing breast cancer. Oncogene; 30: 2547-2557.

Shinkai Y, Rathbun G, Lam KP, Oltz EM, Stewart V, Mendelsohn M, Charron J, Datta M, Young F, Stall AM and . (1992) *RAG-2-deficient mice lack mature lymphocytes owing to inability to initiate V(D)J rearrangement.* Cell; 68: 855-867.

Siegel PM, Dankort DL, Hardy WR and Muller WJ. (1994) *Novel activating mutations in the neu proto-oncogene involved in induction of mammary tumors.* Mol Cell Biol; 14: 7068-7077.

Singh JC, Jhaveri K and Esteva FJ. (2014) *HER2-positive advanced breast cancer: optimizing patient outcomes and opportunities for drug development.* Br J Cancer; 111: 1888-1898.

Tan M, Li P, Klos KS, Lu J, Lan KH, Nagata Y, Fang D, Jing T and Yu D. (2005) *ErbB2 promotes Src synthesis and stability: novel mechanisms of Src activation that confer breast cancer metastasis.* Cancer Res; 65: 1858-1867.

Thomsen M, Galvani S, Canivet C, Kamar N and Bohler T. (2008) *Reconstitution of immunodeficient SCID/beige mice with human cells: applications in preclinical studies.* Toxicology; 246: 18-23.

Turke AB, Song Y, Costa C, Cook R, Arteaga CL, Asara JM and Engelman JA. (2012) *MEK inhibition leads to PI3K/AKT activation by relieving a negative feedback on ERBB receptors.* Cancer Res; 72: 3228-3237.

Wang SE, Xiang B, Guix M, Olivares MG, Parker J, Chung CH, Pandiella A and Arteaga CL. (2008) *Transforming growth factor beta engages TACE and ErbB3 to activate phosphatidylinositol-3 kinase/Akt in ErbB2-overexpressing breast cancer and desensitizes cells to trastuzumab.* Mol Cell Biol; 28: 5605-5620.

Yan M, Parker BA, Schwab R and Kurzrock R. (2014) *HER2 aberrations in cancer: implications for therapy.* Cancer Treat Rev; 40: 770-780.

Yarden Y and Sliwkowski MX. (2001) *Untangling the ErbB signalling network.* Nat Rev Mol Cell Biol; 2: 127-137.

Yarden Y and Pines G. (2012) *The ERBB network: at last, cancer therapy meets systems biology.* Nat Rev Cancer; 12: 553-563.

Zhang S, Huang WC, Li P, Guo H, Poh SB, Brady SW, Xiong Y, Tseng LM, Li SH, Ding Z, Sahin AA, Esteva FJ, Hortobagyi GN and Yu D. (2011) *Combating trastuzumab resistance by targeting SRC, a common node downstream of multiple resistance pathways.* Nat Med; 17: 461-469.

Zhang S, Huang WC, Zhang L, Zhang C, Lowery FJ, Ding Z, Guo H, Wang H, Huang S, Sahin AA, Aldape KD, Steeg PS and Yu D. (2013) *SRC family kinases*

References

as novel therapeutic targets to treat breast cancer brain metastases. Cancer Res; 73: 5764-5774.